REPORT DOCUMENTATION PAGE

Form Approved
OMB No. 0704-0188

PLEASE DO NOT RETURN YOUR FORM TO THE ABOVE ORGANIZATION.

1. REPORT DATE *(DD-MM-YYYY)*	2. REPORT TYPE	3. DATES COVERED *(From - To)*
30-09-2015	Final	Oct 2010 to Sep 2015

4. TITLE AND SUBTITLE

Seabed Scattering from Low Frequency Reverberation Measurements

5a. CONTRACT NUMBER

N0014-11-1-0063

5b. GRANT NUMBER

5c. PROGRAM ELEMENT NUMBER

6. AUTHOR(S)

Zhou, Ji-Xun

Email: jixun.zhou@me.gatech.edu

5d. PROJECT NUMBER

5e. TASK NUMBER

5f. WORK UNIT NUMBER

7. PERFORMING ORGANIZATION NAME(S) AND ADDRESS(ES)

School of Mechanical Engineering
Georgia Institute of Technology
Atlanta, GA 30332-0405

8. PERFORMING ORGANIZATION REPORT NUMBER

9. SPONSORING/MONITORING AGENCY NAME(S) AND ADDRESS(ES)

Ocean Acoustics Program, CODE 322OA
OFFICE OF NAVAL RESEARCH
875 NORTH RANDOLPH ST, SUITE 1425
ARLINGTON, VA 22203-1995

10. SPONSOR/MONITOR'S ACRONYM(S)

ONR

11. SPONSOR/MONITOR'S REPORT NUMBER(S)

12. DISTRIBUTION/AVAILABILITY STATEMENT

Approved for public release; distribution is unlimited

13. SUPPLEMENTARY NOTES

14. ABSTRACT

Four published papers are submitted in lieu of the final technical report:

1. J.X. Zhou and X.Z. Zhang, "Low frequency seabed scattering at low grazing angles," Journal of the Acoustical Society of America, 131 (4), 2611-2621 (Apr 2012).
2. J.X. Zhou and X.Z. Zhang, "Shear wave velocity and attenuation in the upper layer of ocean bottoms from long-range acoustic field measurements," JASA, 132 (6), 3698-3705, (DEC 2012).
3. J.X. Zhou, X.Z. Zhang, Z.H. Peng and Z.L. Li, "Ocean Reverberation: Modeling, Measurements and Inversions," in <ADVANCES IN OCEAN ACOUSTICS>, Editor(s): J.X. Zhou, Z.L. Li and J. Simmen, AIP CP # 1495, Pages: 150-165 (2012).
4. J.X. Zhou and X.Z. Zhang, "Integrating the energy flux method for reverberation with physics-based seabed scattering models: Modeling and inversion," JASA, 134 (1), 55-66 (JUL 2013).

15. SUBJECT TERMS

ocean reverberation, modeling and inversion, seabed scattering, seabottom acoustic model, the energy flux method for reverberation, shallow water acoustics, low grazing angles scattering, shear waves

16. SECURITY CLASSIFICATION OF:			17. LIMITATION OF ABSTRACT	18. NUMBER OF PAGES	19a. NAME OF RESPONSIBLE PERSON
a. REPORT	b. ABSTRACT	c. THIS PAGE			Jixun Zhou
U	U	U	UU	49	19b. TELEPHONE NUMBER *(Include area code)* 404-894-6794

September 30, 2015

TO: Dr. Robert H. Headrick
Ocean Acoustics Program, CODE 322OA
OFFICE OF NAVAL RESEARCH
875 NORTH RANDOLPH ST, SUITE 1425
ARLINGTON, VA 22203-1995
Email: bob.headrick@navy.mil

FROM: Jixun Zhou
School of Mechanical Engineering
Georgia Institute of Technology
Atlanta, GA 30332-0405
Email: jixun.zhou@me.gatech.edu

SUBJECT: Final Technical Report on Award#N0014-11-1-0063
(Titled - SEABED SCATTERING FROM LOW FREQUENCY REVERBERATION MEASUREMENTS)

Attached 4 papers cover the work on the Award#N0014-11-1-0063, and are submitted in lieu of the final technical report:

1. J.X. Zhou and X.Z. Zhang, "Low frequency seabed scattering at low grazing angles," JOURNAL OF THE ACOUSTICAL SOCIETY OF AMERICA, 131 (4), 2611-2621 (APR 2012).
2. J.X. Zhou and X.Z. Zhang, "Shear wave velocity and attenuation in the upper layer of ocean bottoms from long-range acoustic field measurements," JOURNAL OF THE ACOUSTICAL SOCIETY OF AMERICA, 132 (6), 3698-3705, (DEC 2012).
3. J.X. Zhou, X.Z. Zhang, Z.H. Peng and Z.L. Li, "Ocean Reverberation: Modeling, Measurements and Inversions," in <*ADVANCES IN OCEAN ACOUSTICS*>, Editor(s): J.X. Zhou, Z.L. Li and J. Simmen, AIP CP # 1495, Pages: 150-165 (2012).
4. J.X. Zhou and X.Z. Zhang, "Integrating the energy flux method for reverberation with physics-based seabed scattering models: Modeling and inversion," JOURNAL OF THE ACOUSTICAL SOCIETY OF AMERICA, 134 (1), 55-66 (JUL 2013).

Low frequency seabed scattering at low grazing angles

Ji-Xun Zhou[a] and Xue-Zhen Zhang
School of Mechanical Engineering, Georgia Institute of Technology, Atlanta, Georgia 30332-0405

(Received 11 April 2011; revised 7 February 2012; accepted 16 February 2012)

Low-frequency (LF) seabed scattering at low grazing angles (LGA) is almost impossible to directly measure in shallow water (SW), except through inversion from reverberation. The energy flux method for SW reverberation is briefly introduced in this paper. The closed-form expressions of reverberation in an isovelocity waveguide, derived from this method, indicate that in the three-halves law range interval multimode/ray sea bottom scattering with different incident and scattering angles in forming the reverberation may equivalently be represented by the bottom backscattering at a single range-dependent angle. This equivalent relationship is used to derive the bottom backscattering strength (BBS) as a function of angle and frequency. The LF&LGA BBS is derived in a frequency band of 200–2500 Hz and in a grazing angle range of 1.1°–14.0° from reverberation measurements at three sites with sandy bottoms. This is based on three previous works: (1) The closed-form expressions of SW reverberation [Zhou, (Chinese) Acta Acustica **5**, 86–99 (1980)]; (2) the effective geo-acoustic model of sandy bottoms that follows the Biot model [Zhou *et al*., J. Acoust. Soc. Am. **125**, 2847–2866 (2009)] and (3) A quality database of wideband reverberation level normalized to source level [Zhou and Zhang, IEEE J. Oceanic Eng. **30**, 832–842 (2005)].
 [http://dx.doi.org/10.1121/1.3693645]

PACS number(s): 43.30.Gv, 43.30.Pc, 43.30.Dr, 43.30.Ma [NPC] Pages: 2611–2621

I. INTRODUCTION

Acoustic reverberation in shallow water (SW) waveguides has become a hot research topic in recent years. It involves a complex process of both two-way sound propagations and bottom scattering. Figure 1 shows a flow chart of seabed-dominated SW reverberation. The seabottom geoacoustic parameters and velocity profiles in the water column control two-way propagations that can now be dealt with by using existing theoretical formulae and numerical methods, as summarized in a monograph by Jensen *et al*.[1] Thus, as the main source of SW reverberation, seabottom scattering becomes a kernel problem in the development of reverberation models.

In 1999, Preston indicated[2] "Much progress has been made in our understanding of reverberation. However, there remain important unanswered questions and a real scarcity of high-quality basic research data sets." Figure 2 of Ref. 2 shows that currently available BBS data at LF&LGA vary as much as 30 dB at a given angle. This large variation might be caused by different sediment properties, but it might also be due to questionable reverberation data, due to the theoretical formula of reverberation, or the seabed geoacoustic models used in some scattering inversions.

The derivation of a reliable long-range LF reverberation model requires a reliable LF&LGA bottom scattering model that is proven by experimental data. The LF&LGA seabed scattering is almost impossible to directly measure in shallow water, and is generally derived from mid- and long-range reverberation. As Eller argued, "Unless the assumptions used in extracting the scattering coefficients from the received reverberation are very carefully chosen, the resulting coefficients will not represent valid environmental parameters, independent of how the data were obtained and analyzed."[3]

In the past 30 years, one of the major accomplishments in ocean acoustics has been our understanding of seabed scattering. This has been summarized in a monograph of the ONR Underwater Acoustics Series, entitled "*High-Frequency Seafloor Acoustics*."[4] As its introduction indicates, this monograph emphasizes "high frequencies, very roughly, frequencies from 10 kHz to 1 MHz." A natural question is raised from this book: Are those seabed scattering models, which are well developed for seabed boundary roughness and sediment inhomogeneity, suitable/applicable to low grazing angles and low frequencies of 100–3000 Hz? To answer this question, we also need the LF &LGA seabed scattering data that are currently in "a real scarcity."[2]

In addition to a reliable reverberation model, there are two other absolute requirements for the inversion of the LF&LGA scattering from reverberation: (1) carefully calibrated reverberation measurements in a broad band and (2) a ground truth about the seabed geo-acoustic model in the same sea area. Poorly calibrated reverberation data result in incorrect values of the seabed scattering. A previous paper showed that a decrease (increase) in bottom reflection loss can be compensated for by increasing (decreasing) the angular index of bottom scattering.[5] That is, there is an uncertainty caused by an internal coupling between a seabed geoacoustic model and a scattering model.

Taking the above-mentioned three essential conditions of reverberation inversions into account, this paper derives the LF&LGA seabed scattering strength vs angle and frequency in SW with sandy bottoms, based on three previous works: (1) The analytical (closed-form) expressions of SW reverberation;[6–8] (2) an effective geo-acoustic model of sandy bottoms that follows the Biot model as well as

[a]Also at: State Key Laboratory of Acoustics, Institute of Acoustics, Chinese Academy of Sciences, Beijing 100190, China. Author to whom correspondence should be addressed. Electronic mail: jixun.zhou@me.gatech.edu

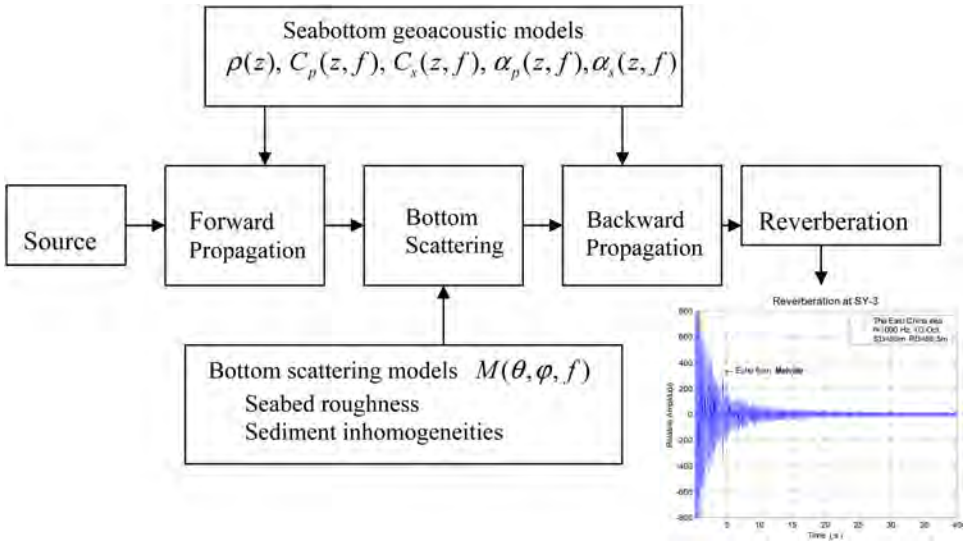

FIG. 1. (Color online) Flow chart of seabed-dominated reverberation in shallow water.

other physics based models;[9,10] and (3) a quality database of wideband reverberation level (RL) normalized to source level (SL).[11] This paper is organized as follows: Sec. II briefly introduces the angular spectrum (energy flux) method for SW reverberation and the closed-form expressions of reverberation in isovelocity shallow water. A theoretical model and a methodology which is used to derive the LF&LGA bottom backscattering strength are described in detail in Sec. III. Section IV describes the seabed geoacoustic model used in the derivation of BBS. The reverberation-derived LF&LGA BBSs as a function of frequency and angles for three sites with sandy bottoms are given in Sec. V. Finally, Sec. VI summarizes and discusses the results of this paper.

II. THE CLOSED-FORM EXPRESSIONS FOR OCEAN REVERBERATION INTENSITY IN SHALLOW WATER

The angular spectrum (energy flux) method for modeling SW reverberation, based on the WKB approximation of normal-mode theory, was first presented three decades ago in archived Chinese journals.[6,7,12,13] These included closed form expressions for reverberation in SW with a down refracting and isovelocity profile or with a varied-depth.[6–8,13–16] Due to its simplicity and intuitive nature, the energy flux method has further been developed and widely used for SW reverberation calculations,[17–30] mainly due to works by Harrison, Holland and Ainslie.[18,20,21,23–30] All the closed-form expressions in isovelocity shallow water, derived by Zhou,[6] Harrison,[18] Ainslie[27,30] and Holland,[24] are almost identical, having only minor differences in constant coefficients. In this paper, Zhou's closed-form expressions for reverberation in isovelocity water are used to extract the frequency and angular dependence of the BBS at LF&LGA from long-range reverberation data.

A. General expressions of the energy flux method for average SW sound intensity and reverberation

The earliest detailed derivation of the energy flux method for SW reverberation, derived from the WKB approximation to the normal-mode solution of the wave equation, was in Chinese.[6] Its English translation has been unavailable to all but a very few western colleagues. It is worthwhile to briefly introduce this method here.

A source level (SL) of 0 dB will be assumed in all subsequent expressions. The sound field intensity in shallow water, normalized to SL, can be expressed as a sum of normal modes:

$$I(r,z;z_0) = \frac{2\pi}{r}\sum\left\{\frac{|\Phi_n(z_0)|^2\,|\Phi_n(z)|^2}{k_n}e^{-2\beta_n r} + \sum\sum_{n\neq m}\frac{\Phi_n(z_0)\Phi_m^*(z_0)\Phi_n(z)\Phi_m^*(z)}{k_n^{1/2}k_m^{*1/2}} \times e^{-[(\beta_n+\beta_m)+i(k_n-k_m)]r}\right\}, \quad (1)$$

where Φ_n is the eigenfunction, k_n is the longitudinal wave number, β_n is the modal attenuation factor of the nth mode, z_0 is the source depth and z is the receiver depth. The first term of Eq. (1) is an incoherent summation of normal-modes. It describes the average intensity of the sound field. Because SW environments are complex and variable in both space and time, it is difficult to predict or measure the fine structure of a SW sound field associated with modal interference. Thus, for many practical applications such as sonar performance predictions, the second term of Eq. (1), which describes the interference fine structure, can be neglected.

According to the WKB approximation, the smoothed (slowly varying) energy depth distribution of the nth mode can approximately be expressed as

$$\overline{|\Phi_n(z)|^2} = \frac{2}{S_n\tan\theta_n(z)}. \quad (2)$$

Here, S_n is the cycle distance of the nth mode-ray given by

$$S_n = 2\int_{\xi_n}^{\eta_n}\frac{dz}{\tan\theta_n(z)} \quad (3)$$

and θ_n is the mode grazing angle. The eigenvalue k_n of the nth mode satisfies the relationship

$$2\int_{\xi_n}^{\eta_n}\sqrt{k^2(z)-k_n^2}dz+\varepsilon_{\xi_n}+\varepsilon_{\eta_n}=2n\pi, \tag{4}$$

where ξ_n and η_n are the upper and lower turning (or reflection) depth of the nth mode, ε_{ξ_n} and ε_{η_n} are the corresponding phase shifts, and $k(z)=\omega/c(z)$. Neglecting other possible losses except bottom reflection loss, the modal attenuation factor, β_n, can be expressed approximately in terms of the bottom reflection coefficient $V(\theta)$:

$$\beta_n=-\frac{\ln|\mathrm{V}(\theta_\mathrm{n})|}{S_n(\theta_n)+\delta_n} \tag{5}$$

where δ_n is a beam displacement on the bottom reflection. If the water depth H satisfies $kH\gg 1$, $\delta_n\ll S_n$; i.e., when the frequency is relatively high, δ_n is negligible.

Each normal-mode can be decomposed into a pair of up- and down-going local quasi-plane waves. We shall call the local plane wave an equivalent "mode-ray." The grazing angle of the mode-ray and the eigenvalue of the nth mode are related by

$$k_n=k(z)\cos\theta_n(z). \tag{6}$$

Ignoring the minor effects of ε_{ξ_n} and ε_{η_n}, differentiating k_n with respect to n in Eq. (4), and using Eqs. (3), (6) and the identity,

$$\frac{d}{dn}\int_{\xi_n}^{\eta_n}f(z,n)dz=\int_{\xi_n}^{\eta_n}f'(z,n)dz+f(\eta_n,n)\frac{d\eta_n}{dn}-f(\xi_n,n)\frac{d\xi_n}{dn} \tag{7}$$

we obtain the known relationship:[1]

$$\frac{dk_n}{dn}=-\frac{2\pi}{S_n}. \tag{8}$$

Using (6) and (8), we have

$$dn=\frac{S_nk(z_0)\sin\theta_n(z_0)d\theta_n(z_0)}{2\pi}. \tag{9}$$

The incoherent summation over modes can be changed to an integration over the mode-ray angle θ. Proceeding from (1), (2), (5), (8), and (9), and adding a term of water absorption, we can derive a general expression for the average field intensity in shallow water given by

$$I(r,z;z_0)=\frac{2}{r}e^{-\alpha r}\int\frac{2e^{2\ln|V(\theta)|r/s_n(\theta)}}{S_n\tan\theta_n(z)}d\theta_n(z_0)=\frac{2e^{-\alpha r}}{r}\int I_{aps}(\theta,r,z;z_0)d\theta_n(z_0), \tag{10}$$

where

$$I_{aps}(\theta,r,z;z_0)=\frac{2e^{-2\beta_n r}}{S_n\tan\theta_n(z)}=\frac{2e^{2\ln|V(\theta)|r/S_n(\theta)}}{S_n\tan\theta_n(z)}. \tag{11}$$

Using different methods, both Brekhovskikh[31,32] and Smith[33] obtained a similar expression. In (10) and (11), α is the water column absorption coefficient; $\theta(z_0)$ is the grazing angle of the mode-rays at the source depth and $\theta(z)$ is the grazing angle at the receiver depth. The quantity defined by Eq. (11), I_{aps} is referred to as the "angular power spectrum" of sound propagation. Smith also called it the "energy density in direction of arrival."[33] The average sound intensity in shallow water depends on water absorption and two other parameters: the bottom reflection coefficient $V(\theta)$ and the cycle distance S_n of the mode-ray. According to Guthrie and Tindle, the "mode rays" (eigenrays) associated with normal modes are spatially fuzzy. The "mode-rays" obey Snell's law: $k_n=k(z)\cos\theta_n(z)=k(z_0)\cos\theta_n(z_0)$. The interference of many adjacent modes forms a physical ray with limited width that converges to a geometric ray at high frequency.[34]

Equation (10) is a simple and intuitive expression for calculating averaged SW field characteristics such as sound propagation, reverberation, noise and their spatial coherence. It is only an angular weighting process. For calculating the average reverberation intensity in shallow water, the two-way propagation angular spectra and the classic seabed scattering function are well connected in the angular domain.

For a frequency band this paper is interested in, and at low order modes-dominated long-range, the water absorption loss may be approximated as the horizontal range times the absorption coefficient α. Using the single scatter approximation, the average reverberation intensity R can be expressed in terms of I_{aps} by[6]

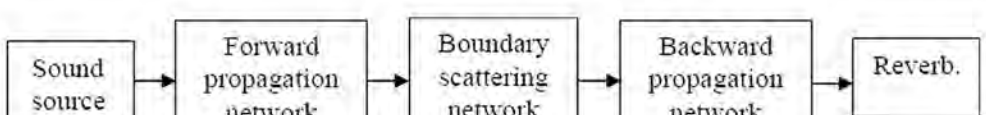

$$R(r,z;z_0)=\iint\overbrace{\frac{e^{-\alpha r}}{r}I_{aps}(\theta,r,H;z_0)}\ \overbrace{A\times M_b(\theta,\phi)}\ \overbrace{\frac{e^{-\alpha r}}{r}I_{aps}(\phi,r,z;H)}\,d\theta d\phi$$
$$=\iint\frac{e^{-\alpha r}}{r}\frac{2e^{2\ln|V(\theta)|r/s_n(\theta)}}{S_n\times\tan\theta_n(H)}\times A\times M_b[\theta_n(H),\varphi_m(H)]\times\frac{e^{-\alpha r}}{r}\frac{2e^{2\ln|V(\varphi)|r/s_m(\varphi)}}{S_m\times\tan\varphi_m(z)}d\theta_n(z_0)d\varphi_m(H) \tag{12}$$

where $I_{aps}(\theta, r, H; z_0)$ is the incident angular power spectrum at a distance of r, incident upon a seabed area A; $I_{aps}(\varphi, r, z; H)$ is the angular power spectrum returned to a receiver at a depth of z from the same bottom scattering area; H is the water depth; $M_b[\theta_n(H), \varphi_m(H)]$ is the bottom scattering function; $\theta_n(H)$ is the incident grazing angle of mode n at the bottom; and $\varphi_m(H)$ is the scattering angle of mode m.

B. The average sound intensity in the Pekeris waveguide (isovelocity water)

The plane-wave reflection coefficient from the half-space seabed at grazing angle θ can be approximated by[35–38]

$$-\ln|V(\theta)| = \begin{cases} Q\theta & 0 \le \theta \le \theta_C \\ -\ln|V_0| = \text{const} & \theta_C \le \theta \le \pi/2, \end{cases} \quad (13)$$

where θ_C is the critical angle, Q is a seabed reflection loss factor; the seabed reflection loss will be $-20\log_{10}|V(\theta)| = 8.686Q\theta$ (dB/rad). V_0 is the bottom reflection coefficient at large grazing angles close to the normal incidence. In isovelocity shallow-water, the cycle distance of the nth mode-ray, $S_n = 2H/\tan(\theta_n)$. From (10) and (13), the average sound intensity as a function of range in the isovelocity shallow-water can be divided into four regions, with different "decay laws" expressed (omitting sound absorption in the water column) by[6,35–37]

(a) For $r_0 < r < r_1$, spherical spreading region $\sim r^{-2}$

$$I_A(r) \approx \frac{4}{-\ln|V_0|}\frac{1}{r^2}. \quad (14)$$

(b) For $r_1 < r < r_2$, cylindrical spreading region $\sim r^{-1}$,

$$I_B(r) = \frac{2\theta_c}{H}\frac{1}{r}. \quad (15)$$

(c) For $r_2 < r < r_3$, three-halves law region $\sim r^{-3/2}$

$$I_C(r) = \sqrt{\frac{\pi}{QH}}\frac{1}{r^{3/2}}. \quad (16)$$

(d) For $r > r_3$, single mode (1st mode) decay region

$$I_D(r) = \frac{2\pi}{kH^2}\frac{1}{r}\exp\left[-\frac{Q\pi^2 r}{k^2H^3}\right]. \quad (17)$$

Three transition distances in the Pekeris model are defined as

$$r_1 = \frac{H}{(-\ln|V_b|)\theta_c}, \quad r_2 = \frac{H}{Q\theta_c^2}, \quad r_3 = \frac{k^2H^3}{Q\pi^2}, \quad (18)$$

where k is the wave number. In general, active sonar predictions are most interested in the mode stripping region C that was defined first by Brekhovskikh as the "three-halves law" region.[36] It is roughly hundreds of meters to several tens of thousands of meters from a sound source.[37]

C. The closed-form expressions of reverberation in the Pekeris model (Ref. 6)

The descriptions of seabed scattering by Urick[39] and Mackenzie-Lambert[40] were extended to more general angular dependence as follows.[6–8] When a plane wave with an intensity of $I_i(\theta)$ is incident upon unit bottom element dA at a grazing angle θ, the backward scattering intensity at one meter from an elementary area in the φ direction can be written as

$$dI_s = \mu I_i(\theta)\sin^m\theta\sin^k\varphi dA. \quad (19)$$

Here μ is the generalized Lambert coefficient, m and k are the angular indexes for incident and scattering waves, respectively.

The insonified area A is defined as $A \approx \pi r c\tau$. Making the small angle approximation, neglecting angles greater than the critical angle, and with the aid of Eqs. (13), (19) and the definition of A, Eq. (12) may be solved to produce the following closed-form solutions, as described in Eqs. (4.1) to (4.3) of Ref. 6.

(1) For the Lambert scattering model ($m = k = 1$):

$$R_{11}(r) = \frac{\mu\pi c\tau}{4Q^2r^3}e^{-2\alpha r}(1 - e^{-(Qr/H)\theta_C^2})^2. \quad (20)$$

(2) For the Omnidirectional model ($m = 1$, $k = 0$):

$$R_{10}(r) = \frac{\mu\pi^{3/2}c\tau}{4H^{1/2}Q^{3/2}r^{5/2}} \times e^{-2\alpha r}(1 - e^{-(Qr/H)\theta_C^2})\phi\left(\sqrt{\frac{Qr}{H}}\theta_C\right). \quad (21)$$

(3) For the Angle-independent scattering model ($m = k = 0$):

$$R_{00}(r) = \frac{\mu\pi^2 c\tau}{4HQr^2}e^{-2\alpha r}\phi^2\left(\sqrt{\frac{Qr}{H}}\theta_C\right), \quad (22)$$

where τ is the pulse duration of the transmitting signal, and c is the sound speed in the water column. The subscript indices of R_{mk}, m and k, are the angular index of incidence and the scattering angle, respectively. $\phi(x)$ is the probability integral

$$\phi(x) = \frac{2}{\sqrt{\pi}}\int_0^x \exp(-t^2)dt.$$

As Sec. IV of Ref. 6 indicates, "although the above-mentioned formulae are derived for $n = (m + k) = 0$, 1 and 2, our numerical calculations show that the results are

approximately applicable to arbitrary values of the bottom scattering index n, i.e., a combination of any k and m, integer or decimal. It only requires a minor modification for the constant coefficient." Thus, the closed-form expressions of long-range reverberation in isovelocity shallow water were generalized to Eq. (4.15) and Eq. (4.17) of Ref. 6 as follows:

(1) When $r_2 > r > r_1$

$$R(r) = \frac{\mu\pi c\tau\theta_c^{(2+n)}}{2^n H^2} \times e^{-2\alpha_v r}\frac{1}{r}. \tag{23}$$

(2) When $r_3 > r > r_2$

$$R(r) = \frac{\mu\pi^{(2-n/2)}c\tau}{4Q^{(1+n/2)}H^{(1-n/2)}} e^{-2\alpha_v r} \times \frac{1}{r^{(2+n/2)}}. \tag{24}$$

Here the bottom scattering index $n = m + k$, i.e., it is a combination of any k and m, integer or decimal. Harrison,[18] Ainslie[27] and Holland[24] have derived expressions for an isovelocity SW that are similar to Eq. (23) and Eq. (24) with a minor difference in the constant coefficients.

III. THEORETICAL MODELS FOR THE *BBS*(θ) DERIVATION FROM REVERBERATION DATA

In isovelocity shallow water, the cycle distance of the nth mode-ray can be expressed by $S_n = 2H/\tan(\theta_n)$. Due to mode stripping, lower modes with small grazing angles dominate the sound field in the three-halves law region where we have $\tan\theta_n \approx \theta_n$. Contributions from higher-order modes with grazing angles larger than the critical angle can be neglected. Using Eq. (13) and Eq. (10), the sound intensity in the three-halves law region can be expressed by:

$$\begin{aligned} I_c(r) &\approx \frac{2}{Hr}e^{-\alpha_v r}\int_0^{\theta_c} e^{-(Qr/H)\theta^2}d\theta \\ &= \sqrt{\frac{\pi}{QH}}\frac{e^{-\alpha_v r}}{r^{3/2}}\phi\left(\sqrt{\frac{Q\,r}{H}}\theta_c\right) = \frac{e^{-\alpha_v r}}{Hr}\times 2\theta_{eff}(r) \\ &\quad \text{for} \quad r_3 > r > r_1. \end{aligned} \tag{25}$$

Here $\theta_{eff}(r)$ is the effective angle of sound propagation defined by[41]

$$\theta_{eff}(r) = \int_0^{\theta_c} e^{-(Qr/H)\theta^2}d\theta \approx \frac{1}{2}\sqrt{\frac{H\pi}{Qr}} \quad \text{for } r_3 > r > r_2, \tag{26}$$

where the transition distances, r_1, r_2 and r_3, are defined in Eq. (18). The angular spectrum of sound propagation in the isovelocity SW is a Gaussian function. It can be replaced by a sharp cut at θ_{eff}. The sound waves propagate within an effective grazing angle range of $\pm\theta_{eff}(r)$; $\theta_{eff}(r)$ depends on the water depth H, propagation distance r and seabed reflection loss factor Q.

Using Eq. (16) and Eq. (26), Eq. (24) may be re-written in the desired form:

$$\begin{aligned} R(r) &= \frac{\mu\pi^{(2-n/2)}c\tau}{4Q^{(1+n/2)}H^{(1-n/2)}}e^{-2\alpha_v r} \times \frac{1}{r^{(2+n/2)}} \\ &= \left(\frac{1}{2}\sqrt{\frac{\pi}{QHr^{3/2}}}\right)e^{-\alpha r}(\pi rc\tau)\left[\mu\left(\frac{21}{\pi 2}\sqrt{\frac{\pi H}{Qr}}\right)^n\right] \\ &\quad \times \left(\frac{1}{2}\sqrt{\frac{\pi}{QHr^{3/2}}}\right)e^{-\alpha r} \\ &= \left[\frac{1}{2}I_C(r,H;z_0)\right]A(r)M_b(\theta_{eg},\theta_{eg})\left[\frac{1}{2}I_C(r,z_0;H)\right]e^{-2\alpha_v r} \\ &= \frac{c\tau\pi^2}{4QHr^2}\left[\mu\theta\left(\theta_{eg}(r)\right)^n\right]e^{-2\alpha_v r}, \end{aligned} \tag{27}$$

where $A(r) = 2\pi r \times c\tau/2$ is the bottom scattering area at a distance of r. $\theta_{eg}(r) = (2/\pi)\theta_{eff}(r) = \sqrt{H/(\pi HQ)}$ $= 0.637\theta_{eff}(r)$. Taking a logarithm for both sides of (27), we have the reverberation level (in dB) as

$$\begin{aligned} RL(r) &= 10\log_{10}A(r) + BBS(\theta_{eg}) - 2TL(r) \\ &\quad - att_w 2r - 6.0, \end{aligned} \tag{28}$$

or

$$\begin{aligned} RL(r) &= 10\log_{10}(c\tau\pi^2/4QHr^2) + BBS(\theta_{eg}) \\ &\quad - att_w \times 2r, \end{aligned} \tag{29}$$

where $BBS(\theta_{eg}) = 10\log_{10}[\mu(\theta_{eg})^n] = 10\log_{10}\left[\mu\left(\frac{2}{\pi}\theta_{eff}(r)\right)^n\right]$ is the bottom backscattering strength at $\theta_{eg}(r)$ that equals to $0.637\theta_{eff}(r)$. att_w is the sound absorption in water (dB/m). Equation (28) is very similar to the boundary reverberation formula suitable to short-range or deep ocean modeling from the ray method (without considering waveguide multipath effect).[39] Equations (27)–(29) show an interesting result: in the mode stripping (three-halves law) region, although the SW reverberation is produced from the bottom scattering by all modes or rays with different incident and scattering angles, the complex multi-incident/scattering angle interactions with a bottom are equivalently replaced by the bottom backscattering (BBS) at a single angle of θ_{eg} (=$0.637\theta_{eff}$), i.e., the reverberation may be expressed as a simple product of the transmission loss to and from the insonified area and the seabed backscattering at a single range-dependent angle, $\theta_{eg}(r)$. A factor of $1/2$ in Eq. (27) for two-way propagation $I_C(r)$, or -6.0 dB in Eq. (28), accounts for the fact that only the down-going waves, i.e., half the energy of normal modes in sound propagation, are considered as an incident wave for bottom scattering. This factor is required by the definitions of the commonly used bottom scattering models. Similarly, only the up-going waves of the bottom-scattered normal-modes are considered in reverberation/scattering calculations.

IV. GEO-ACOUSTIC MODEL FOR SANDY SEA BOTTOMS

LF sound speed and attenuation in sandy seabottoms have recently been analyzed and summarized from long-range field measurements in shallow water.[9] Field

measurements conducted at 20 locations in different coastal zones around the world were analyzed. The sound attenuations in sandy or sand-silt mixture bottoms, inverted from different acoustic field characteristics, exhibit similar magnitude and nonlinear frequency dependence below 2000 Hz at all of these sites (see Fig. 2). The LF field-derived effective seabed geoacoustic model, for both sound speed and attenuation in the sandy bottoms, can be well described by the Biot model as shown in Figs. 2(a) and 2(b) by solid curves.[9] We will use this effective bottom geoacoustic model for inverting the LF&LGA BBS from reverberation data, because half of those LF measurements in Ref. 9 were made at Chinese sea sites that are the same as or close to the sites for the reverberation measurements reported in this paper.

As Ref. 9 indicates, in the basic Biot theory, three parameters largely control the fluid motion that causes the nonlinear dispersion that is important in the coarser granular sediments. These are the permeability κ_s, the porosity β, and the tortuosity α_0 which defines the necessary amount of "added mass" in the Biot-Stoll model. These three parameters define the pore-size parameter. Data/model comparisons (trials) tell us that the LF sound speed ratio is very sensitive to the porosity of sediment and is less sensitive to the permeability and tortuosity. The LF sound attenuation is very sensitive to the permeability of the sediment and is less sensitive to the porosity and tortuosity. Thus, the porosity of 0.42 and the permeability of 1.0×10^{-11} were easily determined as the values that provide the best match between the Biot model and the LF inverted attenuations and speed ratios shown in Fig. 2, as well as the average LF sound attenuations shown in Fig. 11 of Ref. 9. The other eleven Biot parameters are same as those from the SAX99 measurement. The standard deviation of the permeability, inverted from the LF field measurements is less than 0.05×10^{-11}; The porosity deviation is less than 0.015.

The bottom reflection factor Q in Eqs. (13), (27), and (29) can be expressed by[9,11,36–38]

$$Q(f) = 0.0366 \frac{(c_w^2/c_b)(\rho_b/\rho_w)}{\left[1-(c_w/c_b)^2\right]^{3/2}} \times \frac{\alpha_b}{f}, \tag{30}$$

where α_b is the sound attenuation (dB/m) in the bottom and f is the frequency in kHz. c_w and c_b are the sound speed (km/s) in the water and the bottom, respectively. ρ_w and ρ_b are the density (g/cm^3) in the water and the bottom, respectively.

Inputting the LF-field inverted average sound attenuation and speed, shown in Figs. 2(a) and 2(b) by solid lines, into Eq. (30), we have the average bottom loss parameter Q vs frequency shown in Fig. 3 by solid line. The LF fit parameters for the Biot model are listed in Table X of Ref. 9. In contrast to the Hamilton model,[42,43] which should result in a frequency-independent Q, Fig. 3 shows an interesting frequency dependence of the bottom reflection loss at LGA: it increases with increasing frequency, reaches a maximum around the JR (Jackson and Richardson) characteristic frequency of 2.88 kHz [from Eq. (10.52) of Ref. 4; it is different from the Biot characteristic frequency], then decreases with frequency. This frequency dependence of the LGA bottom reflection loss affects the two-way sound propagation in reverberation as well as the frequency dependence of the reverberation-derived bottom scattering. Possible variations of the Q values, caused by standard deviations of the LF

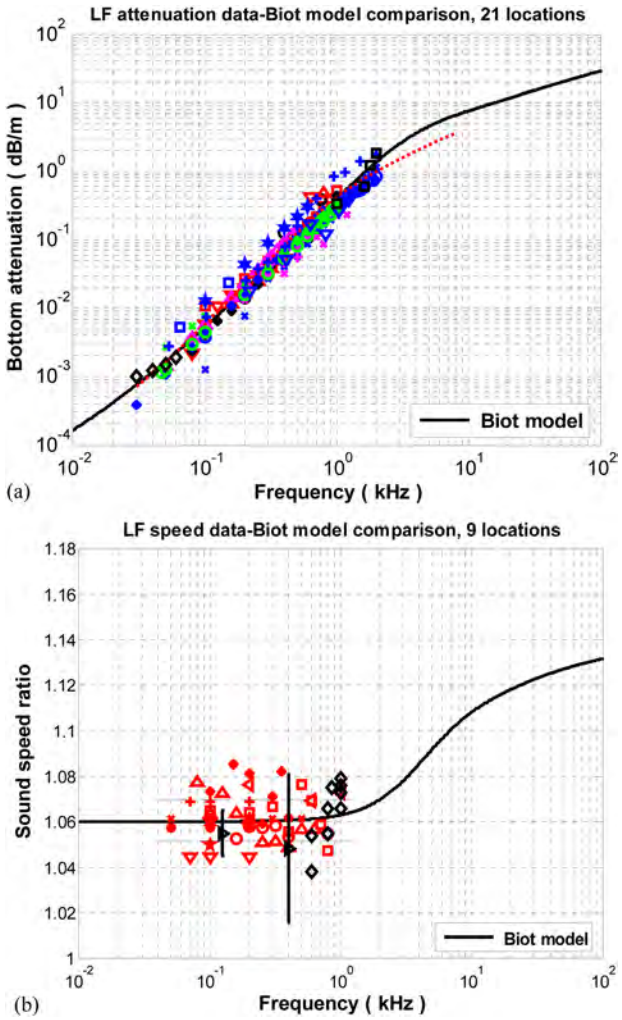

FIG. 2. (Color online) Comparison of the LF field-inverted seabed acoustic parameters with the Biot model (Ref. 9): (a) sound attenuation, (b) sound speed.

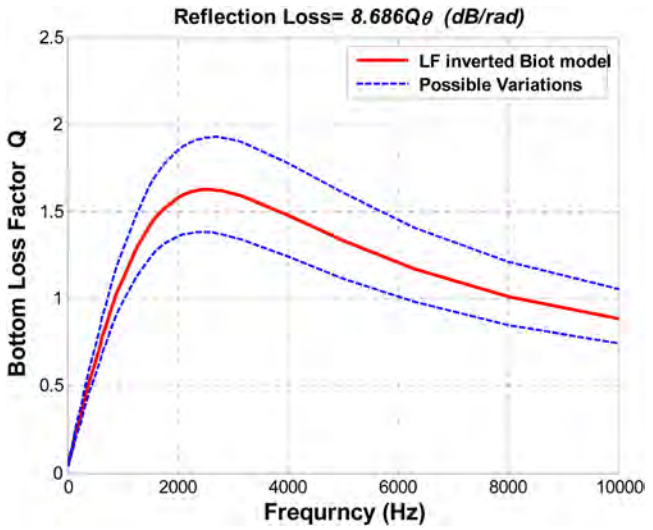

FIG. 3. (Color online) The seabed reflection loss factor Q as a function of frequency for sandy bottoms, derived from the LF field measurements.

field-inverted permeability and porosity, are plotted in Fig. 3 by dashed lines.

V. REVERBERATION MEASUREMENTS AND REVERBERATION-DERIVED *BBS*(θ)

A. Reverberation measurements

A quality database of reverberation is absolutely essential in derivation of bottom scattering strength from reverberation measurements. The "quality" here means that the reverberation data are in a broadband, obtained from carefully calibrated measurements. The data have been normalized to the source level (SL), and have high reverberation-to-noise ratio. However, to get wideband SL-normalized RL is a delicate task that can be subject to error. A prior paper introduced a simple measurement method that could avoid the signal overflow and saturation caused by a powerful explosive source.[11] The SL-normalized RL data in the three-halves law region from this method are used in this paper to derive the BBS (after the RL data are corrected by the Thorp formula for the sound absorption in the ocean[44]).

Reverberation data were collected using 1000-g explosive charges from 4 sites: two from the Yellow Sea (YS); two from the East China Sea (ECS). During the measurements, the sea surfaces were relatively calm. The sea bottoms at the three sites were very flat;[45] the depth deviation was less ± 1 m. The fourth site was nominally flat.[11,45] The average sound velocity profiles (SVP) for the 4 sites, measured at the receiving array sites, are plotted in Fig. 4.

The SVPs at two sites (YS site I and ECS site I), shown in Fig. 4 by solid lines, were isovelocity. The SVP at ECS site II (ASIAEX01), shown by a dashed line, is quasi-isovelocity. At this site, when explosive charges were detonated at a depth of 50 m, RLs received by different hydrophones located at different depths did not show any depth dependence, i.e., the case was close to a Pekeris model. The SVP at YS site II (YS'96), shown by a dotted line, has a strong thermocline. When both sound source and receiver are below the thermocline, the YS'96 site can approximately be treated as a Pekeris model, because numerical simulations show that the maximum RL difference between a real SVP and the Pekeris model is less than 2 dB for frequencies larger than 200 Hz.

B. Using the Lambert law and the Biot geo-acoustic model to derive *BBS*

The semi-empirical Lambert law has widely been used for comparisons with bottom scattering measurements and reverberation modeling, although it has no physical basis. Just for the sake of comparison with the commonly published Lambert coefficients,[46] this section will use the Lambert law ($n = k + m = 2$), reverberation data and the Biot model to derive the Lambert's scattering coefficient, $10 \log_{10} \mu_{LM}$, with respect to frequency.

Figures 5(a) and 5(b) show the initial reference reverberation level (IRRL) at 2 and 4 second after an explosive source is detonated, respectively.[11] The IRRL data were obtained from 4 sites. Equation (24) shows that in the three-halves law region, if the bottom scattering obeys the Lambert law ($n = 2$), the reverberation intensity is independent of water depth, H. Using the IRRL data shown in Figs.

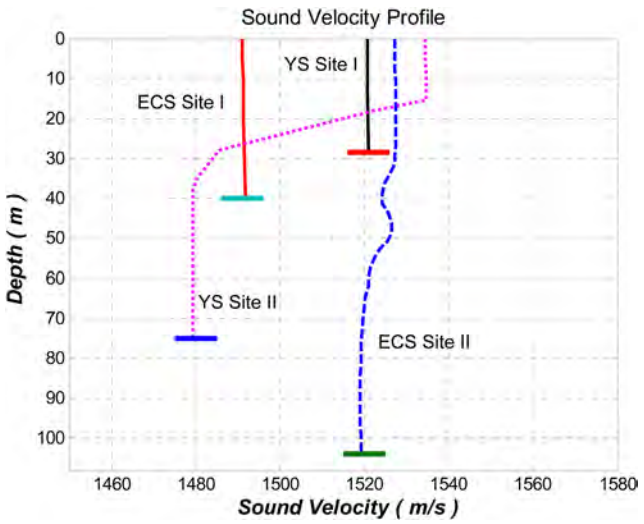

FIG. 4. (Color online) Sound velocity profiles at four sites for reverberation measurements.

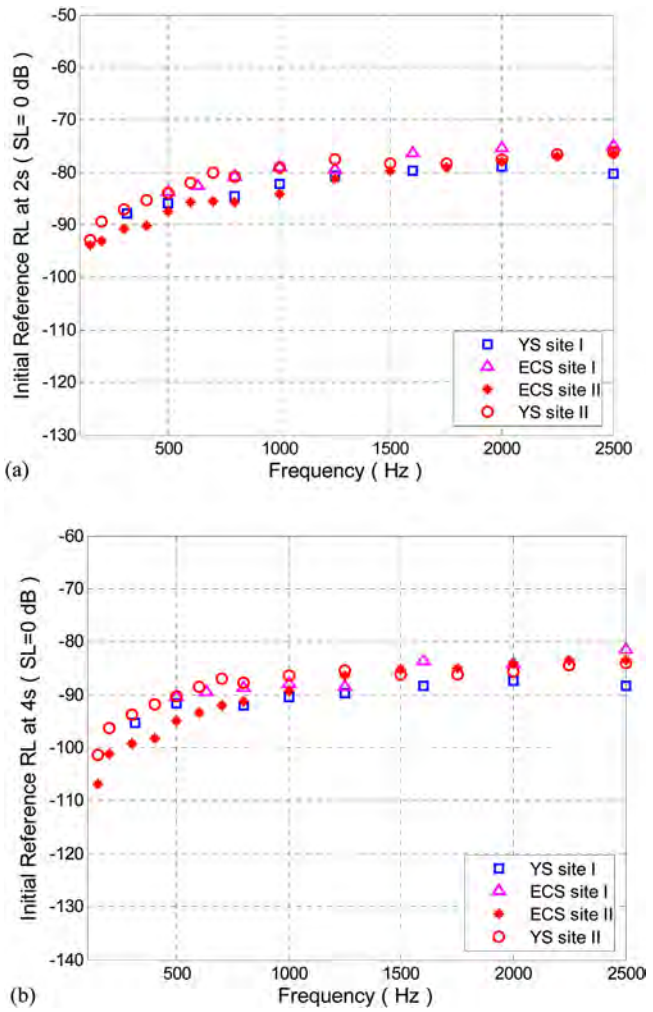

FIG. 5. (Color online) Reverberation level vs frequency from 4 sites: (a) at 2 s; (b) at 4 s.

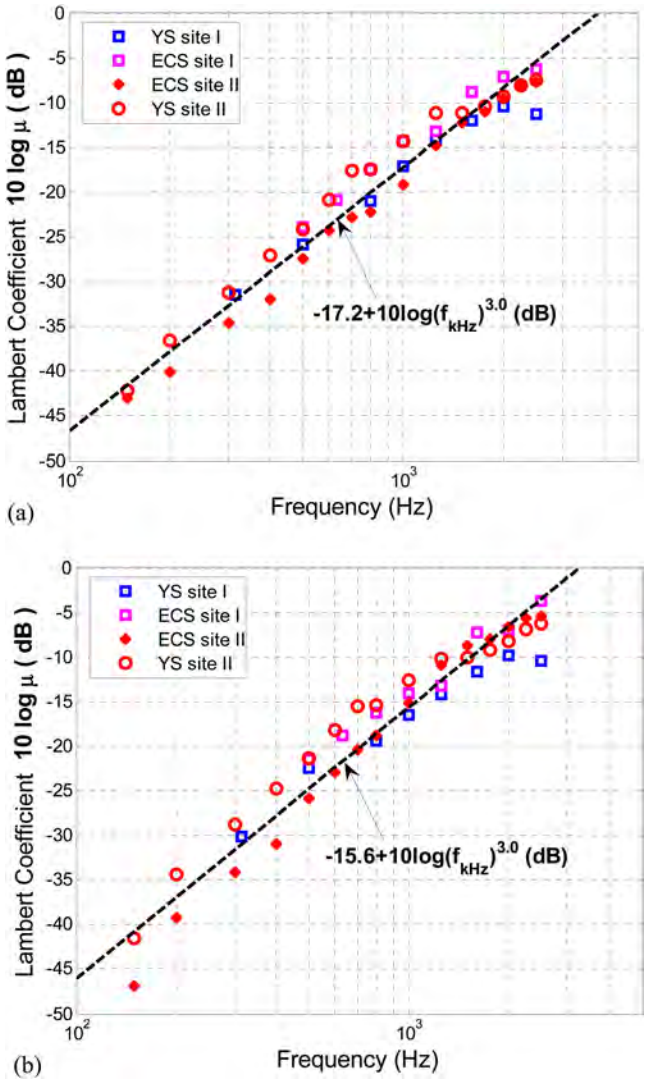

FIG. 6. (Color online) The Lambert's scattering coefficient derived from the Biot model and RLs at (a) 2 s, (b) 4 s.

5(a) and 5(b), the Q values in Fig. 3 and the closed-form expression of Eq. (24), we get the Lambert scattering coefficients shown in Figs. 6(a) and 6(b). The results show that, if the geoacoustic model of sandy bottoms follows the Biot model, the LF Lambert scattering coefficient exhibits strong frequency dependence. Figures 6(a) and 6(b) show that below the JR characteristic frequency, it exhibits frequency-cubed dependence ($\propto f^3$) in the 150–2500 Hz range. Averaged Lambert scattering strength from Figs. 6(a) and 6(b) can approximately be expressed by

$$10\log_{10}\mu_{LM} \approx -16.4 + 10\log_{10}(f/1000)^{3.0}(\mathrm{dB}) \quad \text{for } 150-2500\,\mathrm{Hz}. \tag{31}$$

C. Using the closed form expression for RL and the effective Biot model to derive *BBS*(θ) with arbitrary angular dependence

If both wideband TL and RL are well measured, or if both RL data and the seabed geoacoustic model are available, then Eqs. (28) and (29) can be used to derive an angular dependence of the LF $BBS(\theta)$. In this section, the wideband RL data, obtained from three sites with sandy bottoms, and the average Q values shown in Fig. 3, are used in Eq. (29) to derive the *BBS* vs angle and frequency. The RL data from the YS site II are not used, because the RL data at this site exhibit an uncommon/unknown water volume scattering at long-range (around 20 s).

Equation (18) shows that the three-halves law region is within two transition ranges, r_2 and r_3 . That is, the RL data used to derive $BBS(\theta)$ in this section should satisfy two conditions: (1) A high reverberation/noise ratio (>6 dB); (2) Reverberation time t between $2r_2/c$ and $2r_3/c$ (c is the sound speed in the water column). Based on Eqs. (26) and (29), r_2, r_3, H (water depth) and Q (the bottom loss factor) define a possible angular range of the reverberation-derived $BBS(\theta)$ for a given experimental site.

(1) For the YS site I, where the water depth is 28.5 ± 1.0 m, the RL-derived $BBS(\theta)$ as a function of grazing angle for

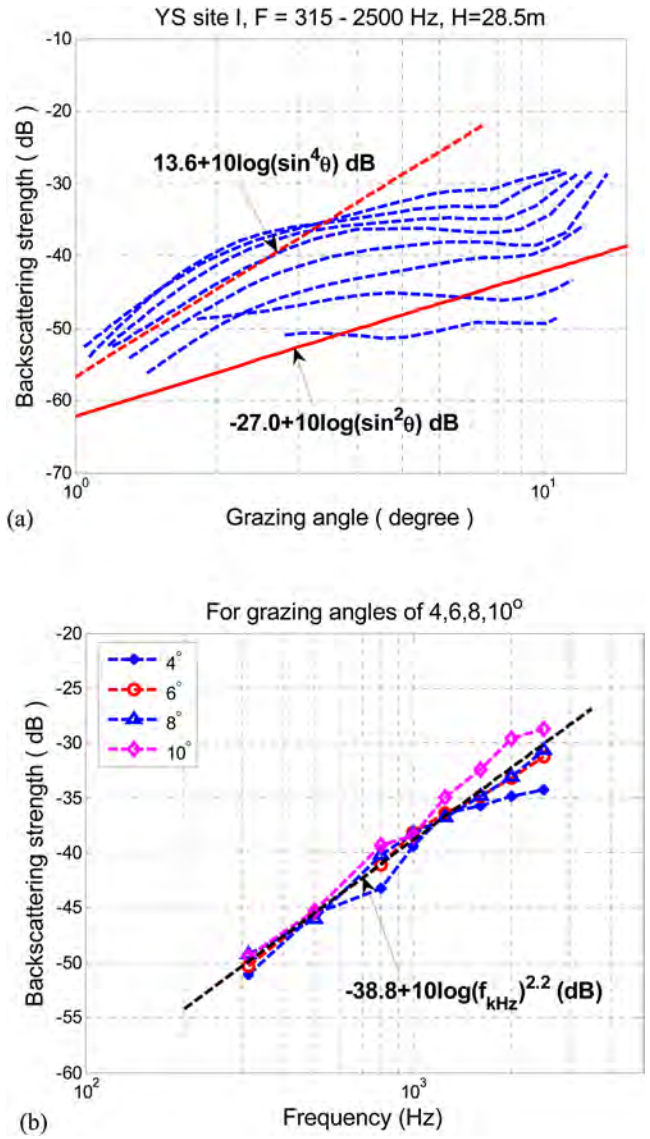

FIG. 7. (Color online) Angular and frequency dependence of the reverberation-derived BBS from the YS Site I. (a). BBS vs angle for eight frequencies, (b) BBS vs frequency at 4°, 6°, 8°, and 10°.

different frequencies is plotted in Fig. 7(a) by dashed lines. Figure 7(a) covers eight center frequencies with 1/3 octave bands (from the bottom line in the figure): 315, 500, 800, 1000, 1250, 1600, 2000, and 2500 Hz. For highlighting the BBS characteristics at LGA, the horizontal axis of Fig. 7(a) is in a logarithmic scale. Data fits show that the BBS at very low grazing angle (1°–4°) in the 800–2500 H range is proportional to $k_s \sin^4\theta$, and $k_s \approx 7-70$. A straight dashed line of $13.6 + 10\log(\sin^4\theta)$ *dB* is shown in Fig. 7(a); it corresponds to $k_s = 23$. For comparison, the semi-empirical Lambert law, $-27 + 10\log(\sin^2\theta)$, is plotted by a straight solid line.

The values of $BBS(\theta)$ at $4°, 6°, 8°$ and $10°$ for different frequencies at the YS Site I are shown in Fig. 7(b). Between 315 Hz and 2500 Hz, this can be approximately expressed by

$$BBS(\theta) \approx -38.8 + 10\log_{10}(f/1000)^{2.2}\,(\mathrm{dB}). \quad (32)$$

(2) For the ECS site I, where the water depth is 40.0 ± 1.0m, the RL-derived $BBS(\theta)$ as a grazing angle for different frequencies is plotted in Fig. 8(a) by dashed lines. Figure 8(a) covers ten center frequencies with 1/3 octave bands (from the bottom line in the figure): 315, 400, 500, 630, 800, 1000, 1250, 1600, 2000, and 2500 Hz. The BBS at 2000 Hz for very low grazing angle (1°–4°) is about $100\sin^4\theta$ shown by a straight dashed line. All of the $BBS(\theta)$ at 4°, 6°, 8° and 10° for different frequencies from the ECS site I are shown in Fig. 8(b). Between 315 Hz and 2500 Hz, it can be approximately expressed by

$$BBS(\theta) \approx -34.5 + 10\log_{10}(f/1000)^{2.0}\,(\mathrm{dB}). \quad (33)$$

(3) For the ECS site II (ASIAEX01), where the seabed is nominally flat,[11,45] with an average water depth of 104 m over the extent of the reverberation measurements, the RL-derived $BBS(\theta)$ as a grazing angle for different

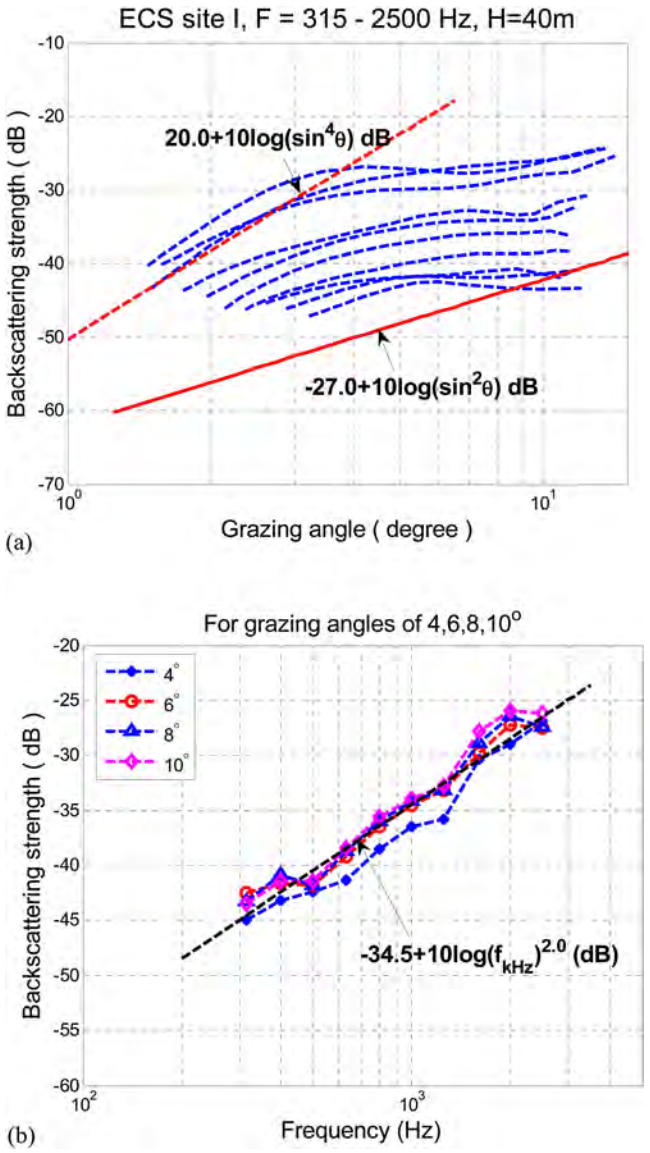

FIG. 8. (Color online) Angular and frequency dependence of the reverberation-derived BBS from the ECS Site I. (a). BBS vs angle for ten frequencies, (b) BBS vs frequency at 4°, 6°, 8°, and 10°.

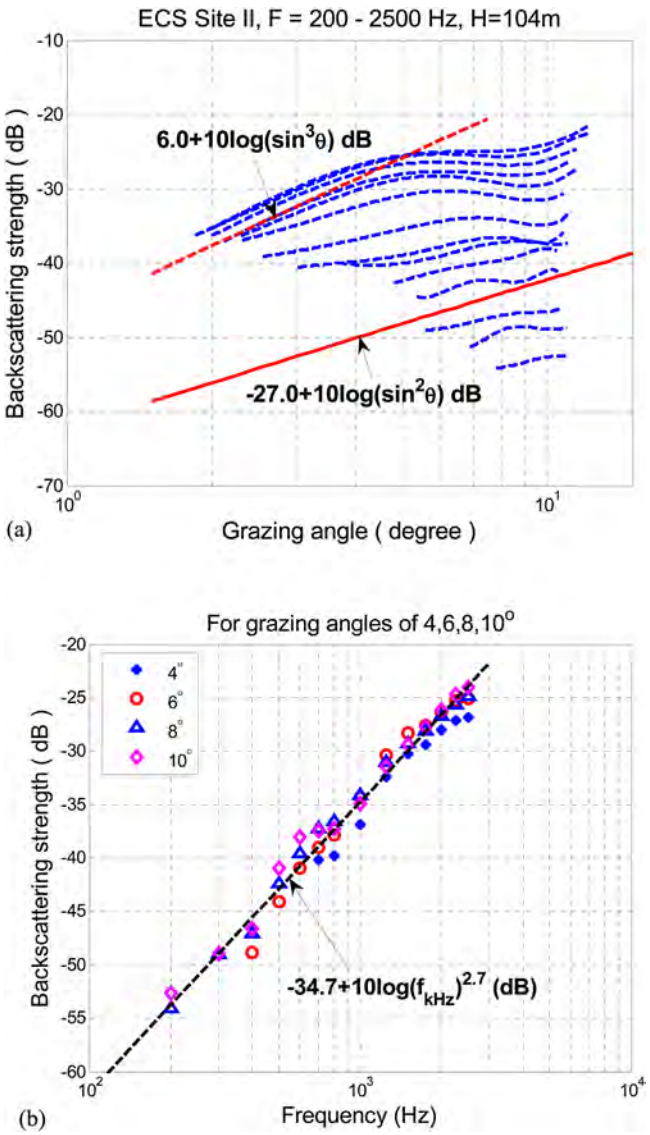

FIG. 9. (Color online) Angular and frequency dependence of the reverberation-derived BBS from the ASIAEX01 Site I. (a). BBS vs angle for fourteen frequencies, (b) BBS vs frequency at 4°, 6°, 8°, and 10°.

frequencies is plotted in Fig. 9(a) by dashed lines. Figure 9(a) covers fourteen center frequencies with 1/3 octave bands (from the bottom line in the figure): 200, 300, 400, 500, 600, 700, 800, 1000, 1250, 1500, 1750, 2000, 2250, and 2500 Hz. The scattering coefficient at 2000 Hz for low grazing angle (1°–4°) is about $4\sin^3\theta$ as shown by a straight dashed line. All $BBS(\theta)$ at $4^\circ, 6^\circ, 8^\circ$ and 10° for different frequency from the ECS site II are shown in Fig. 9(b). Between 200 Hz and 2500 Hz, it can approximately expressed by

$$BBS(\theta) \approx -34.7 + 10\log_{10}(f/1000)^{2.7}(\text{dB}). \quad (34)$$

VI. SUMMATION AND DISCUSSION

The angular spectrum (energy flux) method for calculating SW reverberation has briefly been introduced in this paper. It is based on the WKB approximation to the normal-mode solution for wave equations (ray-mode analogies). In this method, two-way sound propagation and bottom scattering are treated as weighting functions in the angular domain. As an alternative method to SW reverberation modeling, it is simple and intuitive.

The closed-form expressions for SW reverberation in the isovelocity waveguide, derived from the energy flux method, show that the complex seabed scattering by all modes/rays with different incident and scattering angles can equivalently be represented by seabed back-scattering at a single angle (that depends on range, seabed reflection loss and water depth). This equivalent relationship offers a simple method to derive LF&LGA BBS from reverberation measurements [see Eqs. (26)–(29)]. The method is valuable because it allows seabed backscattering strength to be inverted at frequencies and angles where no practical method of measurements exists.

The equivalent relationship and the LF field-derived seabed geo-acoustic model (Biot parameters) are used to extract the bottom backscattering strength in a frequency band of 200–2500 Hz and in a grazing angle range of 1.1°–14.0° from SW reverberation measurements at three sites with sandy bottoms. The results are shown in Figs. 7(a), 8(a), and 9(a). From these figures, many observations can be made: (1) In general, in the 500–2500 Hz range, the SW reverberation-derived BBSs at low grazing angles are larger than the values predicted by the semi-empirical Lambert law. (2) For grazing angles that are larger than about 4°, the BBS has weaker angle dependence than the Lambert law. (3) For the high end of frequencies analyzed in this paper, if grazing angles are smaller than around 4°, the BBS decreases faster than the Lambert law with decreasing angles, the angular exponents may reach 3–4. (4) In a frequency range of 200–2500 Hz (below the JR characteristic frequency), the LF&LGA BBS exhibits strong frequency dependence for all three sites. At low grazing angles of 4°–10° it can approximately be expressed by $BBS = -A + 10\log_{10}(f/1000)^B$ (dB), where A is a range of 34.5–38.8, B is in a range of 2.0–2.7.

The characteristics of the reverberation-derived LF&LGA bottom backscattering strength need a physical explanation. The results might be used to compare with the well-developed HF seabed scattering models summarized by Jackson and Richardson,[6] and to see if those HF seabed scattering models are applicable at low frequencies. It also might be used to analyze the physical mechanisms of bottom scattering, including possible estimates of the seabed roughness spectra or sediment inhomogeneities at low frequencies.[47]

The theoretical expressions used to invert the BBS, Eqs. (24), (26)–(29), are limited to the three-halves law region where $r_3 > r > r_2$. In addition to this limitation, it is often hard to get quality reverberation data at long range because of ocean background noise interference; particularly at lower frequencies. These two factors limit the possible angular ranges of the SW reverberation-derived BBS in this paper.

The LF field-inverted seabed physical parameters for the Biot model[9,10] and the SW reverberation-derived LF&LGA seabed scattering in this paper are limited to sandy or sand-silt mixture seabottoms. Both seabed reflection and scattering models for the BBS derivations are described by the approximate expressions, Eqs. (13) and (19). The shear wave effects are assumed negligible in the frequency range for the BBS derivations. Thus, the reverberation-derived LF&LGA BBSs in this paper are approximation values.

Equations (26)–(29), used to derive the BBS in this paper, show how a variation of the bottom loss factor Q would quantitatively affect the values of the effective angle and reverberation-derived BBS. The Q values in Fig. 3 obtained from the Biot model exhibit very interesting frequency dependence at low grazing angles. The reflection loss amplitude and peak value frequency (around the JR characteristic frequency) are a complex function of the Biot parameters, and are particularly sensitive to the permeability κ_s, the porosity β, and the tortuosity α_0. The uncertainty of the reverberation-derived BBS in this paper will depend on the reliability of the effective Biot model (average parameters) inverted from LF field measurements.[9,10] Our preliminary data-model comparisons also show that around (or higher than) the JR characteristic frequency, the reverberation-derived LGA BBS exhibits much weaker frequency dependence than LF BBS, and it sometimes decreases with increasing frequency. Thus, more work needs to be done in the future to investigate how the Biot parameters and their uncertainties affect the seabed backscattering strength and its frequency dependence, including possible effects of shear wave.

In order to compare with the inversion method used in this paper, one may simultaneously measure both TL and RL from same sites and use Eq. (28) to derive the LF&LGA BBS. It will be desirable in the future to directly integrate physics-based seabed reflection/scattering models[4] into the energy flux method for SW reverberation modeling, and to do data/model comparisons, then from reverberation data to invert the physical parameters of seabed scattering as well as LF&LGA BBS vs frequency and angle.[48]

ACKNOWLEDGMENTS

This work was supported by the ONR OA322 and the CAS. The authors thank Dr. Robert Headrick for his support and helpful comments. We would like to express appreciation

to co-workers at State Key Laboratory of Acoustics, Institute of Acoustics, the Chinese Academy of Sciences for their constructive discussions on this work and for sharing the experimental data. Thanks go to our colleagues, Dr. Peter Rogers and James Martin, for their assistance and encouragement. Dr. Jeffrey Donnell is very much appreciated for copyediting this manuscript. Finally, the authors thank two anonymous reviewers for their valuable comments on the first version of this manuscript.

[1]F. B. Jensen, W. A. Kuperman, M. B. Porter and H. Schmidt, *Computational Ocean Acoustics*, 2nd ed. (Springer, New York, 2011), 794 pp.
[2]J. R. Preston, "Report on the 1999 ONR Shallow-water Reverberation Focus Workshop," Tech. Memorandum No. 99-155, (Appl. Res. Lab., Penn State Univ., State College, December 31, 1999).
[3]A. I. Eller, "Acoustics of shallow water: A status Report," ONR, Washington, DC and AD-A 146089/8/GAR (1985).
[4]D. R. Jackson and M. D. Richardson, *High-frequency Seafloor Acoustics* (Springer, New York, 2007), 616 pp.
[5]J. X. Zhou, X. Z. Zhang, J. S. Martin, and P. H. Rogers, "Reverberation-derived bottom scattering strength in the Yellow Sea," *17th ICA Proceedings* (September 2001, Rome, Italy).
[6]J. X. Zhou, "The analytical method of angular power spectrum, range and depth structure of the echo-to-reverberation ratio in shallow water sound field," (Chinese) Acta Acust. **5**(2), 86–99 (1980). Both the English translation and Chinese original versions of Ref. 6 can be obtained by sending an email to the corresponding author.
[7]J. X. Zhou, D. H. Guan, E. C. Shang, and E. S. Luo, "Long-range reverberation and bottom scattering strength in shallow water," Chin. J. Acoust. **1**, 54–63 (1982).
[8]J. X. Zhou, X. Z. Zhang, and E. S. Luo, "Shallow-water reverberation and small angle bottom scattering," in *Shallow-Water Acoustics*, edited by R. H. Zhang and J. X. Zhou (China Ocean Press, Beijing, 1997), pp. 315–322.
[9]J. X. Zhou, X. Z. Zhang, and D. P. Knobles, "Low-frequency geoacoustic model for the effective properties of sandy seabottoms," J. Acoust. Soc. Am. **125**, 2847–2866 (2009).
[10]J. X. Zhou and X. Z. Zhang, "Physical parameters for four seabed geoacoustic models from low-frequency measurements," in *Shallow-Water Acoustics*, edited by J. Simmen, E. S. Livingston, J. X. Zhou, and F. H. Li, AIP Conf. Proc. **2712**, 163–172 (2010).
[11]J. X. Zhou and X. Z. Zhang, "Shallow-water reverberation level: Measurement techniques and initial reference values," IEEE J. Ocean Eng. **30**, 832–842 (2005).
[12]J. X. Zhou, "The vertical coherence of long-range reverberation in the shallow water homogeneous layer," Acta Oceanol. Sin. **1**(2), 212–218 (1979) (in Chinese).
[13]J. X. Zhou, "Active sonar performance prediction in shallow water of variable depth," the *Proceedings of the Second Acoustics Meeting of China*, Extended abstract, pp. 12–13 (Beijing, May 1979) (in Chinese).
[14]J. X. Zhou, X. Z. Zhang, P. H. Rogers, and D. H. Guan, "Nonreciprocity of long-range reverberation in wedged continental shelf," J. Acoust. Soc. Am. **91**(2), 2343, and NTIS AD-5A254716/4/XAB, 35 pp (August 1992).
[15]J. X. Zhou, X. Z. Zhang, P. H. Rogers, and G. W. Caille, "Average acoustic field in shallow water I: Active sonar performance prediction," J. Acoust. Soc. Am. **96**, 3330 (1994).
[16]J. X. Zhou and X. Z. Zhang, "Average acoustic field in shallow water II: Reverberation and its inverse problem," J. Acoust. Soc. Am. **96**, 3330 (1994).
[17]J. X. Zhou, X. Z. Zhang, E. S. Luo, and D. Z Wang, "Vertical coherence of long-range reverberation in a Pekeris shallow water," J. Acoust. Soc. Am. **93**, 2286 (1993).
[18]C. H. Harrison, "Closed-form expressions for ocean reverberation and signal excess with mode stripping and Lambert's law," J. Acoust. Soc. Am. **114**, 2744–2756 (2003).
[19]J. X. Zhou, X. Z. Zhang, P. H. Rogers, J. A. Simmen, P. H. Dahl, G. L. Jin, and Z. H. "Reverberation vertical coherence and seabottom geoacoustic inversion in shallow water," IEEE J. Ocean Eng. **29**, 988–999 (2004).
[20]C. H. Harrison, "Fast bistatic signal-to-reverberation ratio calculation," J. Comput. Acoust. **13**, 317–340 (2005).
[21]C. H. Harrison, "Closed form bistatic reverberation and target echoes with variable bathymetry and sound speed," IEEE J. Ocean Eng. **30**, 660–675 (2005).
[22]M. K. Prior, "Experimental investigation of the angular dependence of low-frequency seabed reverberation," IEEE J. Ocean Eng. **30**, 691–699 (2005).
[23]C. Holland, "On errors in estimating seabed scattering strength from long-range reverberation," J. Acoust. Soc. Am. **118**, 2787–2790 (2005).
[24]C. W. Holland, "Constrained comparison of ocean waveguide reverberation theory and observations," J. Acoust. Soc. Am. **120**, 1922–1931 (2006).
[25]C. W. Holland, "Mapping seabed variability: Rapid surveying of coastal regions," J. Acoust. Soc. Am. **119**, 1373–1387 (2006).
[26]C. H. Harrison and P. L. Nielsen, "Separability of seabed reflection and scattering properties in reverberation," J. Acoust. Soc. Am. **121**, 108–119 (2007).
[27]M. A. Ainslie, "Observable parameters from multipath bottom reverberation in shallow water," J. Acoust. Soc. Am. **121**, 3363–3376 (2007).
[28]C. W. Holland, "Fitting data, but poor predictions: Reverberation prediction uncertainty when seabed parameters are derived from reverberation measurements," J. Acoust. Soc. Am. **123**, 2553–2562 (2008).
[29]C. W. Holland and D. D. Ellis, "Two modeling approaches for reverberation in a shallow water waveguide where the scattering arises from a sub-bottom interface," J. Comput. Acoust. **17**, 29–43 (2009).
[30]M. A. Ainslie, *Principles of Sonar Performance Modeling* (Springer-Verlag, Berlin, 2010), pp. 495–510.
[31]L. M. Brekhovskikh, "The average field in an underwater sound channel," Sov. Phys. Acoust. **11**, 126–134 (1965).
[32]L. M. Brekhovskikh, "Elements of sound field theory in the ocean," in *Ocean Acoustics*, edited by L. M. Brekhovskikh (Nauka, Moscow, 1974), pp. 79–162 (in Russian).
[33]P. M. Smith, "Average sound transmission in range-dependent channels," J. Acoust. Soc. Am. **55**, 1197–1204 (1974).
[34]K. G. Guthrie and C. T. Tindle, "Ray effects in the normal mode approach to underwater acoustics," J. Sound. Vib. **47**, 403–413 (1976).
[35]E. C. Shang, "Transition ranges of the average sound field in shallow water," Sci. Sin. **19**(6), 794 (1976).
[36]L. M. Brekhovskikh, *Waves in Layered Media* (Academic, New York, 1960).
[37]D. E. Weston, "Intensity-range relations in oceanographic acoustics," J. Sound and Vib. **18**(2), 271–287 (1971).
[38]M. J. Buckingham, "Array gain of a broadside vertical line array in shallow water," J. Acoust. Soc. Am. **65**, 148–161 (1979).
[39]R. J. Urick, *Principles of Underwater Sound*, 3rd ed. (Peninsula, Los Altos, CA, 1983), Chap. 8.
[40]K. V. Mackenzie, "Long-range shallow-water bottom reverberation," J. Acoust. Soc. Am. **34**, 62–66 (1962).
[41]J. X. Zhou, "Vertical coherence of the sound field and boundary loss in shallow water," Chinese Phys. **1**, 494–504 (1981) [(Chinese Acta Acust. **4**, 34–43 (1979)].
[42]E. L. Hamilton, "Compression-wave attenuation in marine sediments," Geophysics **37**, 620–646 (1972).
[43]E. L. Hamilton, "Geoacoustic modeling of the sea floor," J. Acoust. Soc. Am. **68**, 1313–1340 (1980).
[44]W. H. Thorp and D. G. Browning, "Attenuation of low frequency sound in the ocean," J. Sound Vib. **26**, 576–578 (1973).
[45]Q. X. Li, C. H. Chen, and J. S. Xu, *Marine Atlas of the Bohai Sea, Yellow Sea and East China Sea: Geology and Geophysics Section* (China Ocean Press, Beijing, 1991).
[46]F. Desharnais and D. D. Ellis, "Data-model comparisons of reverberation at three shallow-water sites," IEEE J. Ocean Eng. **22**, 309–316 (1997).
[47]A. Turgut, "Inversion of bottom/subbottom statistical parameters from acoustic backscatter data," J. Acoust. Soc. Am. **102**, 833–852 (1997).
[48]J. X. Zhou, X. Z. Zhang, L. Wan, Z. H. Peng, Z. L. Li, and L. H. Guo, "Integrating the energy flux method of shallow-water reverberation with physics-based seabed scattering modes," J. Acoust. Soc. Am. **129**, 2631–2632 (2011).

Shear wave velocity and attenuation in the upper layer of ocean bottoms from long-range acoustic field measurements

Ji-Xun Zhou[a] and Xue-Zhen Zhang
School of Mechanical Engineering, Georgia Institute of Technology, Atlanta, Georgia 30332-0405

(Received 15 April 2012; revised 8 October 2012; accepted 17 October 2012)

Several physics-based seabed geoacoustic models (including the Biot theory) predict that compressional wave attenuation α_2 in sandy marine sediments approximately follows quadratic frequency dependence at low frequencies, i.e., $\alpha_2 \approx kf^n$ (dB/m), $n = 2$. A recent paper on broadband geoacoustic inversions from low frequency (LF) field measurements, made at 20 locations around the world, has indicated that the frequency exponent of the effective sound attenuation $n \approx 1.80$ in a frequency band of 50–1000 Hz [Zhou *et al*., J. Acoust. Soc. Am. **125,** 2847–2866 (2009)]. Carey and Pierce hypothesize that the discrepancy is due to the inversion models' neglect of shear wave effects [J. Acoust. Soc. Am. **124**, EL271–EL277 (2008)]. The broadband geoacoustic inversions assume that the seabottom is an equivalent fluid and sound waves interact with the bottom at small grazing angles. The shear wave velocity and attenuation in the upper layer of ocean bottoms are estimated from the LF field-inverted effective bottom attenuations using a near-grazing bottom reflection expression for the equivalent fluid model, derived by Zhang and Tindle [J. Acoust. Soc. Am. **98**, 3391–3396 (1995)]. The resultant shear wave velocity and attenuation are consistent with the SAX99 measurement at 25 Hz and 1000 Hz. The results are helpful for the analysis of shear wave effects on long-range sound propagation in shallow water. © *2012 Acoustical Society of America*.
[http://dx.doi.org/10.1121/1.4765078]

PACS number(s): 43.30.Ma, 43.30.Pc [NPC] Pages: 3698–3705

I. INTRODUCTION

Low frequency (LF) (compressional) sound velocity and effective attenuation in sandy seabottoms have recently been analyzed and summarized from long-range field measurements in shallow water (SW).[1] The measurements were conducted by different investigators at 20 locations in different coastal zones around the world. The effective seabed attenuations, inverted from these acoustic field measurements with different characteristics, exhibit similar magnitude and nonlinear frequency dependence below 2000 Hz at all of these sites, as shown in Fig. 1. The average LF-field-inverted sound attenuation values from sites 1–20 are listed in Table I as a function of frequency. The numbers of the available data sets for the average are also listed in Table I. Using power law fitting, the average LF effective attenuation α_{2E} in sandy and sand-silt mixture seabottoms can approximately be expressed as the following nonlinear frequency dependence:

$$\alpha_{2E} = (0.367 \pm 0.011)(f/1000)^{(1.801 \pm 0.020)}\ \text{dB/m}, \quad \text{for } 50 - 1000\ \text{Hz}, \tag{1}$$

$$\alpha_{2E} = (0.372 \pm 0.022)(f/1000)^{(1.809 \pm 0.032)}\ \text{dB/m}, \quad \text{for } 50 - 500\ \text{Hz}, \tag{2}$$

where f is frequency in units of Hz. The corresponding average sound velocity ratio at the bottom-water interface in the 50–600 Hz range is 1.061 ± 0.009.[1]

Numerical simulations[2] show that that both LF field-derived sound velocity and attenuation in sandy seabottoms can closely be predicted by the Biot-Stoll model,[3–14] the Buckingham VGS (viscous-grain-shearing) model,[15–17] the Chotiros-Isakson BICSQS (Biot-Stoll with squirt flow and shear) model,[18] and the Pierce-Carey/Williams simpler model[19,20] when the physical parameters of these seabed acoustic models are known. However, there remain important unanswered questions. One of these involves the possible shear wave effects that were assumed to be unimportant in those LF measurements and inversion methods. Another one is, why is the frequency exponent of sound attenuation in Eqs. (1) and (2) around 1.8, not close to 2 that should be "a direct consequence of the Biot theory"?[17–21] There might be different answers to the second question. Carey *et al*. hypothesized that "The discrepancy can be explained because the inverse analysis inferences were made with the neglect of an additional attenuation mechanism where generated lower shear waves carry energy downwards out of the waveguide."[21] Following this hypothesis, this paper attempts to use the LF field-inverted effective sound attenuation shown in Table I to estimate a possible range of the average shear wave velocity and attenuation in the upper layer of sandy bottoms.

II. ESTIMATION OF SHEAR WAVE VELOCITY AND ATTENUATION FROM THE LF FIELD MEASUREMENTS

The LF field geo-acoustic inversions in Ref. 1 assumed that sea bottoms were a half-space equivalent fluid model; i.e., the shear wave was negligible. Thus, inverted sound attenuations (and related Biot parameters) in the bottoms should be considered as equivalent/effective values, $\alpha_{2E}(f)$.

[a]Also at: State Key Laboratory of Acoustics, Institute of Acoustics, Chinese Academy of Sciences, Beijing 100190, China.

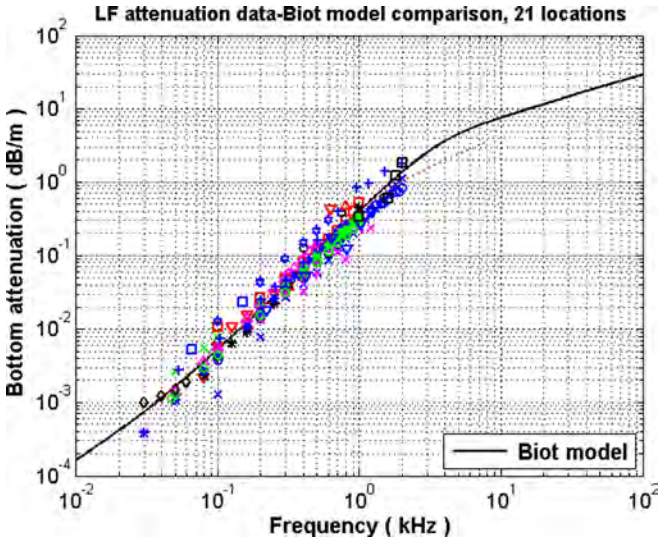

FIG. 1. (Color online) Effective LF sound attenuations in sandy seabottoms (Ref. 1). All data symbols and a dotted line are from the LF field measurements; a solid line is obtained from the Biot-Stoll geoacoustic model.

A. Shear wave effects on the near-grazing acoustic reflection and the equivalent sound attenuation

The LF sound velocity and attenuation in Ref. 1 were inverted from the long-range sound field where lower-order normal modes interact with an upper layer of the bottom at low grazing angles (around a wave length thick). According to the Wentzel–Kramers–Brillouin approximation, the nth modal attenuation coefficient in a SW waveguide, β_n, can be expressed approximately in terms of the bottom reflection coefficient $V(\theta)$,

$$\beta_n = -\frac{\ln|V(\theta_n)|}{S_n(\theta_n)+\delta_n}, \tag{3}$$

where S_n is the cycle distance of the nth mode-ray, δ_n is a beam displacement on the bottom reflection, θ_n is the grazing angle of the nth mode at the water-bottom interface. If the water depth H and wave number k satisfy $kH \gg 1$, δ_n is negligible. The plane wave reflection coefficient from the seabed (fluid or elastic) can always be expressed by its modulus and phase

$$V(\theta) = |V(\theta)|\exp[i\phi(\theta)]. \tag{4}$$

At low grazing angle,[22–26]

$$|V(\theta)| \approx 1 - Q\theta \approx e^{-Q\theta} \quad (\theta \ll 1), \tag{5}$$

$$\phi(\theta) \approx -\pi + P\theta \quad (\theta \ll 1). \tag{6}$$

The quantity Q governs the modal attenuation; it is related to the bottom reflection loss defined by $20\log|V(\theta)| = 8.686Q\theta$ in dB/radian; P is a near-grazing reflection phase shift that is introduced by an imaginary ideal pressure-release boundary located a distance of $P/4\pi$ wavelength below the true seabed boundary, i.e., a "hidden depth" $\Delta H = (P/4\pi)\lambda$. The modal decay factors β_n control the sound propagation loss in SW waveguides. Based on Eqs. (3) and (5), the shear wave must affect long-range SW propagation through the near-grazing bottom reflection factor Q and P.

The characteristics of the seabed reflection loss at low grazing angles were used by Tindle, Zhang, and Chapman to treat the shear wave effects[25–29] that will be briefly described next.

The seabed is assumed as a homogeneous poro-elastic half-space with density ρ_2, compressional wave velocity c_2, and shear wave velocity c_s. The water layer above the seabed has a density ρ_1 and sound velocity c_1 ($c_2 > c_1$, $c_s < c_1$). Attenuation of the compressional waves and shear waves in the seabed is introduced by allowing their velocities to become complex, $c_2 \to c_2(1 - i\varepsilon_2)$ and $c_s \to c_s(1 - i\varepsilon_s)$ with ε_2 and ε_s small dimensionless numbers, i.e., $\alpha_2 = (2\pi f/c_2)\varepsilon_2$ and $\alpha_s = (2\pi f/c_s)\varepsilon_s$ in Np/m.

The main idea introduced by Tindle, Zhang, and Chapman is to have a fluid seabed model that is equivalent to an elastic seabed model, to let three equivalent parameters (ρ_{2E}, c_{2E}, and α_{2E}) do the work of five (ρ_2, c_2, α_2, c_s, and α_s), and to have the same bottom reflection parameters (Q and P) and the same normal-mode decay factors β_n in a shallow-water waveguide. For a low shear velocity ocean bottom with $c_s < c_w$, $\varepsilon_s \ll 1$, $\varepsilon_p \ll 1$, ignoring ε_p^2, ε_s^2, $\varepsilon_p c_s^3$, $\varepsilon_s c_s^3$ and higher order, and leaving the critical angle (equivalent c_2) unchanged

$$c_{2E} = c_2. \tag{7}$$

Tindle, Zhang, and Chapman derived the following approximation expressions for the equivalent sound attenuation (α_{2E}), density ρ_{2E}, near-grazing bottom reflection factors (Q), phase shift (P), and the hidden depth in terms of real acoustic parameters and the angular frequency ω ($=2\pi f$)[25–29]

TABLE I. The average effective sound attenuation from the LF field measurements.

f (Hz)	50	80	100	125	160	200	250	300	315	400	500
α_{2E} (dB/m)	0.00175	0.00330	0.00598	0.00878	0.01510	0.01978	0.02950	0.04271	0.04368	0.07012	0.10926
Data sets	(7)	(7)	(15)	(5)	(10)	(19)	(9)	(15)	(8)	(19)	(19)
f (Hz)	600	630	700	750	800	900	1000	1200	1500	1600	2000
α_{2E} (dB/m)	0.14515	0.18479	0.18888	0.23650	0.22365	0.27511	0.36504	0.47193	0.75464	0.67210	1.17768
Data sets	(12)	(9)	(12)	(6)	(12)	(7)	(13)	(8)	(5)	(3)	(4)

$$\alpha_{2E} = \alpha_2 + \frac{4\omega c_2 c_s^3 (1 - c_1^2/c_2^2)^{3/2}(1 - c_s^2/c_1^2)^{1/2}}{c_1^5(1 - 2c_s^2/c_1^2)^2} + \frac{8\alpha_s c_2 c_s^3 (1 - c_1^2/c_2^2)}{c_1^4(1 - 2c_s^2/c_1^2)}, \quad (8)$$

$$\rho_{2E} = \rho_2[1 - 2c_s^2/c_1^2]^2 \left[1 - \frac{(\alpha_{2E})^2 c_1^2(1 + 2c_1^2/c_2^2)}{2\omega^2(1 - c_1^2/c_2^2)^2}\right]^{-1}, \quad (9)$$

$$Q = 2\frac{\rho_2}{\rho_1}\left\{\frac{1}{2\pi}\frac{c_2}{f}\alpha_2[1-2(c_s/c_1)^2]^2\frac{(c_1/c_2)^2}{[1-(c_1/c_2)^2]^{3/2}} + 4\left(\frac{c_s}{c_1}\right)^3\sqrt{1-(c_s/c_1)^2} + \frac{1}{2\pi}\frac{8c_s}{f}\alpha_s(c_s/c_1)^2 \times \frac{[1-2(c_s/c_1)^2}{[1-(c_1/c_2)^2]^{1/2}}\right\}, \quad (10)$$

$$P = 2Y_0 = 2(\rho_2/\rho_1)\frac{[1 - 2(c_s/c_1)^2]^2}{[1 - (c_1/c_2)^2]^{1/2}}, \quad (11)$$

$$\Delta H = \frac{P}{4\pi}\lambda. \quad (12)$$

In these equations α_2 and α_s are in Np/m. Based on these equations, Chapman clearly indicates "In propagation condition, where only Q and P determine the field, there are many different seabottoms (many families of five parameters) that deliver the same acoustic effect. Conversely, long-range inversion experiments that effectively only measure Q and P cannot hope to produce unambiguous values of five seabed parameters. However, the above equations strongly suggest how estimated parameter values might be correlated. For example, an inversion algorithm that underestimates shear velocity—or perhaps assumes zero shear velocity—would naturally also underestimate the density and overestimate the compressional-wave-attenuation, to compensate. Of course, the ambiguity of these inversions could be resolved by sampling the field at short range, where the acoustic field contains information about seabed interactions at steeper angles."[25] Unfortunately, the acoustic field at short range is often too insensitive to infer compression wave attenuation in the seabed; on other hand, the inverted seabed acoustic parameters that are obtained at short range might not represent the average geoacoustic characteristics of the entire large area used in the sonar performance modeling. Thus, using inversions to estimate the parameters of an effective seabed model "may turn out to be more useful for sonar performance prediction models."[25]

Based on Eq. (8), all the LF field inversions in Ref. 1 that ignored the shear wave effect result in an equivalent bottom attenuation, α_{2E}, that is larger than the real compressional-wave-attenuation, α_2. Tindle, Zhang, and Chapman numerically show that the equivalent fluid approximations are capable of providing a good approximation to the reflection coefficient of a solid seabed (with a low shear wave velocity), as well as a good approximation to SW long-range propagation.[25–29]

B. Shear velocity and attenuation in sandy and sand-silt mixture seabottoms, estimated from the LF field-inverted equivalent sound attenuation

The derivation of shear velocity and attenuation in this section is based on the following four conditions (models, measurements, or assumptions): (i) the LF compressional wave attenuation in ocean bottoms should follow quadratic frequency dependence ($\propto f^{2.0}$)[17–21]; (ii) the averaged LF field-inverted equivalent sound attenuation, α_{2E}, and velocity, c_{2E}, as a function of frequency have been obtained; (iii) three equivalent parameters (ρ_{2E}, c_{2E}, and α_{2E}) in an equivalent fluid seabed model do the work of five (ρ_2, c_2, α_2, c_s, and α_s) in a poro-elastic seabed model for the near-grazing bottom reflection (consequently for SW long-range sound propagation) described by Eqs. (7)–(11);[25–29] and (iv) shear wave velocity and attenuation in sandy/silt bottoms obey the Biot-Stoll geoacoustic model.

Numerical simulations show that when both frame bulk and shear moduli are negligibly small, or two moduli are real (have no an imaginary term), the Biot-Stoll model does predict a quadratic frequency dependence at low frequencies.

As we know,[1] the higher the frequency, the larger the uncertainty of the geoacoustic inversion in shallow water would be. Yet at low frequencies, the sound attenuation, derived from several physics-based geoacoustic models, exhibits quadratic frequency dependence. Taking these two considerations into account, we will only use the LF field-inverted attenuation data, $\alpha_{2E}(f)$, between 50 Hz and 500 Hz (that are listed in Table I).

In the fall of 1999, a comprehensive field experiment named "SAX99" (sediment acoustics experiments) was conducted in the Gulf of Mexico (referred to as SAX99 site).[13,14] During the SAX99 experiment, the Biot parameters of the sediments were extensively measured by using both traditional and newly developed methods. The sound velocity was measured over a frequency range of 125 Hz–400 kHz, and attenuation was measured over a frequency range of 2.6–400 kHz by scientists from different institutions. The data are unique both for the frequency range spanned at a common location and for the extensive environmental characterization. All the results on compressional and shear velocities and attenuations were summarized by Williams *et al.*[13] Reference 1 shows that the LF sound velocity and attenuation in sandy bottoms, inverted from 20 sites, smoothly join with the SAX99 benchmark data set in the mid to high frequency ranges. Thus, the shear velocities at two frequencies of 1000 Hz and 25 Hz from the SAX99[13,14] will be used in this paper as reference values. Shear wave velocities were obtained from the SAX99 experiments using time-of-flight measurements.[13] At 1000 Hz, the average shear velocity was 122 m/s with a range of 97 to 147 m/s; the attenuation of shear waves was found to have a mean of 30.5 dB/m with a range of 21 to 40 dB/m at 1 kHz. At 25 Hz, the mean shear wave velocity was 150 m/s (in the upper layer of about 1 m thick, it was about 100 m/s; beneath this layer, the maximum velocity may approach about 200 m/s); the mean shear wave attenuation was 0.33 dB/m (in the upper layer it was 0.47 dB/m, in the lower stratum it is 0.19 dB/m).[14]

In the basic Biot-Stoll theory, three parameters largely control the fluid motion that causes the nonlinear dispersion that is important in the coarser granular sediments. These are the permeability κ_s, the porosity β, and the tortuosity α_0, which define the necessary amount of "added mass" in the Biot-Stoll model. These three parameters define the pore-size parameter. Data/model comparisons (trials) tell us that the LF sound velocity ratio is very sensitive to the porosity of sediment and is less sensitive to its permeability and tortuosity. The LF sound attenuation is very sensitive to the permeability of the sediment and is less sensitive to its porosity and tortuosity. Thus, the porosity of 0.420 ± 0.015 and the permeability of $(1.00 \pm 0.05) \times 10^{-11}$ were easily determined as the values that provide the best match between the Biot-Stoll model and the LF inverted attenuations and velocity ratios. The other eleven Biot parameters were taken same as those from the SAX99 measurement.[13] All the effective Biot parameters that were used to match the LF field-inverted sound velocity and attenuation are listed in Ref. 1 (Table X, in the column labeled "LF fit"). The frame shear wave modulus μ_0 and shear log decrements δ_s are not important for the compressional wave data-model comparison in Ref. 1; however, they play significant roles in determining the shear wave velocity and attenuation in this paper.

The procedures for deriving shear wave velocity and attenuation from LF field measurements are as follows: (i) by adjusting a pair of frame shear moduli μ_0 and δ_s and using the Biot-Stoll model, calculate shear wave velocity and attenuation vs frequency, i.e., $c_s(f)$ and $\alpha_s(f)$; (ii) input the resultant $c_s(f)$ and $\alpha_s(f)$ into Eq. (8) and use the LF-field inverted equivalent sound attenuation and velocity, $\alpha_{2E}(f)$ and $c_2\,(=c_{2E})$, respectively, to calculate a set of real compressional sound attenuation as a function of frequency, i.e., $\alpha_2(f)$; (iii) when $\alpha_2(f)$ is proportional to $f^{2.000}$, a pair of μ_0 and δ_s, and a pair of $c_s(f)$ and $\alpha_s(f)$ are inverted.

The third term of Eq. (8) indicates that there is shear velocity-attenuation coupling; a decrease in shear velocity can be compensated by an increase in shear wave attenuation; that is, there may be many combinations of c_s and α_s that deliver the same effect. Thus, we use the shear velocity at 25 Hz or at 1000 Hz obtained from the comprehensive SAX99 measurements as a constraining condition. Based on "historical bounds" of frame shear modulus μ_0 and shear log decrements δ_s for sandy/silt bottoms,[30] and μ_0 was varied between $2.61 \times 10^7 - 11.9 \times 10^7$ at 0.01×10^7 intervals with δ_s between 0–0.15 at 0.0001 intervals, we calculate shear velocity and attenuation as inputs for Eq. (8); the LF field-inverted equivalent bottom attenuation α_{2E} is numerically modified toward the compressional wave attenuation α_2. The pair of μ_0 and δ_s values, and the corresponding pair of $c_s(f)$ and $\alpha_s(f)$ values, for which the resultant sound attenuation α_2 has the quadratic frequency dependence $(\propto f^{2.000})$, are both readily uniquely determined. The resultant c_s and α_s as a function of frequency are shown in Figs. 2(a) and 2(b). Solid lines (case A) in these two figures are obtained by using $c_s = 122$ m/s as a constraining condition. It was obtained by the NRL team from the SAX99 site at 1000 Hz.[13] The dashed lines (case B) are obtained by using $c_s = 150$ m/s as a constraining condition. It was obtained at

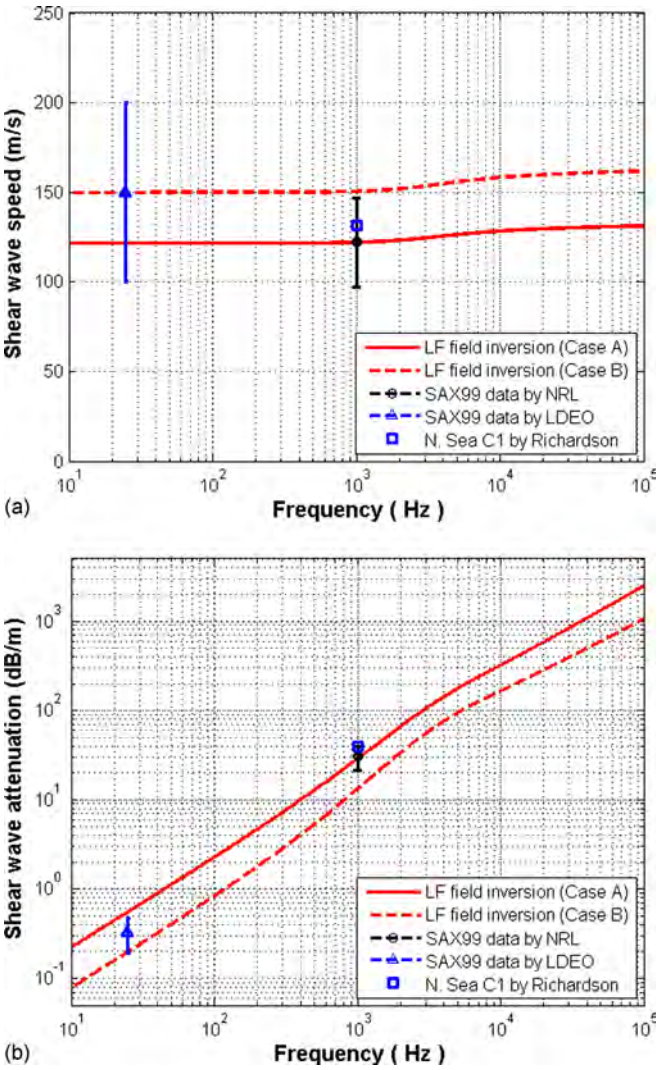

FIG. 2. (Color online) LF field inverted shear wave property in sandy bottoms as a function of frequency: (a) velocity and (b) attenuation.

25 Hz by a team from Lamont-Doherty Earth Observatory (LDEO) of Columbia University.[14] For comparison, both shear velocity and attenuation measured by the SAX99 teams at two frequencies are plotted in Fig. 2. Although only one value of shear velocity at 1000 Hz or 25 Hz from the SAX99 measurements is used as a constraining condition in this work, both the LF field-inverted shear velocity and the attenuation are close to the SAX99 measurements at two frequencies. Based on Buckingham,[15] "the sole reported data taken at a frequency of 1000 Hz" by Richardson from the North Sea site C1 are also plotted in Figs. 2(a) and 2(b).

For case A (the velocity from the SAX99 measurements at 1000 Hz as a constraining condition), the shear wave velocity and attenuation, shown in Fig. 2 by solid lines, correspond to the LF field-inverted complex frame shear modulus

$$\mu = 2.91(1 - 0.0981i) \times 10^7 \text{ Pa}. \tag{13}$$

In case B (the velocity from the SAX99 measurements at 25 Hz as a constraining condition), $c_s(f)$ and $\alpha_s(f)$, shown in Fig. 2 by dashed lines, correspond to the complex frame shear modulus

$$\mu = 4.46(1 - 0.0426i) \times 10^7 \text{ Pa}. \quad (14)$$

Comparing this with Eq. (13), a higher shear wave velocity (frame shear modulus) requires smaller shear wave attenuation (imaginary frame shear modulus). This is the shear wave velocity-attenuation coupling discussed before on Eq. (8).

By using any set of the shear wave velocity and attenuation shown in Fig. 2 as inputs for Eq. (8), the LF field-inverted equivalent sound attenuations $\alpha_{2E}(f)$ are corrected to same compressional wave attenuations, which can be expressed by

$$\alpha_2 = (0.420 \pm 0.035)(f/1000)^{(2.000 \pm 0.045)} \text{ dB/m} \quad \text{for } 50 - 500 \text{ Hz}. \quad (15)$$

The original LF field inverted equivalent sound attenuation from Ref. 1, α_{2E}, and shear wave corrected compressional wave attenuation, α_2, as well as their power-law fittings, expressed by Eqs. (1) and (15), are plotted in Fig. 3.

As an example for comparison, using Eqs. (10)–(12) we calculate the near-grazing bottom reflection loss/phase shift parameters and the hidden depth of shallow water (Q, P, and ΔH) for two cases: with or without shear waves that are plotted in Figs. 4(a)–4(c), respectively. With the exception of the shear modulus expressed by Eq. (13), which is inverted in this paper, other Biot parameters are the same as those listed in Ref. 1 (Table X, the column labeled "LF fit"). For the case of "no shear wave," we assume both frame bulk and shear moduli are real (have no imaginary term). Figure 4(a) shows strong frequency dependence for the near-grazing seabed reflection loss from the sandy ocean bottoms in the cases with or without shear waves. This phenomenon may be extrapolated from papers published by Stoll and Kan,[8] and by Isakson and Neilsen.[31] An interesting frequency dependence shown in Fig. 4(a) predicts that the water-sediment interface for sandy bottoms may act as a filter with respect to

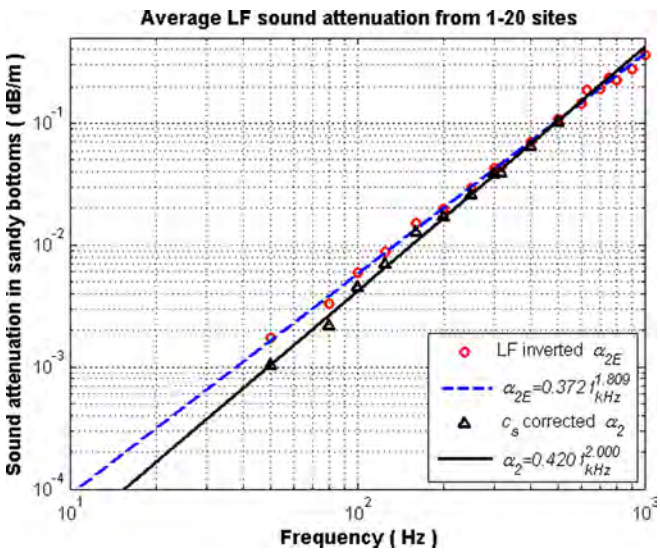

FIG. 3. (Color online) Comparison of the LF field inverted effective bottom sound attenuation α_{2E} with shear wave corrected sound attenuation α_2.

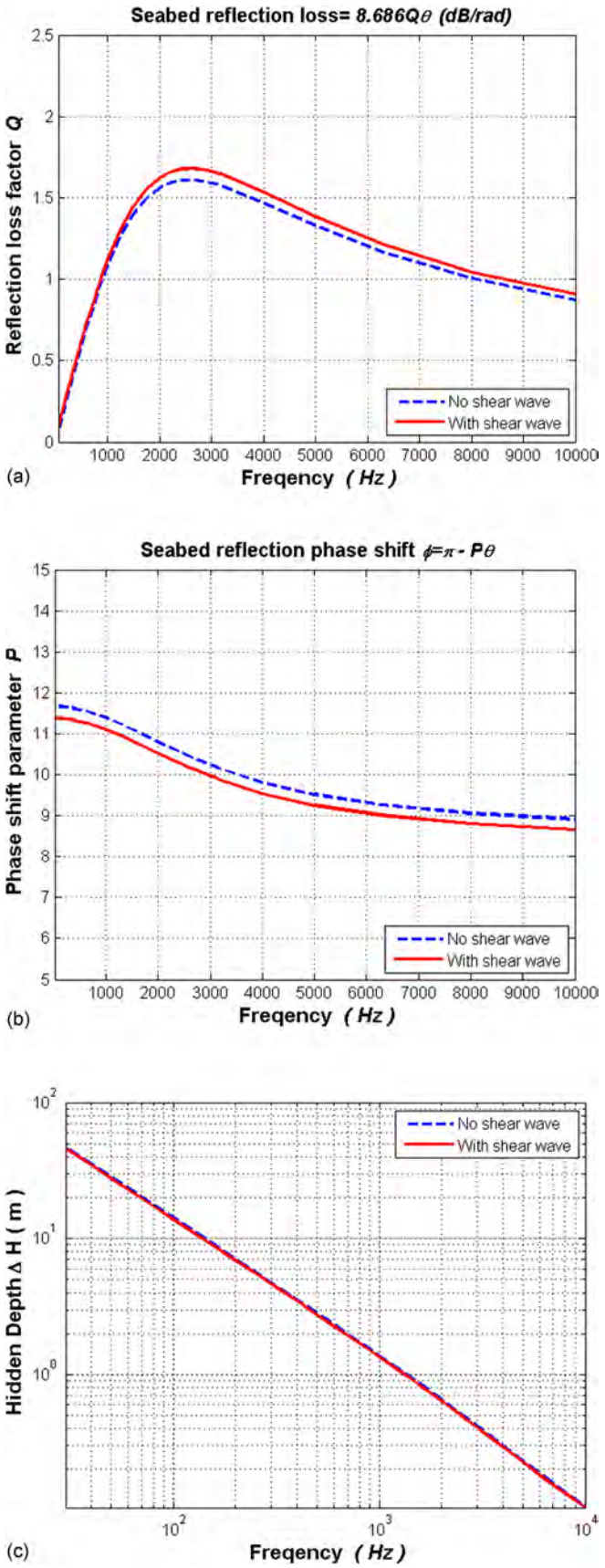

FIG. 4. (Color online) Comparisons between with and without shear waves. (a) The near-grazing bottom reflection loss factor Q, bottom reflection loss defined by $20\log|V(\theta)| = 8.686Q\theta$. (b) The near-grazing bottom reflection phase shift parameter P. (c) The hidden depth of shallow water ΔH.

broadband long-range sound propagation where lower-order modes with low-grazing angles are predominant.

III. SUMMARY AND DISCUSSION

The LF field inverted sound speed and attenuation in sandy seabottoms are "effective" results and yield a frequency exponent of 1.8 for attenuation.[1] Whereas several physical theories on seabed acoustics yield a result of 2.0.[17–20] One of possible sources for this discrepancy may be neglected shear effects.[21] The LF field inversion results for the exponent of 1.8 make the assumption of an all-fluid medium with no shear properties. Based on some theoretical results of Tindle, Zhang, and Chapman,[25–29] the LF field-inverted compressional wave velocity and effective attenuation of Ref. 1 are used to estimate the average shear wave velocity and attenuation, and complex shear modulus for a frequency band of 50–500 Hz in upper layers of sandy and sand-silt mixture ocean bottoms. The resultant shear wave velocity and attenuation are consistent with the SAX99 measurement at 25 Hz and 1000 Hz.

Figure 4(c) shows that from 50 to 500 Hz, the hidden depths in shallow water, ΔH, is equal to about 28.0 m to 2.8 m. The effective penetration depth of sound waves at long ranges is less than ΔH. Thus, resultant shear wave velocity and attenuation shown in Figs. 2(a) and 2(b), as well as the complex shear modulus expressed by Eqs. (13) and (14) can be reasonably considered as average values in an upper layer of about 20 m thick.

In general, "shear wave properties are difficult to measure: their attenuation is high, and it is difficult to generate waves with predominantly transverse particle motions."[32] Buckingham indicated "*In situ* measurements of shear wave properties as functions of frequency are rarer than those of compressional waves. In fact, no published *in situ* measurements of shear-wave dispersion and attenuation over extended frequency ranges are known to the author."[16] Much of the early data on shear wave in the literature from both field and laboratory work is in the high-frequency range. Most of recent *in situ* measurements use interface waves on the bottoms; resultant shear wave speed and attenuation exhibit strong depth dependence beneath the water-seabed interface.[14,32–38] Limited to the authors' knowledge, very few of those data are in a frequency range of 50–1000 Hz that we are interested in. Thus, the LF field inverted shear wave velocity and attenuation, and their possible range presented in this paper, might be helpful for analyzing the effects of the shear wave on LF long-range sound propagation in shallow water.

With the exception of common uncertainties that most geoacoustic inversions meet, the reliability of the LF field-inverted shear wave velocity and attenuation in this paper mainly depends on the quality of the LF field-inverted effective sound attenuation in Ref. 1, and the quality of shear wave velocity measured by the SAX99 group at 25 Hz or 1000 Hz. It also depends on the validity of those seabed geoacoustic models that predict that the compressional attenuation varies as f^{-2} at low frequencies.[17–21] Uncertainties on the LF field-inverted effective sound attenuation were discussed in Ref. 1. Two lines in Figs. 2(a) and 2(b) show variations of the LF field inverted shear wave speed and attenuation caused by two different constraining values of shear wave velocity from two SAX99 teams (25 Hz for deeper sediments, 1000 Hz for a thinner top layer). That is, depending on the constraint that we choose, we may end up with different values for the outputs. However, these variations (uncertainties) have no effect on the physics problems we discussed, including the result shown in Fig. 3. Figures 2(a) and 2(b) and Eqs. (13) and (14) show that a broadband shear wave speed, attenuation and complex frame shear modulus may be estimated from the LF field-inverted effective bottom attenuation plus one value of shear speed (or attenuation) at one single frequency. It will be desirable to simultaneously invert the effective bottom attenuation from the broadband long-range field measurements, and to measure shear wave velocity and attenuation for several frequencies by other methods at the same site, then to have sufficient comparison and validation of the results.

ACKNOWLEDGMENTS

This work was supported by the ONR OA322. The authors thank Dr. Robert Headrick for his support and helpful comments. Thanks go to our colleagues, Dr. Peter Rogers and James Martin, for their assistance and encouragement. Finally, the authors thank Dr. Michael Buckingham and the two anonymous reviewers for their valuable suggestions on the earlier version of this manuscript.

APPENDIX: BIOT-STOLL EXPRESSIONS ON SHEAR WAVE VELOCITY AND ATTENUATION

For a harmonic plane shear wave of $\exp(i\omega t - ik_s x)$ traveling through a sediment medium, in the Biot-Stoll model the frequency equation of shear wave can be expressed by[6,7]

$$\begin{vmatrix} \rho\omega^2 - \mu k_s^2 & \rho_f\omega^2 \\ \rho_f\omega^2 & m\omega^2 - i\omega F\eta/\kappa \end{vmatrix} = (\rho\omega^2 - \mu k^2)(m\omega^2 - i\omega F\eta/\kappa) - \rho_f^2\omega^4 = 0, \tag{A1}$$

where ω is the angular frequency, k_s is wavenumber, and ρ is the total mass density

$$\rho = \beta\rho_f + (1-\beta)\rho_s. \tag{A2}$$

ρ_f is the pore fluid mass density, η is the pore fluid viscosity, κ is the hydraulic coefficient of permeability, β is the porosity, ρ_s is the density of grain, and the frame shear modulus

$$\mu = \mu_0(1 - i\delta_s) \tag{A3}$$

is a complex modulus to account for dissipation loss at grain contact, and δ_s is the shear log decrement. The parameter

$$m = \frac{c\rho_f}{\beta} \tag{A4}$$

accounts for the phase of fluid flow with respect to the macroscopic pressure gradient. The structure constant c, or tortuosity, is equal to 1 for uniform pores that are parallel to the pressure gradient, and is equal to 3 for randomly oriented pores.

The factor F is a viscosity correction to account for frequency-dependent viscous losses of oscillating flow in the sediment pore. Assuming cylindrical pores, Biot derived an expression for the viscosity correction factor F

$$F(\varepsilon) = \frac{1}{4}\frac{\varepsilon T(\varepsilon)}{[1-(2T(\varepsilon)/i\varepsilon)]}, \tag{A5}$$

with

$$T(\varepsilon) = \frac{ber'(\varepsilon) + bei'(\varepsilon)}{ber(\varepsilon) + bei(\varepsilon)} \tag{A6}$$

where ber and bei are the real and imaginary parts of the Kelvin function of the first kind of order zero, ber' and bei' are their derivatives. The argument ε is

$$\varepsilon = a\sqrt{\frac{\omega\rho_f}{\eta}}. \tag{A7}$$

The parameter a is the "pore size parameter" that depends on the shape and size of the sediment pores; it can be expressed by

$$a = \sqrt{\frac{8c\kappa}{\beta}}. \tag{A8}$$

From Eq. (A2), we may derive a complex wave number for shear wave in sediments as

$$k_s^2 = \omega^2\frac{\rho}{\mu}[1-\rho_f^2/\rho m'], \tag{A9}$$

where

$$m' = m - \frac{iF\eta}{\kappa\omega}. \tag{A10}$$

Thus, the shear wave velocity in the sediments is[7,8,10–12]

$$c_s = \mathrm{Re}[(\mu/\rho)^{1/2}(1-\rho_f^2/\rho m')^{-1/2}]. \tag{A11}$$

The shear wave attenuation is

$$\alpha_s = 8.686\,\mathrm{Im}[(\mu/\rho)^{1/2}(1-\rho_f^2/\rho m')^{-1/2}]\,\mathrm{dB/m}. \tag{A12}$$

[1]J. X. Zhou, X. Z. Zhang, and D. P. Knobles, "Low-frequency geoacoustic model for the effective properties of sandy seabottoms," J. Acoust. Soc. Am. **125**, 2847–2866 (2009).
[2]J. X. Zhou and X. Z. Zhang, "Physical parameters for four seabed geoacoustic models from low-frequency measurements," in *Shallow-Water Acoustics*, edited By J. Simmen, E. S. Livingston, J. X. Zhou, and F. H. Li, AIP Conf. Proc. **2712**, 163–172 (2010).
[3]M. A. Biot, "Theory of propagation of elastic waves in a fluid-saturated porous solid. I. Low-frequency range," J. Acoust. Soc. Am. **26**, 168–178 (1956).
[4]M. A. Biot, "Theory of propagation of elastic waves in a fluid-saturated porous solid. II. Higher frequency range," J. Acoust. Soc. Am. **28**, 179–191 (1956).
[5]M. A. Biot, "Generalized theory of acoustic propagation in porous dissipative media," J. Acoust. Soc. Am. **34**, 1254–1264 (1962).
[6]R. D. Stoll, "Acoustic waves in ocean sediments," Geophysics **42**, 715–725 (1977).
[7]R. D. Stoll, "Theoretical aspects of sound transmission in sediments," J. Acoust. Soc. Am. **68**, 1341–1350 (1980).
[8]R. D. Stoll and T. K. Kan, "Reflection of acoustic waves at a water-sediment interface," J. Acoust. Soc. Am. **70**, 149–156 (1981).
[9]R. D. Stoll, "Marine sediment acoustics," J. Acoust. Soc. Am. **77**, 1789–1799 (1985).
[10]T. Yamamoto and A. Turgut, "Acoustic wave propagation through porous media with arbitrary pore size distribution," J. Acoust. Soc. Am. **83(5)**, 1744–1751 (1988).
[11]A. Turgut and T. Yamamoto, "Measurements of acoustic wave velocity and attenuation in marine sediments," J. Acoust. Soc. Am. **87**, 2376–2383 (1990).
[12]M. Badiey, A. H.-D. Chaeng, and Y. Mu, "From geology to geoacoustics-evaluation of Biot-Stoll sound speed and attenuation for shallow water acoustics," J. Acoust. Soc. Am. **103**, 309–320 (1998).
[13]K. L. Williams, D. R. Jackson, E. I. Thorsos, D. J. Tang, and S. G. Schock, "Comparison of sound velocity and attenuation measured in a sandy sediment to predictions based on the Biot theory of porous media," IEEE J. Ocean. Eng. **27(3)**, 413–428 (2002).
[14]R. D. Stoll, "Velocity dispersion in water-saturated granular sediment," J. Acoust. Soc. Am. **111(2)**, 785–793 (2002).
[15]M. J. Buckingham, "Wave propagation, stress relaxation, and grain-to-grain shearing in saturated, unconsolidated marine sediments," J. Acoust. Soc. Am. **108**, 2796–2815 (2000).
[16]M. J. Buckingham, "Compressional and shear wave properties of marine sediments: Comparisons between theory and data," J. Acoust. Soc. Am. **117**, 137–152 (2005).
[17]M. J. Buckingham, "On pore-fluid viscosity and the wave properties of saturated granular materials including marine sediments," J. Acoust. Soc. Am. **122**, 1486–1501 (2007).
[18]N. P. Chotiros and M. J. Isakson, "A broadband model of sandy ocean sediments: Biot-Stoll with contact squirt flow and shear drag," J. Acoust. Soc. Am. **116**, 2011–2022 (2004).
[19]A. D. Pierce and W. M. Carey, "Low-frequency attenuation of acoustic waves in sandy/silty marine sediments," J. Acoust. Soc. Am. **124**, EL308–EL312 (2008).
[20]K. L. Williams, "Sand acoustics: The effective density fluid model, Pierce/Carey expressions, and inferences for porous media modeling," J. Acoust. Soc. Am. **125**, EL164–EL170 (2009).
[21]W. M. Carey, A. D. Pierce, R. E. Evans, and J. D. Holmes, "On the exponent in the power law for the attenuation at low frequencies in sandy sediments," J. Acoust. Soc. Am. **124**(5), EL271–EL277 (2008).
[22]L. M. Brekhovskikh, *Waves in Layered Media* (Academic, New York, 1960), Secs. 27 and 33.
[23]D. E. Weston, "Intensity-range relations in oceanographic acoustics," J. Sound Vib. **18(2)**, 271–287 (1971).
[24]M. J. Buckingham, "Array gain of a broadside vertical line array in shallow water," J. Acoust. Soc. Am. **65**, 148–161 (1979).
[25]D. M. F. Chapman, "What are we inverting for?" in *Inverse Problems in Underwater Acoustics*, edited by M. I. Taroudakis and G. Makrakis (Springer, Berlin, 2001), pp. 1–14.
[26]D. M. F. Chapman, P. D. Ward, and D. D. Ellis, "The effective depth of a Pekeris ocean waveguide, including shear wave effects," J. Acoust. Soc. Am. **85**, 648–653 (1989).
[27]C. T. Tindle and Z. Y. Zhang, "An equivalent fluid approximation for a low shear velocity ocean bottom," J. Acoust. Soc. Am. **91**, 3248–3256 (1992).
[28]Z. Y. Zhang and C. T. Tindle, "Complex effective depth of the ocean bottom," J. Acoust. Soc. Am. **93**, 205–213 (1993).
[29]Z. Y. Zhang and C. T. Tindle, "Improved equivalent fluid approximations for a low shear velocity ocean bottom," J. Acoust. Soc. Am. **98**, 3391–3396 (1995).
[30]R. D. Stoll, "Comments on 'Biot model of sound propagation in water-saturated sand' [J. Acoust. Soc. Am. **97**, 199–214 (1995)]," J. Acoust. Soc. Am. **103**, 2723–2725 (1998).
[31]M. J. Isakson and T. B. Neilsen, "The viability of reflection loss measurement inversion to predict broadband acoustic behavior," J. Acoust. Soc. Am. **120**, 135–144 (2006).

[32]M. Schulkin, "Remote sensing of acoustic properties of shallow water sediments: A review," AD-A192107, Research Report No. APL-UW 8711, Applied Physics Laboratory, University of Washington, September (1987).
[33]E. L. Hamilton, "Shear-wave velocity versus depth in marine sediments: A review," Geophysics **41(5)**, 985–996 (1976).
[34]P. Gabriels, R. Snieder, and G. Nolet, "*In situ* measurements of shear-wave velocity in sediments with higher-mode Rayleigh waves," Geophys. Prospect. **35**, 187–196 (1987).
[35]A. Caiti, T. Akal, and R. D. Stoll, "Estimation of shear wave velocity in shallow marine sediments," IEEE J. Ocean. Eng. **19**(1), 58–72 (1994).
[36]J. A. Collins, G. H. Sutton, and J. I. Ewing, "Shear-wave velocity structure of shallow-water sediments in the East China Sea," J. Acoust. Soc. Am. **100**, 3646–3654 (1996).
[37]J. Xia, R. D. Miller, and C. B. Park, "Estimation of near-surface shear-wave velocity by inversion of Rayleigh waves," Geophysics **64**, 691–700 (1999).
[38]K. Ohta, S. Matsumoto, K. Okabe, K. Asano, and Y. Kanamori, "Estimation of shear wave speed in ocean-bottom sediment using electromagnetic induction source," IEEE J. Ocean. Eng. **33**(3), 233–239 (2008).

Ocean Reverberation: Modeling, Measurements and Inversions

Ji-Xun Zhou[a], Xue-Zhen Zhang[a], Zhaohui Peng[b], and Zhenglin Li[b]

[a] *School of Mechanical Engineering, Georgia Institute of Technology, Atlanta, GA 30332-0405, USA*
[b] *State Key Laboratory of Acoustics, Institute of Acoustics, Chinese Academy of Sciences, Beijing 100190, China.*

Abstract. Research on ocean reverberation has practical and scientific significance. Much progress has been made in the past three decades to improve our understanding of reverberation. However, there remain important unanswered questions and a real scarcity of high-quality basic research data sets. New progress on the reverberation modeling and the low-frequency (LF) seabed scattering characterization in shallow water (SW) requires three essential conditions: 1). A reliable reverberation model using a physics-based seabed scattering function, 2). Carefully calibrated broadband reverberation data, and 3). A ground truth about the seabed geoacoustic model. Some related work on these topics is introduced in this paper. The energy flux method for SW reverberation is briefly introduced. Integration of this method with physics-based seabed scattering models directly and intuitively results in a general expression for SW reverberation. A simple relationship between the classic scattering cross-section and the modal scattering matrix is derived. Some basic research data sets, including the reverberation level/vertical coherence as a function of time, frequency, depth/hydrophone separation and sea state, are reported. Reverberation data and model predictions are in good agreement, which results in some inversion results. The HF seabed scattering models and the energy flux method-derived reverberation model are validated using LF reverberation broadband data.

Keywords: Reverberation, seabed scattering, energy flux method, modal scattering matrix.
PACS: 43.30.Gv, 43.30.Pc, 43.30.Dr, and 43.30.Hw

I. INTRODUCTION

Ocean reverberation is often the most severe limiting factor in relation to the use of active sonar systems in shallow water. Much progress has been made to improve our understanding of reverberation, including reverberation modeling[1-24] and high frequency (HF) seabed scattering.[25] "However, there remain important unanswered questions and a real scarcity of high-quality basic research data sets."[26] SW reverberation involves seabed (surface) scattering as well as two-way sound propagations, which are controlled significantly by a geo-acoustic model of bottom. New progress on reverberation is, in the final analysis, conditioned by our physical understanding of both seabed (and surface) geo-acoustic models and scattering models. Some related work on these topics is introduced in this paper, including theoretical modeling, seabed geaocoustic/scattering models, reverberation data-model comparisons and inversions.

II. THE THORETICAL MODELING: THE ENERGY FLUX METHOD FOR SW REVERBERATION

SW reverberation modeling includes the virtual image method[1], ray method[2], the normal-mode method[3-5], the energy flux method[6-15], the Green's function and the boundary perturbation method[16-20], the two-way coupled mode method[21-22], the finite element method[23], the parabolic equation method[24], etc. This paper mainly introduces the energy flux method for SW reverberation.

A. General Reverberation Expression

The energy flux (angular spectrum) method for modeling SW reverberation, based on the WKB approximation of the normal-mode theory, was first presented in archived Chinese journals.[6-9] Because it is simple and intuitive, the energy flux method has further been developed and widely used for SW reverberation calculations.[10-15]

The sound field in shallow water, generated by a point source (with a source level =0 dB), can be expressed as a summation of normal modes:

$$P(r,z;z_0)=\left(\frac{2\pi i}{r}\right)^{1/2}\sum_n \frac{\Phi_n(z_0)\Phi_n(z)}{k_n^{1/2}}e^{(ik_n-\beta_n)r} \tag{1}$$

The sound intensity is expressed by

$$I(r,z;z_0)=\frac{2\pi}{r}\sum\left\{\frac{|\Phi_n(z_0)|^2|\Phi_n(z)|^2}{k_n}e^{-2\beta_n r} + \sum\sum_{n\neq m}\frac{\Phi_n(z_0)\Phi_m^*(z_0)\Phi_n(z)\Phi_m^*(z)}{k_n^{1/2}k_m^{1/2*}}e^{-[(\beta_n+\beta_m)+i(k_n-k_m)]r}\right\}. \tag{2}$$

where Φ_n is the eigenfunction, k_n is the longitudinal wave number, β_n is the modal attenuation factor of the nth mode, z_0 is the source depth and z is the receiver depth. Details of the interference fine structures are sometimes of no use for sonar performance predictions. Thus, the 2nd term of Eq. (2) can be neglected.

According to Zhou [6]: (a) Using the W.K.B approximation to the mode solution of the wave equation; (b) Expressing (slowly varying) energy depth distribution of the nth mode by

$$\overline{|\Phi_n(z)|^2}=\frac{2}{S_n\tan\theta_n(z)} \tag{3};$$

(c) Decomposing each normal-mode into a pair of up- and down-going local quasi-plane waves (Their grazing angles satisfy $k_n=k(z)\cos\theta_n(z)$); and

(d) Using $dn=S_n k(z_0)\sin\theta_n(z_0)d\theta_n(z_0)/2\pi$ to change the incoherent summation over modes into an integration over the mode-ray angle $\theta_n(z_0)$,

we can derive a general expression for the average field intensity in shallow water given by:

$$I(r,z;z_0)=\frac{2}{r}e^{-\alpha_w r}\int\frac{2e^{-2\beta_n r}}{S_n\tan\theta_n(z)}d\theta_n(z_0) \qquad (4)$$

Here, S_n is the cycle distance of the n[th] mode-ray which is related to modal wave numbers by

$$S_n=2\pi/(k_n-k_{n+1}) \qquad (5)$$

α_w is the water column absorption coefficient; $\theta(z_0)$ is the grazing angle of the mode-rays at the source depth and $\theta(z)$ is the grazing angle at the receiver depth (not just at the source/receiver location). The modal attenuation factor, β_n, can be expressed approximately in terms of the bottom reflection coefficient, $V(\theta)$:

$$\beta_n=-\frac{\ln|\mathrm{V}(\theta_\mathrm{n})|}{S_n(\theta_n)+\Delta_n} \qquad (6)$$

where Δ_n is a beam displacement on the bottom reflection. Using different methods, both Brekhovskikh[27, 28], Smith[29] , Brekhovskikh and Lysanov[30] , and Katsnelson and Petnikov[31] obtained an expression that is similar to (4).

For calculating the average reverberation intensity in shallow water, as weighting functions, the two-way propagation angular spectra and the classic seabed scattering function (cross section) are well connected in the angular domain:

$$\begin{aligned}R(r,z;z_o)&=\frac{4}{r^2}e^{-2\alpha_w r}\iint\frac{\exp[\dfrac{2\ln|V[\theta_m(h)]|}{S_m}r]}{S_m\tan\theta_m(h)}\times A\\&\times\sigma[\theta_m(h),\theta_n(h)]\times\frac{\exp[\dfrac{2\ln|V[\theta_n(h)]|}{S_n}r]}{S_n\tan\theta_n(z)}d\theta_m(z_0)d\theta_n(h) \qquad (7)\\&=\frac{4}{r^2}e^{-2\alpha_w r}\int R_{aps}(r,z,z_0)d\theta_n(h)\end{aligned}$$

Here h is the water depth, $\sigma[\theta_m(h),\theta_n(h)]$ can be any seabed scattering cross section with different scattering mechanisms in consideration. A is a seabed scattering area. The angular spectrum of reverberation is expressed by:

$$R_{aps}(r,z,z_0)=\int\frac{\exp[\dfrac{2\ln|V[\theta_m(h)]|}{S_m}r]}{S_m\tan\theta_m(h)}\times A\times\sigma[\theta_m(h),\theta_n(h)]\times\frac{\exp[\dfrac{2\ln|V[\theta_n(h)]|}{S_n}r]}{S_n\tan\theta_n(z)}d\theta_m(z_0) \qquad (8)$$

B. A Reverberation Expression in the Angular Domain for the Pekeris Waveguide

For a special case, in the Pekeris waveguide (an iso-velocity water), Eq. (7) becomes:

$$R(r)=\frac{\pi c_w\tau_0}{h^2 r}e^{-2\alpha_w r}\iint e^{\frac{\ln|V(\theta_m)|}{h}r\tan\theta_m}\times\sigma_b(\theta_m,\theta_n)\times e^{\frac{\ln|V(\theta_n)|}{h}r\tan\theta_n}d\theta_m d\theta_n \qquad (9)$$

Here the seabed scattering area $A\approx\pi r c_w\tau_0$. That is, the waveguide dispersion spreading[5] has been assumed to be much less than the signal pulse duration, τ_0.

C. A General Reverberation Expression in the Modal Domain for a non-Pekeris Waveguide

For a non-Pekeris SW waveguide, Eq. (7) is changed back to a summation over the mode numbers, resulting in a general expression in the modal domain:

$$R(r,z;z_0)=\frac{\pi^2}{r^2}e^{-2\alpha_w r}\sum_m\sum_n\frac{\overline{|\Phi_m(z_0)|^2}\;\overline{|\Phi_n(z)|^2}}{k_m k_n}e^{-2(\beta_m+\beta_n)r}\times A\times\sigma(\theta_m,\theta_n)\times\overline{|\Phi_m(h)|^2}\;\overline{|\Phi_n(h)|^2} \qquad (10)$$

Using (5) and the property of the slowly depth-varying energy dependence of the normal mode $\overline{|\Phi_n(z)|^2}$, Eq. (10) can be expressed by:

$$R(r,z;z_0)=\frac{c_w\tau_0}{\pi r}e^{-2\alpha_w r}\sum_m\sum_n\frac{k_m(k_m-k_{m+1})^2\exp(-2\beta_m r)}{\left[k_w^2(z_0)D(z_0)+k_w^2(z_0)-k_m^2\right]^{1/2}\left[k_w^2(h)D(h)+k_w^2(h)-k_m^2\right]^{1/2}}$$
$$\times\sigma(\theta_m,\theta_n)\times\frac{k_n(k_n-k_{n+1})^2\exp(-2\beta_n r)}{\left[k_w^2(h)D(h)+k_w^2(h)-k_n^2\right]^{1/2}\left[k_w^2(z)D(z)+k_w^2(z)-k_n^2\right]^{1/2}} \qquad (11)$$

where $D(z)$ is a small modification factor introduced by Zhang and Jin[4] to overcome a problem when a receiver is near a turning point,

$$D(z)=0.875\left|\frac{1}{\pi f}\frac{dc(z)}{dz}\right|^{2/3} \qquad (12)$$

Eq. (11) is a simple and practical expression for SW reverberation in the modal domain. Using the classic cross sections of seabottom scattering $\sigma(\theta_m,\theta_n)$ and any available normal-mode code, Eq. (11) can be used to calculate reverberation intensity in a SW waveguide with an arbitrary velocity profile. It only requires two parameters: real and imaginary parts of the modal eigenvalue, k_m and β_m.

D. Reverberation Vertical Coherence in Shallow Water

Spatial coherence in shallow water may be defined as a measure of arrival angles' spreading of signals. The vertical coherence of the SW sound field and the angular power spectrum of the arrival direction have a relationship that is similar to the Fourier transform:[7, 32-34]

$$\rho_v(\Delta z,r,z;z_0)=\frac{\int I_{aps}(\theta,r,z;z_0)e^{-jk\Delta z\sin(\theta)}d\theta}{\int I_{aps}(\theta,r,z;z_0)d\theta} \qquad (13)$$

Where Δz is the vertical separation of a pair of hydrophones, and k is the wave number. Using a seabed scattering cross-section and the reverberation angular

spectrum $R_{aps}(r,z,z_0)$ in (8), an expression for a normalized vertical cross-correlation can be obtained either in the angular domain or in the modal domain.[34]

E. The Effective Geoacoustic Model for Sandy Seabottoms

Without a reliable geoacoustic model, all data-model comparisons in forward physics problems of reverberation, or reverberation inversion results, are questionable.

The debate on the sound speed dispersion and the frequency dependence of sound attenuation in seabottoms has persisted for decades. One of our recent papers analyzes and summarizes low-frequency (LF) measurements in shallow water that have resulted in the identification of nonlinear frequency dependence of sound attenuation in the effective media of sandy seabottoms (shown in Fig. 1). Both the LF field-derived sound speed and the attenuation can be well described by the Biot-Stoll model, using parameters that are consistent with either theoretical considerations or experimental measurements.[35] Based on this effective Biot model from the LF field measurements, the bottom reflection loss at low grazing angles is shown in Fig. 2. The interesting frequency dependence in Fig. 2 predicts that the water-sediment interface for sandy bottoms may act as a filter with respect to the broadband long-range sound field where lower-order modes with low-grazing angles are predominant. It also affects the frequency dependence of both long-range reverberation and its inverted geophysical parameters.

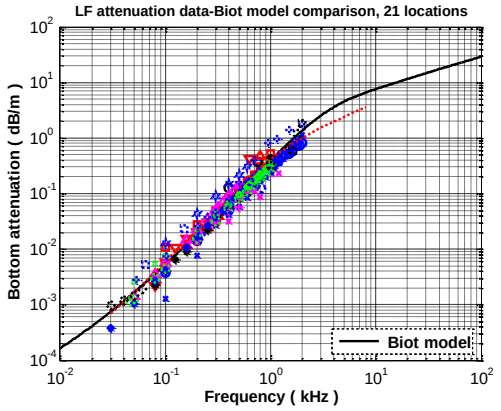

FIG. 1. Effective sound attenuation in sandy bottoms from LF field measurements[35]

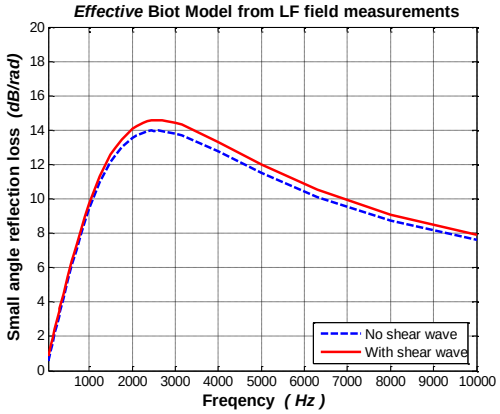

FIG. 2. Bottom reflection loss vs. frequency at low grazing angles

F. Seabed Scattering Models

1. Semi-empirical Seabed Scattering Cross-sections

For convenience, semi-empirical seabed scattering cross-sections are often assumed separable for incident angle and scattering angle[6,8]

$$\sigma(\theta_i,\theta_s) = \mu \sin^{n/2}\theta_i \sin^{n/2}\theta_s \qquad (14)$$

A special case for $n=2$ is the Lambert law, which is widely used for HF data-model comparisons. However, this model has no physical basis.

2. Physics-based Seabed Scattering Cross-sections

In the past 30 years, one of the major accomplishments in ocean acoustics is the improvement in our understanding of seabed scattering, resulting from a significant effort, both in at-sea measurement and in theoretical modeling, made by many investigators. These accomplishments, including the rough bottom scattering (RBS) model and the sediment volume scattering (SVS) model, have been summarized in an underwater acoustics monograph by Jackson and Richardson.[25] According its introduction, "This monograph will emphasize small spatial scale and 'high frequencies', very roughly, frequencies from 10 kHz to 1 MHz". We will use SW reverberation data to test their suitability at low frequencies.

G. Modal Scattering Matrix in SW Waveguide

Using the energy flux method for SW reverberation, we have proved that, in Eq. (10) the modal scattering matrix in the SW waveguide between mode *m* and mode *n* can be expressed by:

$$MSM(m,n) = \sigma(\theta_m,\theta_n) \times \overline{|\Phi_m(h)|^2}\ \overline{|\Phi_n(h)|^2}$$
$$= \frac{\Phi_m^2(h)}{|1+V_{ww}(\theta_m)|^2} \times \sigma(\theta_m,\theta_n) \times \frac{\Phi_n^2(h)}{|1+V_{ww}(\theta_n)|^2} \qquad (15)$$

Here $\theta_m = \cos^{-1}[k_m / k_w(h)]$, and $\Phi_m(h)$ is the amplitude of the mth mode at the water-bottom interface. $V_{ww}(\theta)$ is the bottom reflection coefficient of mode-decomposed plane waves. $\sigma(\theta_m,\theta_n)$ can be any physics-based seabed scattering cross section. For example, inputting the roughness bottom scattering (RBS) model into (15) can directly result in an expression for modal scattering matrix in the SW waveguide that is the same as that derived from the Green's function and the boundary perturbation method by Tracey and Schmidt.[16,17]

H. A Simple Formula to Derive LF Seabed Scattering at Low Grazing Angles in the Pekeris Waveguide

Low-frequency seabed scattering at low grazing angles (LGA) is almost impossible to directly measure in shallow water (SW), except through inversion from reverberation. The closed-form expressions for SW reverberation in the isovelocity waveguide derived from the energy flux method show that, at a given distance in the three-half law region the complex, seabed scattering by all modes/rays with different incident and scattering angles can equivalently be represented by the seabed back-scattering at a single angle of $\theta_{eg}(r) = \sqrt{h/(\pi Q r)}$. This equivalent angle depends on distance r, seabed reflection loss factor Q and water depth h.[36] The simple equivalent relationship can be expressed by:

$$BBS(\theta_{eg}) = RL(r) - 10\log_{10}(c\tau_0\pi^2 / 4QHr^2) + att_w \times 2r \qquad (16) \text{ or}$$

$$BBS(\theta_{eg}) = RL(r) + 2TL(r) + 6.0dB - 10\log_{10} A(r) + att_w \times 2r \qquad (17)$$

Here att_w is the sound absorption in the water column in dB/m. τ_0 is the signal duration. $A = \pi rc\tau_0$ is the seabed scattering area. Eq. (16) or (17) can be used to derive the LF&LGA seabed back scattering strength by measuring the reverberation level (RL) or/and transmission loss (TL). The method is valuable because it allows the seabed backscattering strength to be inverted at frequencies and angles where no practical method of measurements exists.

III. REVERBERATION MEASUREMENTS

A quality database of reverberation measurements is an absolutely essential component of any effort to understand the shallow-water reverberation problem. However, to get wideband reverberation data for both short- and long-range data in a frequency range of 100-3000 Hz is a delicate task that can be subject to errors.[37] Through years' efforts, a quality database of broadband reverberation has been set up/accumulated. This database has been (and will be) used to compare with theoretical reverberation models and to characterize the LF seabed scattering. Some examples selected from this database are shown in this section.

A. Reverberation Level $RL(t, f)$ as a Function of Time and Frequency

Reverberation measurements were carefully calibrated. RL was normalized to the source level (SL). Fig.3 shows $RL(t)$ of 700-2500 Hz, obtained on June 3, 2012 at the ASIAEX site in the East China Sea. Fig.4 shows $RL(f)$ at 4 seconds after an explosive source is detonated, obtained from four sites.

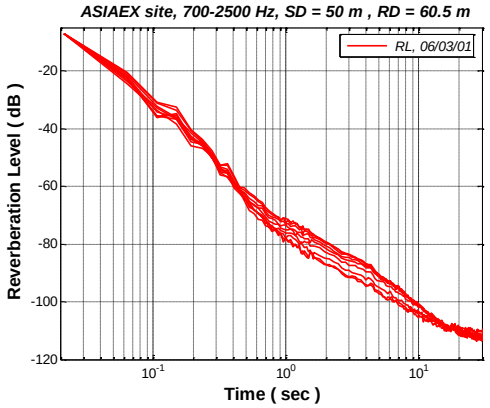

FIG. 3. $RL(t)$ at the ASIAEX site.

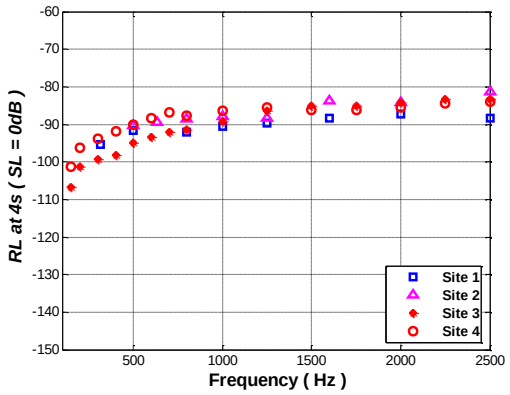

FIG. 4. $RL(t)$ at 4s from 4 sites

B. *RL* Depth Dependence and Interference Phenomenon

The first China-US joint ocean acoustics experiment (YS96) was conducted in the summer of 1996 in the Yellow sea with a strong thermocline. The reverberation data exhibited some special characteristics, including strong depth dependence, a regular interference, a resonant volume-scattering etc.[38,39] Fig. 5a shows the $RL(t, r; z_0)$ at 800 Hz when a hydrophone is located below the thermocline

($RD = 60\,m$), and two sources are located below and above the thermocline, respectively ($SD = 50\,m$, *or* $7\,m$). Fig. 5b shows that the *RL* exhibits a regular interference structure with increasing time (distance), when a receiver is in the thermocline (*RD=22 m*) and the source is below the thermocline (*SD=50*).

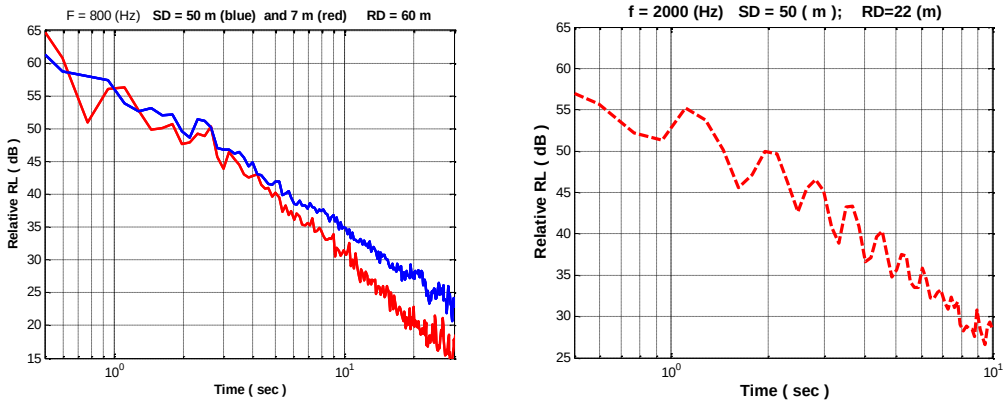

(a) (b)

Fig. 5. Reverberation data at the YS96 site show (a) Strong depth dependence, (b) Regular interference oscillations when a receiver is in the thermocline.

C. Unknown Resonant Volume Scattering in Water Column

Reverberation data at the YS96 site also showed an interesting resonant volume-scattering in the water column as shown in Fig. 6: 1). Around 20-23 seconds after the explosive sources were denoted (about *15-16 km* away from a source), all 5 shot-produced reverberation data exhibited strong water volume scattering between 700 *Hz* and 3000 *Hz*, peaked around 1500 *Hz*. It was about 7-10 *dB* higher than bottom scattering-induced RL from same distance. The horizontal size (dimension) of a scattering volume was about 2000 meters. The reverberation at 29 km away from the source, produced by shot I, also had a stronger wideband volume scattering. But the horizontal size of the scattering volume was much smaller. 2) For shot III (2 minutes after the first shot I), an apparent fish (group) produced resonant scattering around 300 Hz at around 29 km away from the source/receiver location. The scattering strength at 300 Hz was about 20 dB higher than the bottom scattering from same distance. However, the wideband volume scattering at same distance shown in the shot I disappeared. Both the source and the receiver were located below the thermocline. The scattering mechanism that responded to the observed volume scattering is unknown.

D. Reverberation Vertical Coherence

Reverberation vertical coherence (RVC) from three sites has been analyzed and added to our quality data base for further reverberation modeling and for the LF seabed scattering characterizations. For example, Figs.7a-7b show the RVC as function of time, frequency and hydrophone separation, obtained from the YS'96 site and the ASIAEX site, respectively.

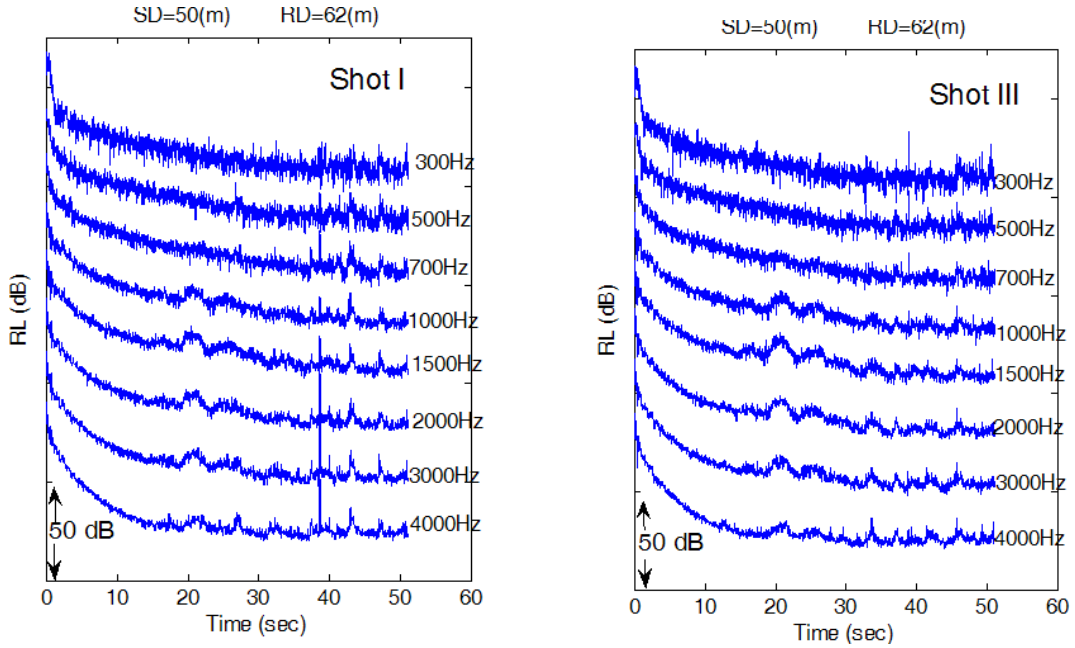

FIG. 6. Reverberation data at the YS96 site show resonant scattering in the water column around 20s to 23 s, peaked around at 1500 Hz

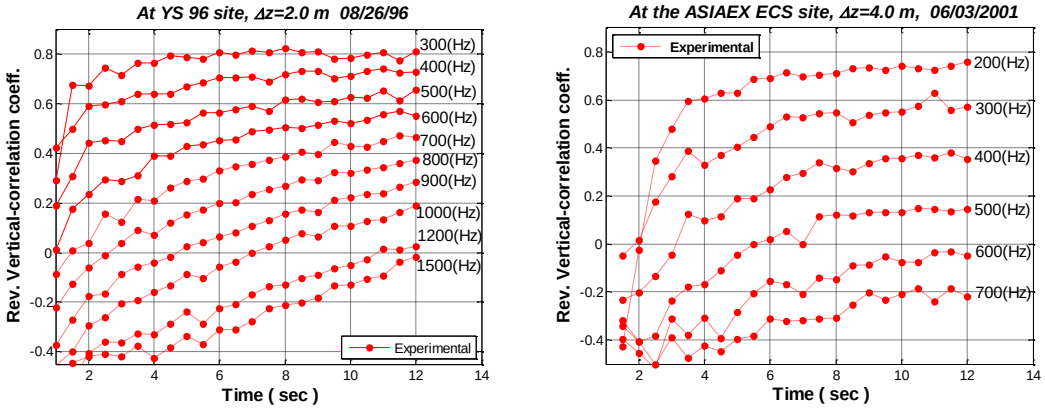

FIG. 7. Reverberation vertical coherence measured at
(a) The YS96 site ($\Delta z = 2.0\ m$), (b) At the ASIAEX site ($\Delta z = 4.0\ m$).

E. Effects of Sea State on $RL(t,z;z_0)$ and $RVC(\Delta z,t,f)$

Wideband reverberation measurements were repeatedly conducted at a fixed location in the center of the ASIAEX ECS site. Data were collected on June 3rd and June 5th, 2001 using the same measurement system. Sound-speed profiles during the two measurement periods were similar to each other. However, wind speed and RMS surface-wave height (σ) changed from 2.74 m/s and 0.10 m on June 3rd to 7.45 m/s and 0.33 m on June 5th. (See Fig. 8, where the wind speed was measured at 14 m elevation). Thus, these measurements offer an opportunity to evaluate sea surface effects on reverberation level (RL), reverberation vertical coherence (RVC), and

RVC-inverted bottom acoustic parameters in shallow water (SW).[40,41] Two sets of data for RVC and RL in a frequency range of 100-2500 Hz show differences that are the apparent effects of the surface roughness. In contrast to many peoples' intuition: with increasing sea state, the RVC increases (shown in Fig. 9), but the RL decreases (shown in Fig. 10).

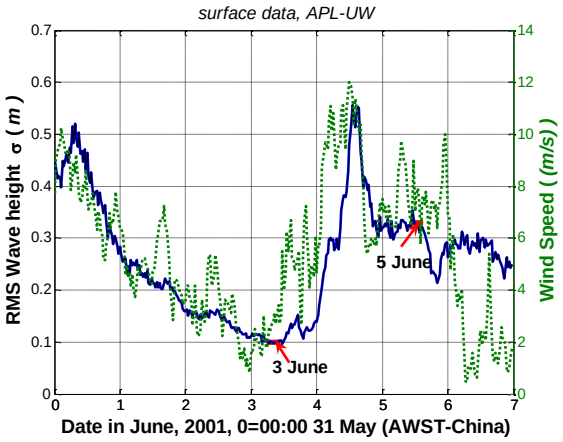

FIG. 8. Wind speed and surface wave height variability during the ASIAEX experiment. (Collected and analyzed by Peter Dahl, APL-UW)

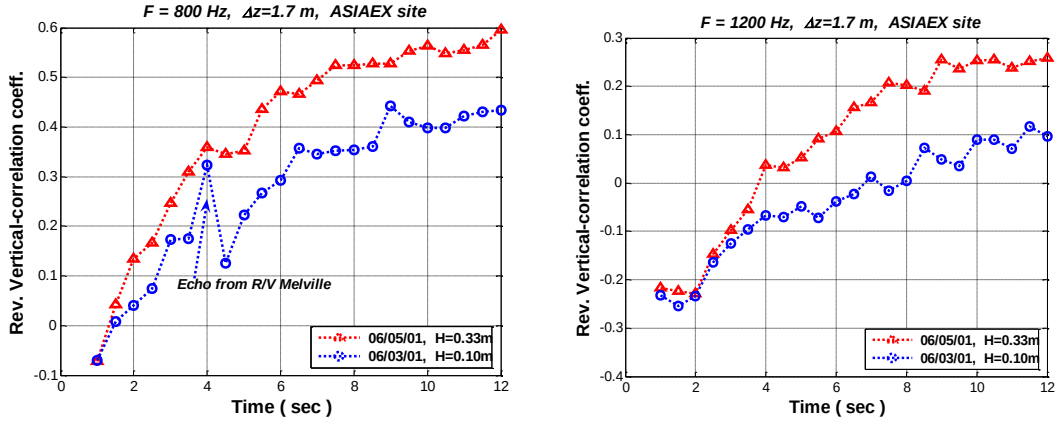

FIG. 9. The RVC increases with increased sea state, (a) 800 Hz, (b) 1200 Hz

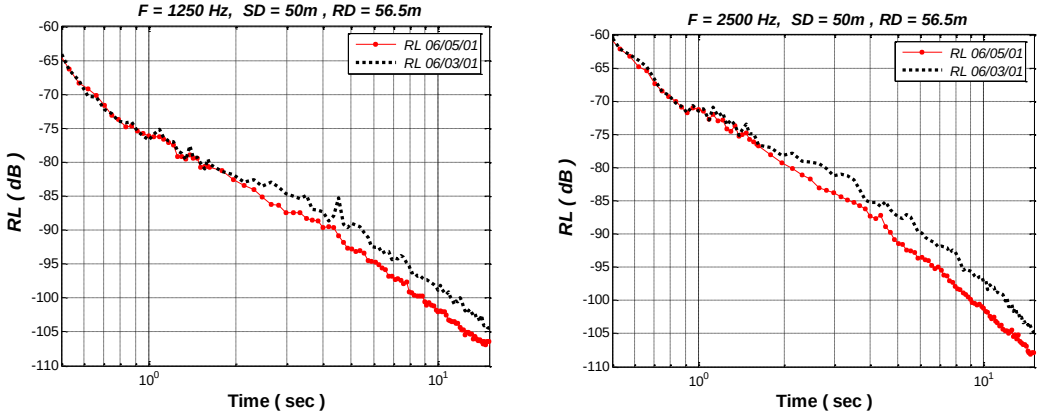

FIG. 10. The RL decreases with increased sea state, (a) 1250 Hz, (b) 2500 Hz

IV. REVERBERATION DATA-MODEL COMPARISON AND INVERSION

A. Data-model Comparisons Using Physics-based Seabed Scattering Model

Two reverberation measurements were conducted in the East China Sea. Two sound velocity profiles (SVP) are shown in Fig. 11. The SVP at the ECS site I was almost iso-velocity (the Pekeris shallow water). The SVP at the ASIAEX site on June 3, 2001 had a weaker negative gradient.

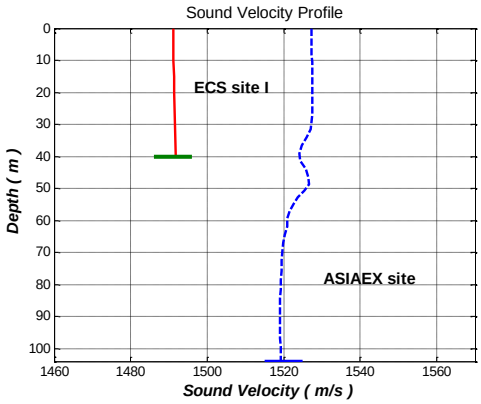

FIG. 11. Sound velocity profiles at two sites during reverberation measurements

The effective Biot seabed geoacoustic model[35] derived from the LF field measurements is used in our reverberation modeling. The physics-based rough seabed scattering cross section and the sediment volume cross section have been extensively tested with HF data[25], and are used in Eq. (9) and Eq. (11) for data-model comparisons. Figs. 12a and 12b show the reverberation data-model comparisons at the ECS site I, using Eq. (9) in the angular domain for a Pekeris waveguide. Figs. 13a and 13b show the data-model comparisons at the ASIAEX site, using Eq. (11) in the modal domain for the non-Pekeris waveguide. All required spectral strength ω_2 and the exponent γ_2 for the bottom roughness spectrum, and the sediment volume scattering cross-section σ_V for the sediment volume scattering are shown in these figures. The data and the model predictions are in good agreement. That is, the physics-based HF seabed scattering models can be used to predict LF reverberation using a right set of seabed geoacoustic and scattering parameters. Our reverberation expressions in both the angular and the modal domain are also validated.

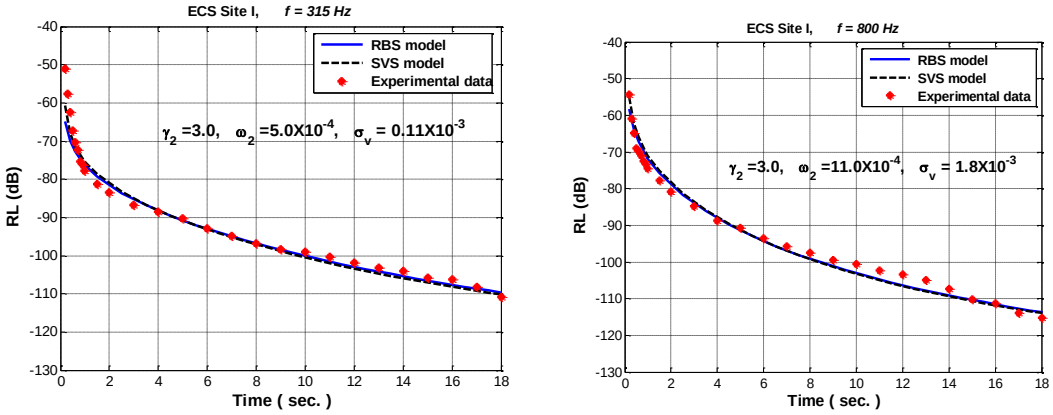

(a) (b)

FIG. 12. Data-model comparison at the ECS site I (the Pekeris waveguide) using Eq. (9), (a) 315 Hz, (b) 800 Hz

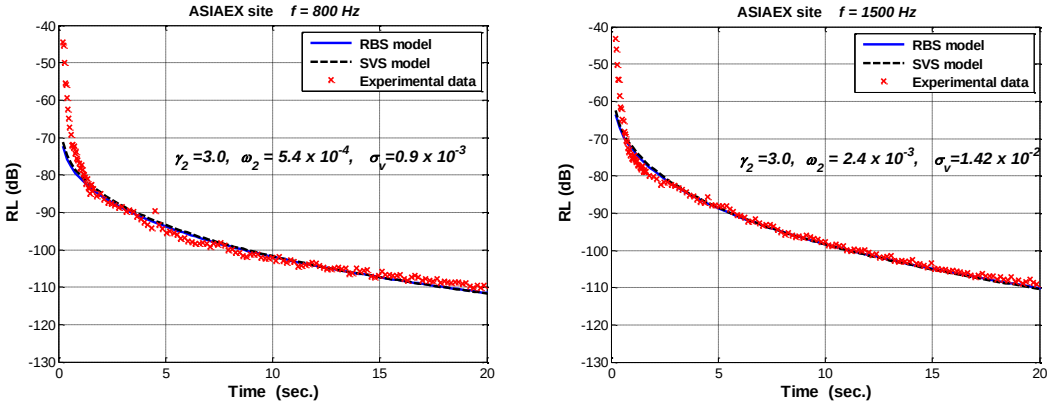

(a) (b)

FIG. 13. Data-model comparison at the ASIAEX site (non-Pekeris waveguide), using Eq. (11) (a) 800 Hz, (b) 1500 Hz

B. Low Grazing Angle Scattering at Low Frequencies[36]

The equivalent relationship between the multi-mode/ray scattering and one specific angle backscattering (Eq. 16) and the LF field derived effective Biot seabed geoacoustic model are used to extract the bottom backscattering strength as a function of angle and frequency. Figs.14a and 14b show the RL inverted bottom backscattering strength as a function of grazing angle and frequency. Apparently, the LF bottom scattering exhibits strong frequency dependence. At the small grazing angles of $4^{\circ}, 6^{\circ}, 8^{\circ}$ and 10°, the bottom backscattering strength between 200 Hz and 2500 Hz can approximately be expressed by $BBS(\theta) = -34.7 + 10\log_{10}(f/1000)$[27] (dB).

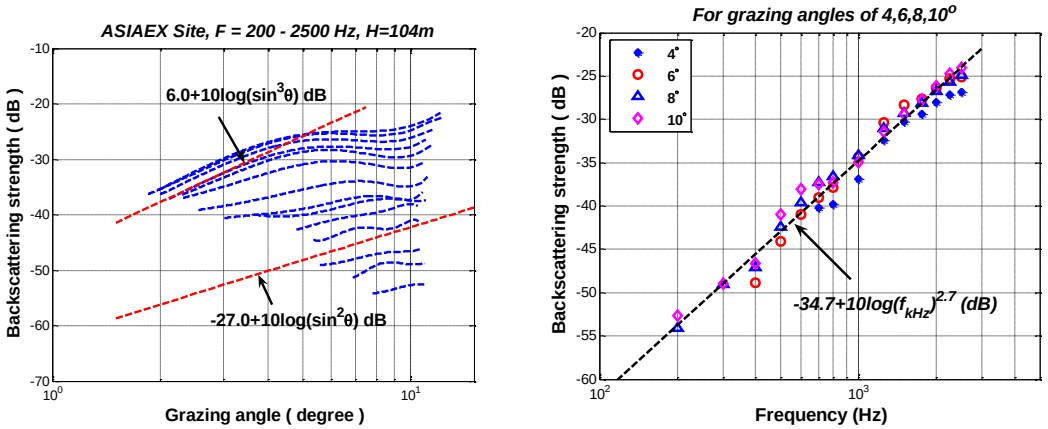

(a) (b)

FIG. 14. RL inverted LF bottom backscattering strength vs. (a) angle, (b) frequency

C. RVC-inverted bottom acoustic parameters[34,41]

Reverberation vertical coherence has been used to derive effective seabottom sound speed, attenuation and reflection loss. Fig. 15a shows the best match between the measured and theoretical RVC at 400 Hz for the ASIAEX site using a pair of values for bottom sound velocity and attenuation. Fig. 15b shows the effective boundary (bottom and surface) reflection loss difference at the ASIAEX site, inverted from RVC on 3 June and 5 June, respectively. It shows that higher boundary loss corresponds to the increase of the sea state. This figure also shows that the additional surface loss in shallow water is less than the coherent mean reflection loss predicted by the perturbation theory with the Pierson-Moskowitz model, because some forward scattered energy returns to the waveguide. These results were obtained using the semi-empirical seabed scattering model. In the future, it is desirable to use physics-based seabed scattering models to get better results, including the sea surface forward scattering.

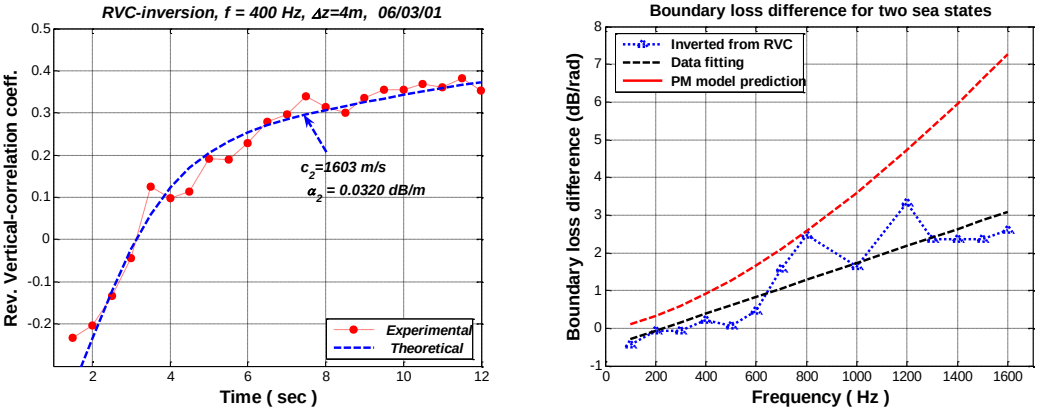

(a) (b)

FIG. 15. RVC-inverted seabottom parameters at the ASIAEX site. (a) Bottom velocity and attenuation at 400 Hz, (b) RVC-inverted boundary loss difference for two sea states on 3 and 5 June, 2001.

D. Reverberation-inverted LF seabed scattering parameters

The reverberation data-model comparisons in Sec. IV (A) have proved that the well developed HF physics-based seabed scattering model can directly be used to predict LF SW reverberation. However, the broadband reverberation-inverted LF seabed scattering parameters are different from those values often used for HF modeling or testing. For example, the HF roughness spectrum exponent is restricted to the range of with a mean of 3.0. But, the long-range reverberation inverted LF roughness spectrum exponent has a much smaller value with a mean of 1.3. The HF sediment volume scattering cross section σ_V is generally assumed to have linear frequency dependence. However, the broadband LF long-range reverberation-inverted σ_V exhibits much stronger frequency dependence, up to the fourth power of the frequency.

V. SUMMARY

The energy flux method for SW reverberation based on the WKB approximation of normal-mode theory, first presented three decades ago in archived Chinese journals, is briefly introduced with new results. Benefiting from the accomplishments of the seabed scattering research community, we have integrated the energy flux method for SW reverberation with the physics-based seabed scattering models, and obtained a general expression for SW reverberation in the angular domain (Eq. 7) or in the modal domain (Eq. 11). The integration also directly results in a simple relationship between the classic boundary scattering cross-section and the modal scattering matrix in SW waveguide expressed by Eq. (15). The development of a high quality reverberation data base has become a pressing task for SW reverberation modeling and for LF seabed scattering characterization. Some data on RL and RVC as a function of time, frequency, depth/hydrophone separation and sea state, are reported. The reverberation data and the energy flux method-derived reverberation model are in good agreement. Reverberation-based inversion results, briefly reported in this paper, include the low grazing angle seabed scattering strength vs. angle and frequency, seabottom velocity and attenuation, additional sea surface reflection loss, and the LF seabed scattering parameters for the rough seabed scattering and the sediment volume scattering section, etc.

ACKNOWLEDGMENTS

This work was supported by ONR OA322 and CAS.

REFERENCES

1. K. V. Mackenzie, "Long-range shallow-water bottom reverberation," J. Acoust. Soc. Am. **34**, 62-66 (1962).
2. C. Y. Wu, ACTA ACUSTICA (Chinese) **4,** 114-119 (1979) C.Y. Wu, "Calculation of shallow water reverberation intensity based on ray theory, Part (1)," in Acta Acustica (Chinese) **4**, 114-119 (1979). Part (2) in Acta Acustica (Chinese), 5, 210-220 (1980).
3. H.P. Bucker and H.E. Morris, "Normal-mode reverberation in channels or Ducts," J. Acoust. Soc. Am. **44**, 827-828 (1968).
4. R.H. Zhang and G.L. Jin, "Normal-mode theory of average reverberation intensity in shallow-water," J. Sound Vib., **119**, 215-223 (1987).
5. D.D. Ellis, "A shallow-water normal-mode reverberation model," J. Acoust. Soc. Am. **97**, 2804-2814 (1995).
6. J.X. Zhou, "The Analytical method of angular power spectrum, range and depth structure of the Echo-to-Reverberation Ratio in Shallow Water Sound Field,"ACTA ACUSTICA (Chinese), **5** (2), 86-99 (1980).
7. J.X. Zhou, "The vertical coherence of long-range reverberation in the shallow water homogeneous layer," ACTA OCEANOLOGIA SINICA, **1** (2), 212-218 (Dec. 1979) (in Chinese).
8. J. X. Zhou, D.H. Guan, E.C. Shang and E.S. Luo, "Long-range reverberation and bottom scattering strength in shallow water," Chin. J. Acoust. **1**, 54-63 (1982).
9. J.X. Zhou, X.Z. Zhang and E.S. Luo, "Shallow-water reverberation and small angle bottom scattering," in <Shallow-water Acoustics> edited by R.H. Zhang and J.X. Zhou, pp. 315-322 (China Ocean Press, 1997)
10. C.H. Harrison,"Closed-form expressions for ocean reverberation and signal excess with mode stripping and Lambert's law," J. Acoust. Soc. Am. **114**, 2744-2756 (2003).
11. C.H. Harrison, "Closed form bistatic reverberation and target echoes with variable bathymetry and sound speed," IEEE J. Ocean Eng. **30**, 660-675 (2005).
12. C.W. Holland, "Constrained comparison of ocean waveguide reverberation theory and observations," J. Acoust. Soc. Am. **120**, 1922-1931 (2006).
13. M. A. Ainslie, "Observable parameters from multipath bottom reverberation in shallow water," J. Acoust. Soc. Am. **121,** 3363-3376 (2007).
14. C.W. Holland, "Fitting data, but poor predictions: Reverberation prediction uncertainty when seabed parameters are derived from reverberation measurements," J. Acoust. Soc. Am. **123**, 2553-2562 (2008).
15. M. A. Ainslie, *Principles of Sonar Performance Modeling*, (Springer-Verlag Berlin Heidelberg 2010), pp. 495-510.
16. B.H. Tracey and H. Schmidt, "Seismo-acoustic field statistics in shallow water," IEEE J. Ocean. Eng. **22**, 317-331 (1997)].
17. H.C. Song, S. Kim, W.S. Hodgikiss and W.A. Kuperman, "Environmentally adaptive reverberation nulling using a time reversal mirror," J. Acoust. Soc. Am., **116** (2), 762-768 (2004).
18. E.C. Shang, T.F. Gao and J.R. Wu, "A shallow-water reverberation model based on perturbation theory," IEEE J. Oceanic Eng., **33** (4), 451-461 (2008).
19. A. Galinde, N. Donabed, M. Andrews, S. Lee, N.C. Markris and P. Ratial, "Range-dependent waveguide scattering model calibrated for bottom reverberation in a continental shelf environment," J. Acoust. Soc. Am. **123**, 1270-1281 (2008).
20. D.J. Tang and D.R. Jackson, "Application of small-roughness perturbation theory to reverberation in range-dependent waveguide," J. Acoust. Soc. Am. **131**, 4428-4441 (2012).
21. S. A. Stotts and R.A. Koch, "Rough surface scattering in a Born approximation from a two-way coupled-mode formalism," J. Acoust. Soc. Am. **125**, EL242-EL248 (2009).
22. S.A. Stotts, D.P. Knobles and R.A. Koch, "Scattering in a Pekeris waveguide from a rough bottom using a two-way coupled mode approach," J. Acoust. Soc. Am. **129**, EL172-178 (2011).
23. M.J. Isakson and N.P. Chotiros, "Finite element modeling of reverberation and transmission loss in shallow water waveguides with rough boundaries," J. Acoust. Soc. Am. **129**, 1273-1279 (2011).
24. J.F. Lingevich and K.D. LePage, "Parabolic equation simulations of reverberation statistics from non-Gaussian-distributed bottom roughness," IEEE J. Ocean. **35**,199-208 (2010).

25. D.R. Jackson and M.D. Richardson, *High-frequency Seafloor Acoustics,* (Springer, New York, 2007).
26. J.R. Preston, "Report on the 1999 ONR Shallow-water Reverberation Focus Workshop," Tech. Memorandum No. 99-155, Applied Research Laboratory, Penn State University, 31 Dec., 1999.
27. L.M. Brekhovskikh, "The Average Field in an Underwater Sound Channel," Sov. Phys. Acoust., **11**(2), 126-134 (1965).
28. L.M. Brekhovskikh, "Elements of sound field theory in the ocean," in <*Ocean Acoustics*>,ed. By LM. Brekhovskikh , pp.79-162, Nauka, Moscow 1974 (in Russian)
29. P.M. Smith, "Average sound transmission in range-dependent channels," J. Acoust. Soc. Am. **55**, 1197-1204 (1974).
30. L.M. Brekhovskikh and Y.P. Lysanov, <*Fundaments of Ocean Acoustics*>,3rd Edition, (Springer-Verlag, New York, 2003) Sec. 5.6
31. B. G. Katsnelson and V.G. Petnikov, <*Shallow-Water Acoustics*>, (Springer-Praxis, New York, 2002), Sec. 3.5.
32. P.M. Smith, "Spatial coherence in multipath or multimodal channels,"J. Acoust. Soc. Am. **60**, 305-310 (1976).
33. J.X. Zhou, "Vertical coherence of the sound field and boundary loss in shallow water," Chinese Phys., **1**, 494-504(1981).[Acta Acust., **4** ,34-43 (1979)]
34. J.X. Zhou, X.Z. Zhang, P.H. Rogers, J.A. Simmen, P. H. Dahl, G.L. Jin and Z.H. Peng, "Reverberation vertical coherence and seabottom geoacoustic inversion in shallow water," IEEE J. Ocean Eng. **29**, 988-999 (2004).
35. J.X. Zhou, X.Z.Zhang, and D.P. Knobles, "Low-frequency geoacoustic model for the effective properties of sandy seabottoms," J. Acoust. Soc.Am., **125**, 2847-2866 (2009).
36. J.X. Zhou and X.Z. Zhang, "Low frequency seabed scattering at low grazing angles," J. Acoust. Soc.Am., **131**, 2611-2621 (2012).
37. J.X. Zhou and X.Z. Zhang, "Shallow-water reverberation level: measurement techniques and initial reference values," IEEE J. Ocean Eng. **30**, 832-842 (2005).
38. J.X. Zhou, X.Z. Zhang, and G.L. Jin, "Reverberation characteristics in shallow water with a strong thermocline," J. Acoust. Soc. Am. **107**, 2920 (2000).
39. F. Li, G. Jin, R. Zhang, J. Liu, and L. Guo, "An oscilation phenomenon of reverberation in shallow water with a thermocline," *J. Sound Vib.*, **252**, 457-468(2002).
40. F.H. Li, J.J. Liu and R.H. Zhang, "A model/data comparison for shallow-water reverberation," IEEE J. Ocean Eng. **29**, 1060-1066 (2004).
41. J.X. Zhou, X.Z.Zhang Z. H. Peng and J.S. Martin,"Sea surface effects on shallow-water reverberation," J. Acoust. Soc.Am., **121**, 98-107 (2007).

Integrating the energy flux method for reverberation with physics-based seabed scattering models: Modeling and inversion

Ji-Xun Zhou[a] and Xue-Zhen Zhang
School of Mechanical Engineering, Georgia Institute of Technology, Atlanta, Georgia 30332-0405

(Received 23 August 2012; revised 29 March 2013; accepted 26 April 2013)

During the past 30 years, one of the major accomplishments in ocean acoustics is the improvement of understanding seabed scattering, resulting from a significant effort of both at-sea measurement and theoretical modeling. [Jackson and Richardson: *High-Frequency Seafloor Acoustics*, 2007]. Benefiting from this accomplishment, this paper integrates the energy flux method for shallow-water (SW) reverberation [Zhou, (Chinese) Acta Acust. **5**, 86–99 (1980)] with the physics-based seabed scattering models. This integration directly and intuitively results in general expressions for SW reverberation in the angular and modal domains. The latter expression is the same as the modal reverberation expression derived from the Green's function and boundary perturbation method by Tracey and Schmidt [IEEE J. Ocean. Eng. **22**, 317–331(1997)]. The integration also results in a simple relationship between the classic boundary scattering cross sections and the modal scattering matrix in SW waveguides. The bottom roughness spectrum and sediment volume scattering cross section at low grazing angles are inverted in a frequency range of 150–2500 Hz from the wideband long-range reverberation data by using the Biot seabed geoacoustic model. The results may offer some reference data sets for future analysis of the low-frequency seabed scattering mechanisms.
 [http://dx.doi.org/10.1121/1.4807562]

PACS number(s): 43.30.Gv, 43.30.Pc, 43.30.Dr, 43.30.Bp [NPC] Pages: 55–66

I. INTRODUCTION

Acoustic reverberation in shallow-water (SW) waveguides has recently become a research area of intensely increasing interest. Much progress has been made in two areas: SW reverberation modeling and seabed scattering. However, these two research communities have not yet had enough communication with each other.

SW reverberation modeling includes the virtual image method,[1] the ray method,[2,3] the normal-mode method,[4–8] the energy flux method,[9–20] the Green's function and boundary perturbation method,[21–28] the two-way coupled mode method,[29,30] the finite element method,[31] the parabolic equation method,[32] etc. However, most of these models have not yet fully taken advantage of the progress made by the seabed scattering community.

In general, seabed scattering is a dominant mechanism of generating SW reverberation. In the past 30 years, one of the major accomplishments in ocean acoustics is the improvement in our understanding of seabed scattering, resulting from a significant effort of both at-sea measurement and theoretical modeling made by many investigators. These accomplishments, including the rough bottom scattering (RBS) model and the sediment volume scattering (SVS) model, have been summarized in an underwater acoustics monograph by Jackson and Richardson.[33] However, there remains a real scarcity of seabed scattering data sets in the low frequency (LF) range of 100–2600 Hz that can be used to compare with the RBS and SVS models.

Motivated by the above-mentioned three "howevers," this paper integrates the energy flux method of SW reverberation with the physics-based seabed scattering models. The integration directly and intuitively results in a practical expression for long-range SW reverberation in terms of seabed physical/scattering parameters.

The present paper first introduces a theoretical model for SW reverberation using the energy flux method, then characterizes the LF seabed scattering at low grazing angles from broadband reverberation data using the Biot geoacoustic model. The paper is organized as follows. Section II briefly introduces the energy flux (angular spectrum) method for SW reverberation, which is based on the Wentzel-Kramers-Brillouin (WKB) approximation.[9] For readers' convenience, two physics-based seabed scattering models that are widely used for high frequency (HF) seafloor scattering, the RBS model and the SVS model,[33] are briefly introduced in Sec. III. Section IV integrates the energy flux method of SW reverberation with these physics-based RBS and SVS models. The integration results in a practical expression for SW reverberation in the angular domain or in the mode domain. A simple relationship between the bottom scattering cross sections and the modal scattering matrix in the SW waveguides obtained from the integration is described in Sec. V. For validating the energy flux method-derived reverberation expressions with the HF RBS and SVS models, data-model comparisons for the ASIAEX site are given in Sec. VI. Section VII characterizes the LF seabed scattering at low grazing angles using broadband long-range reverberation data and the Biot geoacoustic model. Finally, Sec. VI summarizes and discusses the results of this paper.

[a]Author to whom correspondence should be addressed. Also at: State Key Laboratory of Acoustics, Institute of Acoustics, Chinese Academy of Sciences, Beijing 100190, China. Electronic mail: jixun.zhou@me.gatech.edu

II. THE ENERGY FLUX METHOD FOR SW REVERBERATION

The angular spectrum (energy flux) method for modeling SW reverberation, based on the WKB approximation of normal-mode theory, was first presented in archived Chinese journals.[9–13] Due to its simplicity and intuitiveness, the energy flux method has further been developed and widely used for SW reverberation calculations.[9–20] This method is briefly introduced here, and the interested reader is referred to the basic concepts in Sec. II and Sec. IV of Ref. 9.

The sound field in SW, generated by a point source (with a source level, $SL = 0$ dB), can be expressed as a summation of normal modes[34]

$$P(r,z;z_0) = \left(\frac{2\pi i}{r}\right)^{1/2} \sum_n \frac{\Phi_n(z_0)\Phi_n(z)}{k_n^{1/2}} e^{(ik_n-\beta_n)r}. \tag{1}$$

The sound intensity is expressed by

$$I(r,z;z_0) = \frac{2\pi}{r}\left\{\sum \frac{|\Phi_n(z_0)|^2\,|\Phi_n(z)|^2}{k_n} e^{-2\beta_n r} + \sum\sum_{n\neq m} \frac{\Phi_n(z_0)\Phi_m^*(z_0)\Phi_n(z)\Phi_m^*(z)}{k_n^{1/2}k_m^{1/2*}} \times e^{-[(\beta_n+\beta_m)+i(k_n-k_m)]r}\right\}, \tag{2}$$

where Φ_n is the normalized eigenfunction, k_n is the longitudinal wave number, β_n is the modal attenuation factor of the nth mode (i.e., the complex wave number $K_n = k_n + i\beta_n$). z_0 is the source depth and z is the receiver depth. The first term of Eq. (2) is an incoherent summation of normal modes. It describes the average intensity of the sound field. For many practical applications such as sonar performance predictions, an average estimate of the sound intensity is quite sufficient, i.e., the second term of Eq. (2), which describes the interference fine structure, can be neglected.

According to the WKB approximation, the smoothed (slowly varying) energy depth distribution of the nth mode can approximately be expressed as

$$\overline{|\Phi_n(z)|^2} = \frac{2}{S_n \tan\theta_n(z)}. \tag{3}$$

Here, S_n is the cycle distance of the nth mode that is the sum of the geometric cycle distance S_{ng} and the beam displacement Δ_n:[35]

$$S_n = S_{ng} + \Delta_n = 2\int_{\xi_n}^{\eta_n} \frac{dz}{\tan\theta_n(z)} + \Delta_n, \tag{4}$$

and θ_n is the mode angle. Δ_n is a beam displacement on the bottom reflection. If the bottom reflection is expressed by $V(\theta) = |V(\theta)|\exp(i\varphi_b)$, with a phase of φ_b, then $\Delta_n = d\varphi_b/dk_n$. The eigenvalue k_n of the nth mode satisfies relationship

$$2\int_{\xi_n}^{\eta_n} \sqrt{k_w^2(z) - K_n^2}\,dz + \varepsilon_{\xi_n} + \varepsilon_{\eta_n} = 2n\pi, \tag{5}$$

where ξ_n and η_n are the upper and lower turning (or reflection) depths of the nth mode, ε_{ξ_n} and ε_{η_n} are the corresponding phase shifts, and $k_w(z) = \omega/c(z)$ is the wave number in water. The modal attenuation factor, β_n, can be expressed approximately in terms of the bottom reflection coefficient $V(\theta)$,

$$\beta_n = -\frac{\ln|V(\theta_n)|}{S_n(\theta_n)}. \tag{6}$$

Each normal mode can be decomposed into a pair of up- and down-going local quasi-plane waves. We shall call the local plane wave an equivalent "mode ray." The angle of the mode ray and the eigenvalue of the nth mode are related by

$$k_n = k_w(z)\cos\theta_n(z). \tag{7}$$

It is well known

$$\frac{dk_n}{dn} = -\frac{2\pi}{S_n}. \tag{8}$$

Using Eqs. (7) and (8), we have

$$dn = \frac{S_n k_w(z_0)\sin\theta_n(z_0)d\theta_n(z_0)}{2\pi}. \tag{9}$$

The incoherent summation over modes can be changed to an integration over the mode-ray angle θ. Proceeding from Eqs. (2), (3), (6), (8), and (9), and adding a term of water absorption, we can derive a general expression for the average field intensity in SW given by

$$I(r,z;z_0) = \frac{2}{r}e^{-\alpha_w r}\int \frac{2e^{2\ln|V(\theta)|r/s_n(\theta)}}{S_n\tan\theta_n(z)}d\theta_n(z_0) = \frac{2e^{-\alpha_w r}}{r}\int I_{aps}(\theta,r,z;z_0)d\theta_n(z_0) \tag{10}$$

where

$$I_{aps}(\theta,r,z;z_0) = \frac{2e^{-2\beta_n r}}{S_n\tan\theta_n(z)} = \frac{2e^{2\ln|V(\theta)|r/S_n(\theta)}}{S_n\tan\theta_n(z)}. \tag{11}$$

Using different methods, Brekhovskikh,[36,37] Smith,[38] Brekhovskikh and Lysanov,[39] and Katsnelson and Petnikov[40] obtained an expression that is similar to Eq. (10). In Eq. (11), α_w is the water column absorption coefficient; $\theta(z_0)$ is the grazing angle of the mode rays at the source depth, and $\theta(z)$ is the grazing angle at the receiver depth (note: Here "depth" means in the whole water column not just at the source/receiver location). The quantity defined by Eq. (11), I_{aps}, is referred to as the "angular power spectrum" of sound propagation.[9] Smith also called it the "energy density in direction of arrival" (Ref. 38). The average sound intensity in SW depends only on water absorption and two other parameters: The bottom reflection coefficient $V(\theta)$ and the cycle distance S_n of the mode ray.

Equation (10) is a simple and intuitive expression for calculating averaged SW field characteristics such as sound propagation, reverberation, noise, and their spatial

coherence. It is only an angular weighting process. For calculating the average reverberation intensity in SW, the two-way propagation angular spectra and the classic seabed scattering function (cross section) are naturally connected in the angular domain.

Using the single scatter approximation, the average reverberation intensity R can be expressed in terms of I_{aps} by[9]

$$\begin{aligned} R(r,z;z_0) &= \int\int \frac{e^{-\alpha r}}{hr} I_{aps}(\theta_m, r, h; z_0) \times A \times \sigma_b(\theta_m, \theta_n) \\ &\quad \times \frac{e^{-\alpha r}}{hr} I_{aps}(\theta_n, r, z; h) d\theta_m d\theta_n \\ &= \frac{4}{r^2} e^{-2\alpha_w r} \int\int \frac{\exp(\{2\ln|V[\theta_m(h)]|/S_m\}r)}{S_m \tan\theta_m(h)} \\ &\quad \times A\sigma[\theta_m(h), \theta_n(h)] \\ &\quad \times \frac{\exp(\{2\ln|V[\theta_n(h)]|/S_n\}r)}{S_n \tan\theta_n(z)} d\theta_m(z_0) d\theta_n(h), \end{aligned} \tag{12}$$

where $I_{aps}(\theta_m, r, h; z_0)$ is the incident angular power spectrum at a distance of r, incident upon a seabed scattering area A; $I_{aps}(\theta_n, r, z; h)$ is the angular power spectrum returned to a receiver at a depth of z from the same bottom scattering area; h is a water depth; $\sigma_b[\theta_m(h), \theta_n(h)]$ is the bottom scattering cross section per unit area; $\theta_m(h)$ is the incident grazing angle of mode m at the bottom; and $\theta_n(h)$ is the scattering angle of mode n.

III. TWO PHYSICS-BASED SEABED SCATTERING MODELS

The bistatic seabed scattering models for high frequencies have extensively been investigated, tested against data with good results, and summarized in a comprehensive monograph (Ref. 33). These HF scattering models have been extended to the geoacoustic bottom interaction model (GABIM) for LF range.[41] For the simplicity on the reverberation data-model comparisons, the present study will use two (commonly adopted) physics-based models: The RBS model and the SVS model described in Ref. 33. For readers' convenience, all notations in the expressions for these two scattering models in present paper will be same as those used by Jackson and Richardson.[33]

A. The RBS model

The bistatic scattering cross section for the RBS model in the small-roughness perturbation approximation is[33]

$$\sigma_{rbs}(\theta_i, \theta_s) = k_w^4 |A_{ww}|^2 W(\Delta K), \tag{13}$$

$$W(\Delta K) = \frac{\omega_2}{(\Delta K)^{\gamma_2}}. \tag{14}$$

For the homogeneous fluid model,

$$A_{ww} = \frac{1}{2}[1 + V_{ww}(\theta_i)][1 + V_{ww}(\theta_s)]G, \tag{15}$$

where

$$G = \left(1 - \frac{1}{a_\rho}\right)[\cos\theta_i \cos\theta_s \cos\phi_s - B] - 1 + \frac{1}{a_p^2 a_\rho}, \tag{16}$$

$$B = \frac{\sin\theta_{pi} \sin\theta_{ps}}{a_p^2 a_\rho}, \tag{17}$$

$$\sin\theta_{pi} = \sqrt{1 - a_p^2 \cos^2\theta_i}, \tag{18}$$

$$\sin\theta_{ps} = \sqrt{1 - a_p^2 \cos^2\theta_s}, \tag{19}$$

$$a_p = \frac{\nu_p}{1 + i\delta_p}, \tag{20}$$

$$\delta_p = \frac{\nu_p c_w \ln(10)}{40\pi f} \alpha_p \ = \left(\frac{c_b \times \alpha_p}{2\pi f \times 8.686}\right), \tag{21}$$

where $W(\Delta K)$ is the roughness spectrum, which is the Fourier transform of the interface relief covariance. Equation (14) is one of the simplest and most often used isotropic forms, the "power law." ΔK is the magnitude of the two-dimensional "wave vector." The parameters of the spectrum are the "spectral strength" ω_2 and the "spectral exponent" γ_2. The definition of angular coordinates used in these equations is shown in Fig. 2.4 of Ref. 33, θ_i and θ_s are the *incident* and the *scattering grazing angle*, respectively. ϕ_s is the *bistatic angle*. $V_{ww}(\theta)$ is a sound reflection coefficient from the seabottom evaluated at the grazing angle θ. a_p is the complex ratio of sediment compressional wave speed to water sound speed (ν_p is a real parameter of the speed ratio, $\nu_p = c_b/c_w$). a_ρ is the sediment-water density ratio, δ_p is the ratio of the imaginary and real parts of sound speed in the sediment. α_p is the sound attenuation in the sediment in dB/m.

B. The SVS model

The geometry relevant to the simplest fluid SVS models is shown by Fig. 14.1 of Ref. 33. If the volume scattering strength is assumed to be depth independent and can be treated in terms of an effective interface scattering strength (the decibel equivalent of scattering cross section per unit solid angle per unit area), the equivalent interface bistatic cross section for SVS can be expressed by

$$\sigma_{svs}(\theta_i, \theta_s) = \frac{|V_{wp}(\theta_i)|^2 |V_{wp}(\theta_s)|^2 \sigma_V}{2k_w |a_\rho|^2 \mathrm{Im}[P(\theta_i) + P(\theta_s)]}, \tag{22}$$

where

$$P(\theta) = \sqrt{a_p^{-2} - \cos^2\theta}. \tag{23}$$

The pressure transmission coefficient (V_{wp}) is

$$V_{wp} = \frac{2z_{wp}}{z_{wp} + 1}, \tag{24}$$

$$z_{wp}(\theta) = \frac{a_\rho a_p \sin\theta_w}{\sin\theta_p}. \tag{25}$$

According to Jackson and Richardson, Eqs. (22)–(23) "form the basis for several SVS models, which differ only in the assumptions used to obtain the volume scattering cross section, σ_V. The simplest approach is to treat σ_V, empirically, that is as a quantity that must be obtained by fitting data rather than calculated on the basis of theory."[33] σ_V has the units of $m^2/m^3 = m^{-1}$. The transmission coefficient V_{wp} and the seabottom reflection coefficient V_{ww} have a relationship

$$V_{wp} = 1 + V_{ww}. \tag{26}$$

Thus Eq. (22) can also be rewritten as

$$\sigma_{svs}(\theta_i, \theta_s) = \frac{|1 + V_{ww}(\theta_i)|^2 |1 + V_{ww}(\theta_s)|^2 \sigma_V}{2k_w |a_\rho|^2 \,\mathrm{Im}[P(\theta_i) + P(\theta_s)]}. \tag{27}$$

IV. INTEGRATING THE ENERGY FLUX METHOD OF REVERBERATION WITH PHYSICS-BASED SEABED SCATTERING MODELS

A. In the angular domain

Equation (12) forms a general SW reverberation expression in the angular domain with the physics-based seabed scattering model. It is a double-integral over incident/scattering grazing angles. All classic seabed scattering cross sections expressed as a function of incident/scattering grazing angles and frequency can be well integrated with two-way propagation in the angular domain, including the RBS model and the SVS model, expressed by Eq. (13) or (22).

For a special case, in the Pekeris waveguide (iso-velocity water), the cycle distance of the nth mode ray is given by

$$\begin{aligned} S_m &= 2h/\tan(\theta_m) - [(\partial\varphi_b/\partial\theta)|_{\theta=\theta_n}/k_w \sin\theta_n] \\ &\approx 2h/\tan(\theta_m). \end{aligned} \tag{28}$$

Equation (12) becomes

$$\begin{aligned} R(r) \approx \frac{\pi c_w \tau_0}{h^2 r} e^{-2\alpha_w r} \int\int e^{(2\ln|V(\theta_m)|/S_m)r} \times \sigma_b(\theta_m, \theta_n) \\ \times e^{(2\ln|V(\theta_n)|/S_n)r} d\theta_m d\theta_n. \end{aligned} \tag{29}$$

In derivation, the seabed scattering area at mid- to long-range has been assumed as $A = 2\pi r \times dr \approx 2\pi r \times (c_w\tau_0/2) = \pi r c_w \tau_0$. The waveguide dispersion spreading[7] has been assumed to be much less than the signal pulse duration, τ_0 (or less than a time window for reverberation data processing). For the Pekeris waveguide (iso-velocity water), Eq. (29) is much simpler for calculating SW reverberation.

B. In the modal domain

From Eqs. (3) and (9), we have

$$\begin{aligned} d\theta_m(z_0) &= \frac{2\pi dm}{S_m k(z_0) \sin\theta_m(z_0)} \times \frac{\cos\theta_m(z_0)}{\cos\theta_m(z_0)} \\ &= \overline{|\Phi_m(z_0)|^2}\, \frac{\pi dm}{k_m}, \end{aligned} \tag{30}$$

$$d\theta_n(h) = \frac{2\pi dn}{S_n k(h) \sin\theta_n(h)} \times \frac{\cos\theta_n(h)}{\cos\theta_n(h)} = \overline{|\Phi_n(h)|^2}\, \frac{\pi dn}{k_n}. \tag{31}$$

Using Eqs. (3), (30), and (31), the SW reverberation expression that integrates over mode-ray angles, Eq. (12), can be converted back to a summation over normal modes

$$\begin{aligned} R(r, z; z_0) = \frac{\pi^2}{r^2} e^{-2\alpha_w r} \sum_m \sum_n \frac{\overline{|\Phi_m(z_0)|^2}\, \overline{|\Phi_n(z)|^2}}{k_m k_n} \\ \times e^{-2(\beta_m + \beta_n)r} \times A\sigma(\theta_m, \theta_n) \\ \times \overline{|\Phi_m(h)|^2}\, \overline{|\Phi_n(h)|^2}. \end{aligned} \tag{32}$$

For the slowly depth-varying energy dependence of the normal mode in Eqs. (3) and (32), Ellis[7] and Yang[6] had the following expression:

$$\overline{|\Phi_n(z)|^2} = \frac{1}{4}\left[\Phi_n^2(z) + \frac{1}{k_w^2(z) - k_n^2}\left(\frac{d\Phi_n}{dz}\right)^2\right]. \tag{33}$$

To overcome a problem when a receiver is near a turning point, where $k_w(z) \approx k_n(z)$, alternatively, Zhang and Jin have proposed the following expression:[5]

$$\overline{|\Phi_n(z)|^2} = \frac{2k_n}{S_n[k_w^2(z)D(z) + k_w^2(z) - k_n^2]^{1/2}}, \tag{34}$$

where

$$D(z) = 0.875\left|\frac{1}{\pi f}\frac{dc(z)}{dz}\right|^{2/3}. \tag{35}$$

Using Eqs. (8) and (34), Eq. (32) can be re-written as

$$\begin{aligned} R(r, z; z_0) = \frac{c_w \tau_0}{\pi r} e^{-2\alpha_w r} \sum_m \sum_n \frac{k_m (k_m - k_{m+1})^2 \exp(-2\beta_m r)}{[k_w^2(z_0)D(z_0) + k_w^2(z_0) - k_m^2]^{1/2}[k_w^2(h)D(h) + k_w^2(h) - k_m^2]^{1/2}} \\ \times \sigma(\theta_m, \theta_n) \times \frac{k_n (k_n - k_{n+1})^2 \exp(-2\beta_n r)}{[k_w^2(h)D(h) + k_w^2(h) - k_n^2]^{1/2}[k_w^2(z)D(z) + k_w^2(z) - k_n^2]^{1/2}}. \end{aligned} \tag{36}$$

This is a simple and practical expression for SW reverberation in the modal domain. For arbitrary velocity profiles, Eq. (36) can be used to calculate SW long-range reverberation intensity by using the classic cross sections of seabottom scattering and any available normal-mode code. It only requires two parameters: Real and imaginary parts of the modal eigenvalue, k_m and β_m.

V. THE MODAL SCATTERING MATRIX DERIVED FROM THE ENERGY FLUX METHOD

A. A simple relationship between the modal scattering matrix and the seabed scattering cross sections

Equation (32) can be re-written as

$$R(r,z;z_0)=\frac{\pi^2}{r^2}e^{-2\alpha_w r}\sum_m\sum_n\frac{\overline{|\Phi_m(z_0)|^2}\,\overline{|\Phi_n(z)|^2}}{k_m k_n}\times e^{-2(\beta_m+\beta_n)r}\times A\times MSM(m,n). \tag{37}$$

Here $MSM(m,n)$ is defined as the modal scattering matrix in the SW waveguide between mode m and mode n, expressed by the classic seabed scattering cross sections

$$MSM(m,n)=\sigma(\theta_m,\theta_n)\times\overline{|\Phi_m(h)|^2}\,\overline{|\Phi_n(h)|^2}. \tag{38}$$

A simple relationship between the waveguide modal scattering matrix and the plane wave scattering cross section is derived as follows.

The continuity of pressure and normal component particle velocity at the water-sediment interface requires that the normal mode function and its derivative with respect to depth z have the relationship[24,43]

$$q_m=\frac{1}{\Phi_m(z)}\frac{d\Phi_m(z)}{dz}\bigg|_h=(\rho_w/\rho_b)\sqrt{k_m^2-k_b^2}, \tag{39}$$

where the subscripts w and b denote the water and bottom at the interface $z=h$. Using Eq. (39), Eq. (33) can be written as

$$\begin{aligned}\overline{|\Phi_m(h)|^2}&=\frac{\Phi_m^2(h)}{4}\left[1+\frac{1}{k_w^2(h)-k_m^2}\frac{1}{\Phi_m^2(h)}\left(\frac{d\Phi_m(z)}{dz}\bigg|_h\right)^2\right]\\&=\frac{\Phi_m^2(h)}{4}\left[1+\left(\frac{1}{k_w(h)\sin\theta_m}\frac{\rho_w}{\rho_b}\sqrt{k_m^2-k_b^2}\right)^2\right]\\&=\frac{\Phi_m^2(h)}{4}\left[1+\left(\frac{1}{\sin\theta_m}\frac{\rho_w}{\rho_b}\sqrt{\cos^2\theta_m-a_p^{-2}}\right)^2\right].\end{aligned} \tag{40}$$

Using Eqs. (18) and (24)–(26), (or using 8.46, 8.49, and 8.53 in Ref. 33), we have

$$\frac{1}{|1+V_{ww}(\theta_m)|^2}=\frac{1}{4}\left|1+\left(\frac{1}{\sin\theta_m}\frac{\rho_w}{\rho_b}\sqrt{\cos^2\theta_m-a_p^{-2}}\right)^2\right|. \tag{41}$$

Here V_{ww} is the reflection coefficient with the scripts ww added to indicate that the incident and reflected fields are both in the water. Substituting Eq. (41) into (40) results in

$$\overline{|\Phi_m(h)|^2}=\frac{\Phi_m^2(h)}{|1+V_{ww}(\theta_m)|^2}. \tag{42}$$

Thus the modal scattering matrix in SW waveguides, Eq. (38), can be re-written as

$$MSM(m,n)=\frac{\Phi_m^2(h)}{|1+V_{ww}(\theta_m)|^2}\times\sigma(\theta_m,\theta_n)\times\frac{\Phi_n^2(h)}{|1+V_{ww}(\theta_n)|^2}. \tag{43}$$

Here $\theta_m=\cos^{-1}[k_m/k_w(h)]$. $\Phi_m(h)$ is the amplitude of mth mode at the water-bottom interface. $\sigma(\theta_m,\theta_n)$ can be either the RBS cross section or the SVS cross section.

Using a two-way coupled-mode representation, Stotts and Koch first derived the expression of Eq. (43) for the RBS model.[29] Equation (43), derived from the energy flux method for SW reverberation in this paper, shows that it should be applicable to any seabed scattering cross section, including the RBS and SVS models.

The relationship between the plane wave scattering cross section $\sigma(\theta_m,\theta_n)$ and the waveguide mode scattering matrix MSM, expressed by Eq. (43), has an interesting physical explanation. $\sigma(\theta_m,\theta_n)$ is the classic seabed scattering cross section per unit seabed area. It is defined as the scattering intensity at a unit distance caused by an incident plane wave with unit amplitude; for the MSM in a waveguide, the equivalent incident wave intensity (decomposed from mth mode) and the scattering intensity (decomposed from nth mode) at a unit distance, are scaled by a factor of $\Phi_m^2(h)/|1+V_{ww}(\theta_m)|^2$ and $\Phi_n^2(h)/|1+V_{ww}(\theta_n)|^2$, respectively. The factor is approximately corresponded to the down- or up-going (incident or scattering) wave intensity at the water-bottom interface, decomposed from a mode WKB expression.

B. The modal scattering matrixes for the RBS model and SVS model

Substituting Eqs. (13) and (15)–(20) into Eq. (43), we have the $MSM(m,n)$for the RBSg model as follows:

$$\begin{aligned}MSM_{rbs}(m,n)&=\frac{\Phi_m^2(h)}{|1+V_{ww}(\theta_m)|^2}\times k_w^4|A_{ww}|^2W(\Delta K)\times\frac{\Phi_n^2(h)}{|1+V_{ww}(\theta_n)|^2}\\&=\frac{1}{4}\Phi_m^2(h)\times k_w^4|G|^2W(\Delta K)\times\Phi_n^2(h)\\&=\frac{1}{4}\Phi_m^2(h)\times b_{mn}^2W(\Delta K)\times\Phi_n^2(h),\end{aligned} \tag{44}$$

where

$$b_{mn}=k_w^2G=\left(1-\frac{\rho_w}{\rho_b}\right)k_mk_n+\left(1-\frac{\rho_b}{\rho_w}\right)q_mq_n+k_w^2-\frac{\rho_w}{\rho_b}k_b^2. \tag{45}$$

q_n is defined by Eq. (39). The MSM for the RBS model, derived from the integration of the reverberation energy flux method with RBS model, expressed by Eqs. (44) and (45), is same as the result derived by Tracey and Schmidt[23] and by Song *et al.*,[24] using the boundary perturbation method. Song *et al.* called b_{mn} as "the modal backscattering strength" between modes m and n.[24]

In the same way, substituting Eq. (27) into Eq. (43), we have the MSM for the SVS model

$$\begin{aligned} MSM_{SVS}(m,n) &= \frac{\Phi_m^2(h)}{|1+V_{ww}(\theta_m)|^2} \\ &\times \frac{|V_{wp}(\theta_m)|^2|V_{wp}(\theta_n)|^2\sigma_v}{2k_w|a_\rho|^2\mathrm{Im}[P(\theta_m)+P(\theta_n)]} \\ &\times \frac{\Phi_n^2(h)}{|1+V_{ww}(\theta_n)|^2} \\ &= \Phi_m^2(h) \times \frac{\sigma_v}{2k_w|a_\rho|^2\mathrm{Im}[P(\theta_m)+P(\theta_n)]} \\ &\times \Phi_n^2(h), \end{aligned} \tag{46}$$

where V_{wp} is the pressure transmission coefficient of the compressional wave from the water into the bottom. $p(\theta)$ is defined by Eq. (23).

VI. DATA-MODEL COMPARISONS

For validating the energy flux method-derived reverberation expressions integrated with the HF RBS and SVS models, some examples are shown in this section.

A. Reverberation measurements

Reverberation data were collected on June 3, 2001 at the Asian Sea International Experiment (ASIAEX) site in the East China Sea using 38- and 1000-g explosive charges. The reverberation levels (RL) averaged over three shots were analyzed as a function of time for different center frequencies in 1/3-octave bands and normalized to the source level (SL).[14] The source depths were around 50 m; the receiver depth was 56.5 m. The horizontal distances between the sources and the receiver were in a range of 8.2–15.7 m. Thus the RL can be well described as the monostatic. (More details on the RL measurements can be found in Refs. 14 and 44.) The water depth was about 104 m. The sea bottom was nominally flat. During the reverberation measurements on June 3, the sea surfaces were relatively calm: Wind speed and the *rms* surface-wave height were 2.74 m/s and 0.10 m, respectively.[44] The average sound velocity profile at the receiving array site is plotted in Fig. 1.

B. Seabed geoacoustic and scattering models

A recent paper on broadband geoacoustic inversions from LF field measurements, made at 20 locations around the world by many investigators, has resulted in an effective seabed geoacoustic model.[42] The sound attenuations in sandy or sand-silt mixture bottoms, inverted from different acoustic field characteristics, exhibit similar magnitude and nonlinear

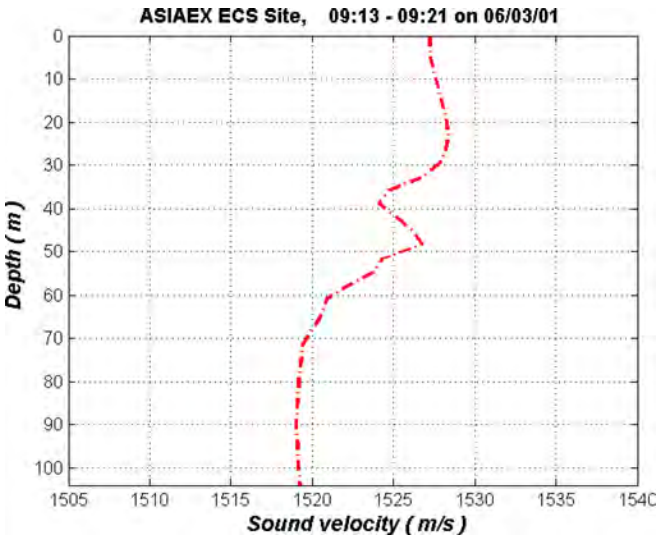

FIG. 1. (Color online) Sound velocity profile at the ASIAEX site during the reverberation measurements.

frequency dependence at all of these locations, including the ASIAEX site. The LF field-derived sound speed and attenuation in the sandy bottoms satisfy the Kramers-Kronig relationship,[42] and may be equally well described by four physics-based models: The Biot-Stoll model, the Buckingham VGS model, the Chotiros-Isakson BICSQS model, and the Pierce-Carey model.[45] In this paper, we use a Biot geoacoustic model that matches the LF field measurements. All the effective Biot parameters are listed in a column of "LF fit," Table 10 of Ref. 42. Related bottom sound attenuation and the velocity ratio at the bottom-water interface, derived from the effective Biot model, are listed in Table I.

The RBS model and SVS model introduced in Sec. III are used for reverberation computations.

C. Reverberation data are in good agreement with the theoretical model

The reverberation expression in the modal domain, Eq. (36), is used to calculate RL in this section. First, we assume that the "spectral exponent" γ_2 of the seabed roughness spectrum in Eq. (14) equals 3.0 (as many HF seabed scattering papers suggested), then we adjust the "spectral strength" ω_2 to find the best match (by vision) between the numerical RLs and the experimental data. For the SVS model in Eq. (27), we adjust the parameter σ_V to find the best match. The data-model comparisons at 800, 1500, and 2500 Hz are shown in Figs. 2(a) to Fig. 2(c). These figures show that both the RBS model and SVS model, well developed by the HF seabed scattering community, can be used to predict LF SW reverberation using a set of right seabed geoacoustic and scattering parameters. The SW reverberation expression derived from the integration of the energy flux method with these seabed scattering models is also validated by Figs. 2(a)–2(c), as well as by the results in the next section.

Figures 2(a)–2(c) show that the measured reverberation levels at very short ranges are larger than the theoretical predictions. This result indicates that the modal expression for

TABLE I. Bottom attenuation and velocity ratio at the water-bottom interface, derived from the Biot model that matches the LF field measurements (Ref. 42).

f (Hz)	150	200	300	400	500	600	700	800	1000	1250	1500	1750	2000	2250	2500
C_b/C_w	1.0604	1.0605	1.0606	1.0608	1.0611	1.0614	1.0618	1.0622	1.0632	1.0646	1.0663	1.0681	1.0700	1.0721	1.0741
α_p (dB/m)	0.0110	0.0187	0.0401	0.0694	0.1064	0.1509	0.2026	0.2613	0.3979	0.6012	0.8344	1.0909	1.3643	1.6486	1.9386

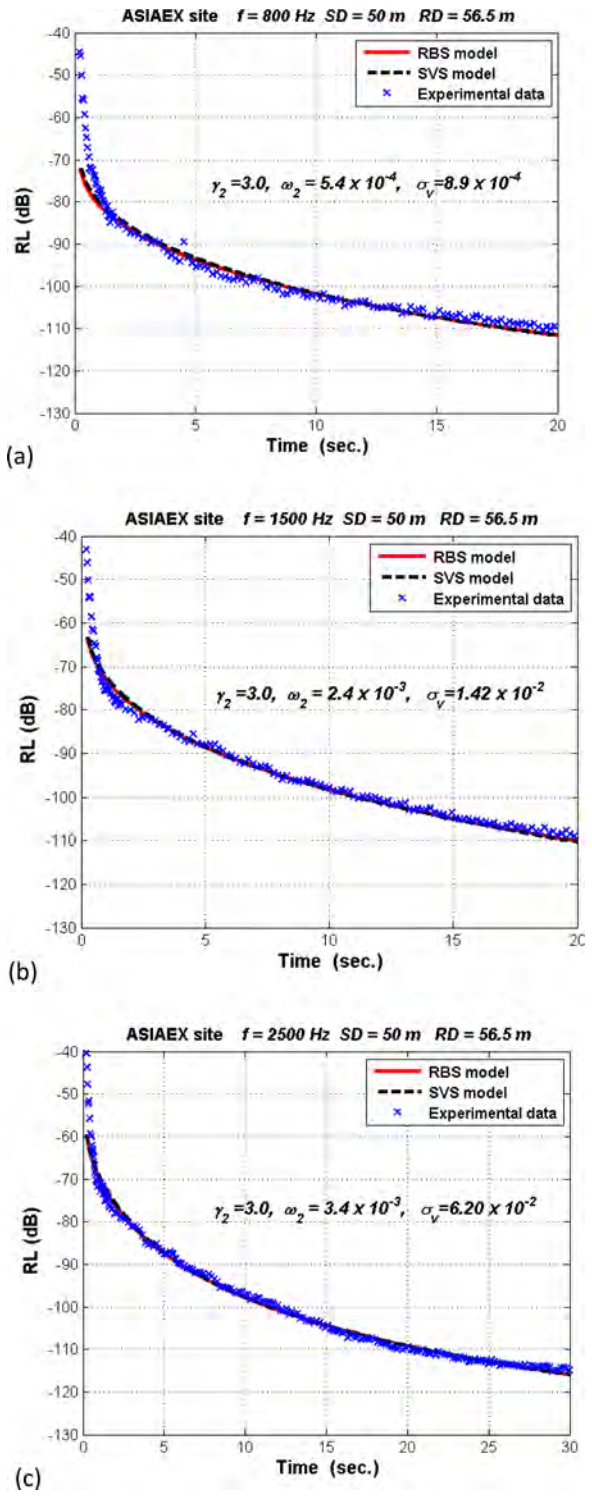

FIG. 2. (Color online) Comparisons between theoretical $RL(t)$ (using the RBS and SVS models) and reverberation data at given frequencies. (a) 800 Hz, (b) 1500 Hz, (c) 2500 Hz.

SW reverberation, Eq. (36), can not be used for predicting the SW reverberation at short range. One of the reasons is that the reverberation modeling in this paper assumes that the amplitudes of the down- and up-going waves, decomposed from the modes, are equal. This assumption requires that the bottom reflection coefficient is close to one, i.e., the reverberation data-model comparison should be made at long ranges where the low-order modes with low-grazing angles dominate the sound field. In fact, the modal wave numbers are complex (due to the bottom attenuation), the amplitudes for the down-going/incident wave and up-going/scattering wave, decomposed from the mode WKB expression, are not equal. This factor can not be ignored for short-range reverberation.

VII. CHARICTERIZATION OF THE LF SEABOTTOM SCATTERING FROM LONG-RANGE REVERBERATION

A. *RL*(*t*) at a given single frequency is used to invert the scattering parameters for the RBS and SVS model

Assuming the $\gamma_2 = 3.0$, the reverberation level as a function of time, $RL(t)$, at given frequencies is used to find the best match between measurements and models, as we did in Sec. VI. The theoretical RL is numerically evaluated by using Eq. (36) and a mode code of Modal Acoustic Transmission Loss (MOATL),[46] using different ω_2 for the RBS model or σ_V for the SVS model. When the numerical RL curve matches the experimental $RL(t)$ data, ω_2 or σ_V is determined at the given frequency. All resultant scattering parameters from the best matches for both the RBS and SVS models at different frequencies are listed in Table II.

1. Internal parameter coupling between γ_2 and ω_2 in the RBS model

For the HF, the bottom roughness is assumed to be a random process described by (a two parameter, isotropic, two dimensional roughness spectral density) Eq. (14). In general, γ_2 and ω_2 are assumed as constant. The roughness spectrum exponent is restricted to the range of $2 \le \gamma_2 \le 4$ with a mean of 3.0. Figures 2(a)–2(c) and Table II show that when the spectral exponent $\gamma_2 = 3.0$, the data-model fittings at different frequencies require the RBS model to have very different values of the spectral strength ω_2. Numerical simulations show that at a given single frequency, there are various combinations of γ_2 and ω_2 in the RBS mode that can match the measurements. As an example, Figs. 3(a) and 3(b) show that three different pairs of γ_2 and ω_2 would result in an identical $RL(t)$. An increase (decrease) in γ_2 can be compensated for by an increase (decrease) in ω_2. Thus it is impossible to uniquely invert the bottom roughness spectral density from SW reverberation at one single frequency. It

TABLE II. $RL(t)$-inverted LF seabed scattering parameters, assuming $\gamma_2 = 3.0$.

f (Hz)	150	200	300	400	500	600	700	800	1000	1250	1500	1750	2000	2250	2500
$\omega_2(\times 10^{-4})$	0.6	0.8	0.9	1.2	2.7	3.1	4.6	5.4	8.0	18.0	24.0	28.0	34.0	42.0	34.0
$\sigma_V(\times 10^{-4})$	0.029	0.067	0.16	0.43	1.50	2.42	5.68	8.90	20.0	72.0	142.0	240.0	382.0	626.0	620.0

needs wideband reverberation measurements as described in Sec. VII B.

2. Strong frequency dependence of the LF volume scattering cross section σ_V

In the HF range, the sediment volume cross section, σ_V, is often quantified by the following dimensionless parameter[33]

$$\sigma_2 = \sigma_V/\alpha_p, \text{ or } \sigma_V = \sigma_2\alpha_p, \tag{47}$$

where α_p is the bottom attenuation in dB/m. For high frequencies, α_p is close to linear frequency dependence, σ_2 is taken to be frequency independent, then Eq. (22) or (27) will yield a scattering cross section (σ_{svs}) that is nearly frequency independent.[33] However, Figs. 2(a)–2(c) and Table II show that at low frequencies, the reverberation-derived volume scattering cross section, σ_V, has much stronger frequency dependence.

All σ_V in Table II, inverted from $RL(t)$ at different frequencies, are plotted in Figs. 4(a) and 4(b) against the bottom attenuation and frequency, respectively. Data fitting results in the following approximate relations:

$$\sigma_V \approx 0.0170\alpha_p^{2.057}, \tag{48}$$

$$\sigma_V = (0.00235 \pm 0.00019)(f/1000)^{(3.822\pm0.092)}, \tag{49}$$

where α_p is the bottom attenuation in dB/m, f is frequency in Hz.

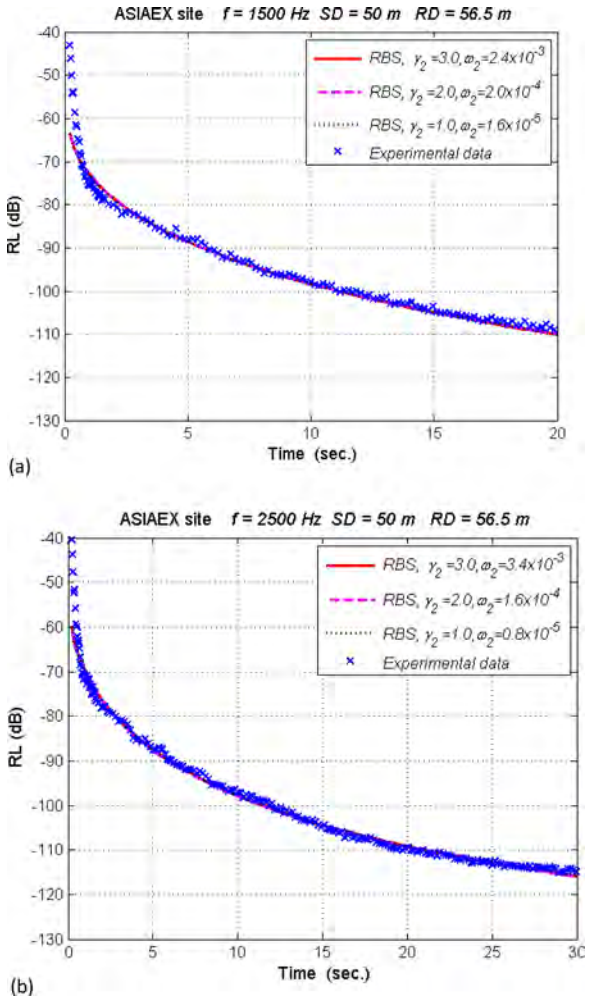

FIG. 3. (Color online) Three different pairs of γ_2 and ω_2 result in an identical $RL(t)$. An increase (decrease) in γ_2 can be compensated for by an increase (decrease) in ω_2.

B. Wideband $RL(f)$ at giving reverberation times is used to invert the scattering parameters for the RBS and SVS models

The reverberation level as a function of frequency, $RL(f)$, at given times is used to invert the LF seabottom scattering at low grazing angles. For the RBS model, both γ_2 and ω_2 are assumed as adjustable. For the SVS model, as mentioned in the last section, the HF expression of Eq. (47) needs to be modified for LF reverberation modeling. We assume

$$\sigma_V = \sigma_2^*\alpha_p^{n_V}. \tag{50}$$

For a given time, a theoretical RL as a function of frequency, $RL(f)$, is numerically evaluated by using Eq. (36) and a mode code of MOATL for a pair of γ_2 and ω_2 (for the RBS model) or a pair of σ_2^* and n_V (for the SVS model). The pair of γ_2 and ω_2, or the pair of σ_2^* and n_V, for which the numerical $RL(f)$ curves best match the experimental $RL(f)$ data, is both readily and uniquely determined. The resultant best matches between theoretical predictions and measurements are shown in Figs. 5(a) to 5(h) All the $RL(f)$-inverted parameters at different times for the bottom roughness spectrum (γ_2 and ω_2) and for the SVS cross section [σ_2^* and n_V in Eq. (50)] are listed in Table III. The standard deviations between the measurements and theoretical results are also listed in Table III.

C. Characteristics of the LF RBS model and SVS model at low grazing angles

To ensure that the characteristics of seabed scattering derived from reverberation are limited to low frequencies and low grazing angles and to reduce possible bottom scattering contributions from deeper layers of sediments, in this section, we just use the results derived from $RL(f)$ in a range

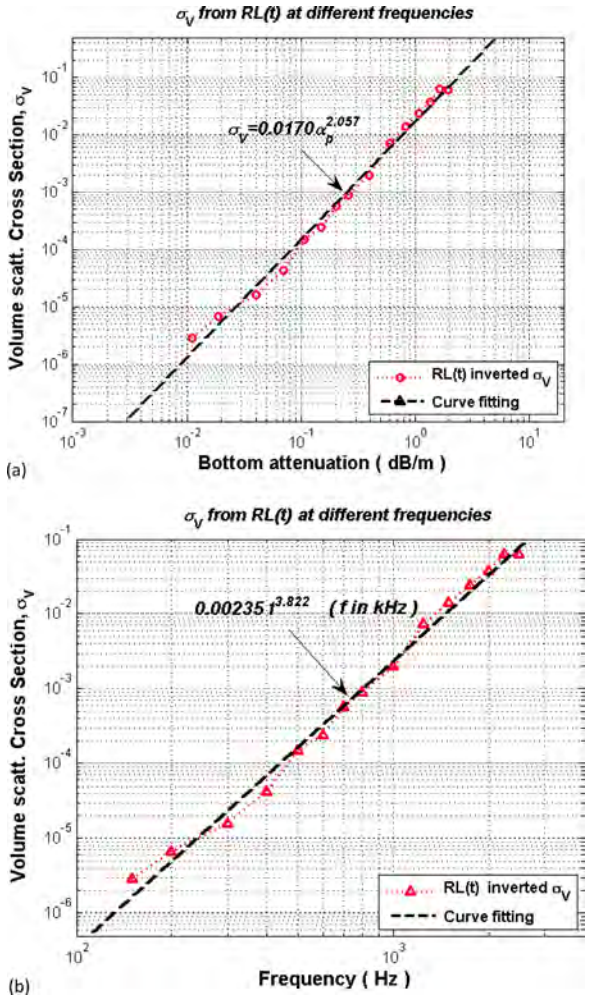

FIG. 4. (Color online) The sediment volume scattering cross section σ_V, inverted from $RL(t)$ at different frequencies. (a) σ_V vs the bottom attenuation, (b) σ_V vs frequency.

of 3–12 s; the ranges from the source to the seabed scattering areas are about 22–88 times of the water depth. The choice of the RL data between 3 and 12 s is based on the following considerations: (1) As we discussed in a previous paper,[14] to get quality wideband reverberation levels (RL) normalized to the source level (SL) simultaneously for both short and long range is a very delicate task that can be subject to errors. At short-range, the measurements often encounter signal overflow or saturation and possible nonlinear gain problems in the reverberation measurement system caused by a powerful explosive source. (2) Due to strong environmental noise interference, it is very hard to get long-range RL with a higher reverberation-to-noise for lower frequencies, such as 150 and 200 Hz. Thus the quality of RL data between 3 and 12 s should be more reliable when a broadband of 150–2500 Hz is used. (3) The RBS cross section σ_{rbs} and the equivalent interface bistatic cross section for SVS σ_{svs}, expressed by Eqs. (13) and (27), are derived from the perturbation approximations. They are more accurate at low- to mid-grazing angles, and not good for very large grazing angles. The RL data between 3 and 12 s ensure all inverted seabed scattering are for low grazing angles in the whole frequency band of 150–2500 Hz. (4) The reverberation expressions in this paper are better for long range reverberation predictions (see the discussion made in the last paragraph of Sec. VI). (5) The seabed effective geoacoustic model in this paper is derived from LF long-range field measurements and is assumed as a homogenous half space. The long-range reverberation data ensure only a top layer of the bottom is under the consideration for the LF seabed scattering characterization.

1. The LF bottom roughness spectrum from long-range reverberation

In contrast to Figs. 2 and 3, obtained from $RL(t)$ at given single frequencies, Fig. 5 and Table III show that the wideband reverberation data as a function of frequency, $RL(f)$, between 150–2500 Hz at different reverberation times may uniquely determine the bottom roughness spectrum. For example, based on Table III, the average LF bottom roughness spectrum parameters for low grazing angles at the ASIAEX site, derived from $RL(f)$ data between 3 and 12 s in a frequency band of 150–2500 Hz, are close to

$$\gamma_2 \approx 1.3, \quad \omega_2 \approx 2.8 \times 10^{-5}. \tag{51}$$

These values are different from those commonly used for HF.

Table III also shows that with decreasing time/range (corresponding to increased grazing angles of the seabed scattering), $RL(f)$-inverted γ_2 and ω_2 seem to increase. γ_2, inverted from short-range reverberation at 1.5 and 2 s, may reach to 2.2–2.3. The reason for this is not clear at this moment. It might be due to the scattering contributions from deeper layers of sediments at short range for lower frequencies or due to the problems/physics discussed in the first paragraph of Sec. VII C. In addition, the theoretical RL values at shorter range are also less accurate. Thus the results from 1.5 and 2.0 s are included in Table III just for reference/discussion.

2. The LF volume scattering cross section σ_V from long-range reverberation

All the $RL(f)$ inverted σ_V from 3 to 12 s in Table III are plotted in Fig. 6(a). Using the power law fitting, the average volume cross section in sediments can be expressed by

$$\sigma_V = 0.0171\alpha_p^{(2.038\pm0.001)}. \tag{52}$$

Using the frequency dependence of the bottom attenuation listed in Table I, all the σ_V obtained from 3 to 12 s are plotted against the frequency in Fig. 6(b). From the power law fitting, the average volume cross section from all $RL(f)$ between 3 and 12 s can be expressed by

$$\sigma_V = (0.00238\pm0.00004)(f/100)^{(3.805\pm0.021)}. \tag{53}$$

Equations (52) and (53) are very close to Eqs. (48) and (49), where α_p is the bottom attenuation in dB/m, f is frequency in Hz. The long-range reverberation-derived LF σ_V exhibits strong frequency dependence that is very different from that in the HF range. The results in Fig. 6 are also almost the

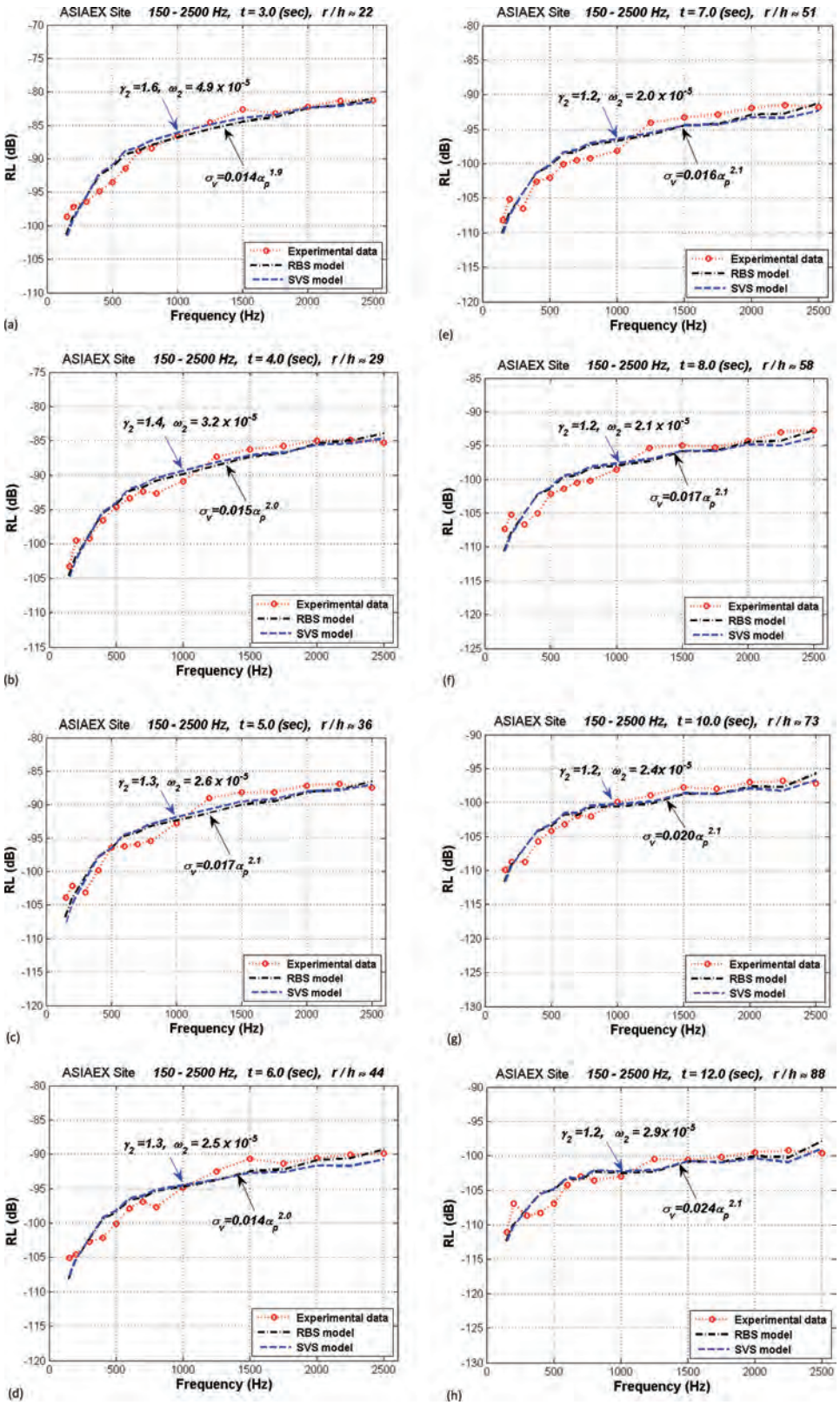

FIG. 5. Comparisons between theoretical $RL(f)$ (using the RBS and SVS models) and reverberation data at given times. (a) 3.0 s, (b) 4.0 s, (c) 5.0 s, (d) 6.0 s, (e) 7.0 s, (f) 8.0 s, (g) 10.0 s, and (h) 12.0 s.

same as those in Fig. 4, obtained from $RL(t)$ at different frequencies.

As this time, we do not know why the LF bottom roughness spectrum and the SVS cross section at low grazing angles, derived from wideband long-range reverberation, have different characteristics from those commonly used for HF. We also do not know which of these should be a dominant LF seabed scattering mechanism for long-range reverberation. These questions are outside of the present paper's scope. Hopefully, the LF seabed scattering parameters at low grazing angles inverted from long-range reverberation measurements in this paper can offer some reference data sets for future analysis of the LF seabed scattering mechanisms.

TABLE III. LF seabed scattering parameters inverted from *RL(f)* at different reverberation times.

Models		RBS: Bottom roughness spectrum $W(\Delta K) = \omega_2/(\Delta K)^{\gamma_2}$			SVS: Volume scattering cross section: $\sigma_V = \sigma_2 \alpha_p^{n_v}$		
Rev. time (s)	$r/h \approx$	γ_2	$\omega_2 \times 10^{-5}$	Std_{RBS}	σ_2^*	n_V	Std_{SVS} (dB)
1.5*	11	2.3	23.7	2.031	0.010	1.5	2.294
2.0*	15	2.2	18.3	1.411	0.009	1.5	1.649
3.0	22	1.6	4.9	1.419	0.014	1.9	1.603
4.0	29	1.4	3.2	1.192	0.015	2.0	1.348
5.0	37	1.3	2.6	1.719	0.017	2.1	1.874
6.0	44	1.3	2.5	1.473	0.014	2.0	1.668
7.0	52	1.2	2.0	1.547	0.016	2.1	1.725
8.0	59	1.2	2.1	1.672	0.017	2.1	1.855
10.0	73	1.2	2.4	1.191	0.020	2.1	1.243
12.0	88	1.2	2.9	1.513	0.024	2.1	1.578

VIII. SUMMATION AND DISCUSSION

The energy flux (angular spectrum) method for SW reverberation, based on the WKB approximation to the normal-mode solution, has been integrated with the physics-based RBS and SVS models. The integration also results in a simple relationship between the classic seabed scattering cross sections and the modal scattering matrix in waveguides. Taking advantage of the progress made by the seabed scattering community, and using commonly known seabed geoacoustic/scattering models, the resultant SW reverberation expressions in the angular domain or in the modal domain can conveniently be used for predicting SW reverberation for the Pekeris waveguide or non-Pekeris waveguide, respectively. Comparisons of the reverberation model with the reverberation data, collected from the ASIAEX site in a frequency range of 150–2500 Hz, show that the the RBS model or the SVS model can directly be used for the LF reverberation modeling.

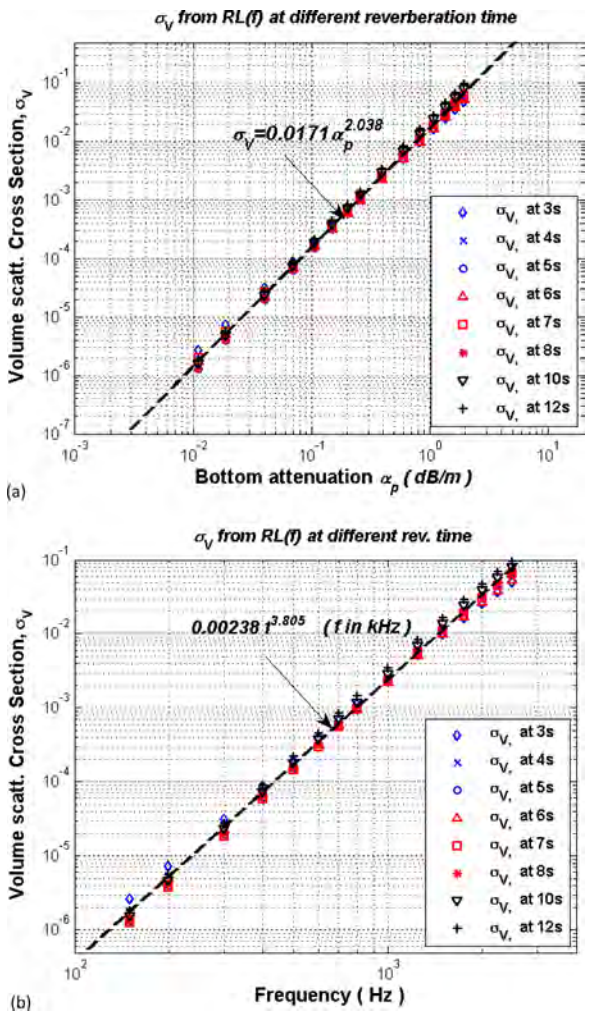

FIG. 6. (Color online) The sediment volume scattering cross sectionσ_V, inverted from $RL(f)$ at different times. (a) σ_V vs the bottom attenuation, (b) σ_V vs frequency.

The reverberation data at the ASIAEX site are used for characterization of the LF seabed scattering at low grazing angles. The results show that the reverberation level as a function of time, $RL(t)$, at one single frequency cannot uniquely determine the seabed scattering parameters. The wideband reverberation data can uniquely determine a set of the bottom roughness spectra or the SVS cross section. The bottom roughness spectrum and the SVS cross section, inverted from the broadband long-range reverberation data at the ASIAEX site, exhibit different characteristics from those commonly used in HF. For example, for the HF, the roughness spectrum exponent is restricted to the range of $2 \leq \gamma_2 \leq 4$ with a mean value of 3.0. But the long-range reverberation inverted LF roughness spectrum exponent $\gamma_2 \approx 1.3$. The HF SVS cross section σ_V is generally assumed to have linear frequency dependence. However, in the 150–2500 Hz range, the long-range reverberation-inverted σ_V exhibits much stronger frequency dependence: $\sigma_V \propto f^{3.8}$.

All the reverberation inversions in this paper are constrained by the Biot geoacoustic model for the bottom. The reverberation data from the ASIAEX site can almost be equally well predicted by the RBS model and SVS model. To analyze which one (or both) is a dominating LF scattering mechanism at low grazing angles, it is desirable to have geophysical measurements on the bottom roughness spectrum and sediment inhomogeneities for the seabed scattering modeling. Further research is called for understanding the mechanism of the reverberation-inverted LF seabed

scattering characteristics and analyzing the uncertainties in reverberation inversion with more measurements.

ACKNOWLEDGMENTS

This work was supported by the ONR OA322 and the CAS. The authors thank Dr. Robert Headrick for his support and helpful comments. We would like to express appreciation to co-workers at the State Key Laboratory of Acoustics, Chinese Academy of Sciences Institute of Acoustics, Dr. Zhaohui Peng, Dr. Zhenglin Li, Dr. Lianghao Guo, and Dr. Fenghua Li for their constructive discussions on this work and for sharing the experimental data. Finally, thanks go to our colleagues, Dr. Peter Rogers and James Martin, for their assistance and encouragement.

[1]K. V. Mackenzie, "Long-range shallow-water bottom reverberation," J. Acoust. Soc. Am. **34**, 62–66 (1962).
[2]C. Y. Wu, "Calculation of shallow water reverberation intensity based on ray theory. Part 1 (in Chinese)," Acta Acust. **4**, 114–119 (1979).
[3]C. Y. Wu, "Calculation of shallow water reverberation intensity based on ray theory. Part 2 (in Chinese)," Acta Acust. **5**, 210–220 (1980).
[4]H. P. Bucker and H. E. Morris, "Normal-mode reverberation in channels or ducts," J. Acoust. Soc. Am. **44**, 827–828 (1968).
[5]R. H. Zhang and G. L. Jin, "Normal-mode theory of average reverberation intensity in shallow-water," J. Sound Vib. **119**, 215–223 (1987).
[6]T. C. Yang, "Scattering from boundary protuberances and reverberation imaging," J. Acoust. Soc. Am. **93**, 231–242 (1993).
[7]D. D. Ellis, "A shallow-water normal-mode reverberation model," J. Acoust. Soc. Am. **97**, 2804–2814(1995).
[8]V. A. Grigor'ev, V. M. Kuz'kin, and B. G. Petnikov, "Low-frequency bottom reverberation in shallow-water ocean regions," Acoust. Phys. **50**, 37–45 (2004).
[9]J. X. Zhou, "The analytical method of angular power spectrum, range and depth structure of the echo-to-reverberation ratio in shallow water sound field (in Chinese)," Acta Acust. **5**(2), 86–99 (1980).
[10]Both the English translation and Chinese original versions of Ref. 9 can be obtained by sending an email to: jixun.zhou@me.gatech.edu.
[11]J. X. Zhou, "The vertical coherence of long-range reverberation in the shallow water homogeneous layer (in Chinese)," Acta Ocean. Sin. **1**(2), 212–218 (1979).
[12]J. X. Zhou, D. H. Guan, E. C. Shang, and E. S. Luo, "Long-range reverberation and bottom scattering strength in shallow water," Chin. J. Acoust. **1**, 54–63 (1982).
[13]J. X. Zhou, X. Z. Zhang, and E. S. Luo, "Shallow-water reverberation and small angle bottom scattering," in *Shallow-Water Acoustics*, edited by R. H. Zhang and J. X. Zhou (China Ocean Press, Beijing, 1997), pp. 315–322.
[14]J. X. Zhou and X. Z. Zhang, "Shallow-water reverberation level: Measurement techniques and initial reference values," IEEE J. Ocean. Eng. **30**, 832–842 (2005).
[15]C. H. Harrison, "Closed-form expressions for ocean reverberation and signal excess with mode stripping and Lambert's law," J. Acoust. Soc. Am. **114**, 2744–2756 (2003).
[16]C. H. Harrison, "Closed form bistatic reverberation and target echoes with variable bathymetry and sound speed," IEEE J. Ocean. Eng. **30**, 660–675 (2005).
[17]C. W. Holland, "Constrained comparison of ocean waveguide reverberation theory and observations," J. Acoust. Soc. Am. **120**, 1922–1931 (2006).
[18]M. A. Ainslie, "Observable parameters from multipath bottom reverberation in shallow water," J. Acoust. Soc. Am. **121**, 3363–3376 (2007).
[19]C. W. Holland, "Fitting data, but poor predictions: Reverberation prediction uncertainty when seabed parameters are derived from reverberation measurements," J. Acoust. Soc. Am. **123**, 2553–2562 (2008).
[20]M. A. Ainslie, *Principles of Sonar Performance Modeling* (Springer-Verlag, Berlin, 2010), pp. 495–510.
[21]D. J. Tang, "Theoretical analysis on reverberation in shallow water (in Chinese)," CAS Institute of Acoustics Technical Report, Beijing, China (1985).
[22]E. C. Shang, "Some new challenges in shallow water acoustics," in *Progress in Underwater Acoustics*, edited by H. M. Merklinger (Plenum, New York, 1986), pp. 461–472.
[23]B. H. Tracey and H. Schmidt, "Seismo-acoustic field statistics in shallow water," IEEE J. Ocean. Eng. **22**, 317–331 (1997).
[24]H. C. Song, S. Kim, W. S. Hodgikiss, and W. A. Kuperman, "Environmentally adaptive reverberation nulling using a time reversal mirror," J. Acoust. Soc. Am. **116**(2), 762–768 (2004).
[25]J. R. Wu and E. C. Shang, "Relationship between integrated bottom scattering strength and modal backscattering matrix," IEEE J. Ocean. Eng. **32**(4), 872–878 (2007).
[26]E. C. Shang, T. F. Gao, and J. R. Wu, "A shallow-water reverberation model based on perturbation theory," IEEE J. Ocean. Eng. **33**(4), 451–461 (2008).
[27]A. Galinde, N. Donabed, M. Andrews, S. Lee, N. C. Markris, and P. Ratial, "Range-dependent waveguide scattering model calibrated for bottom reverberation in a continental shelf environment," J. Acoust. Soc. Am. **123**, 1270–1281 (2008).
[28]D. J. Tang and D. R. Jackson, "Application of small-roughness perturbation theory to reverberation in range-dependent waveguide," J. Acoust. Soc. Am. **131**, 4428–4441 (2012).
[29]S. A. Stotts and R. A. Koch, "Rough surface scattering in a Born approximation from a two-way coupled-mode formalism," J. Acoust. Soc. Am. **125**, EL242–EL248 (2009).
[30]S. A. Stotts, D. P. Knobles, and R. A. Koch, "Scattering in a Pekeris waveguide from a rough bottom using a two-way coupled mode approach," J. Acoust. Soc. Am. **129**, EL172–178 (2011).
[31]M. J. Isakson and N. P. Chotiros, "Finite element modeling of reverberation and transmission loss in shallow water waveguides with rough boundaries," J. Acoust. Soc. Am. **129**, 1273–1279 (2011).
[32]J. F. Lingevich and K. D. LePage, "Parabolic equation simulations of reverberation statistics from non-Gaussian-distributed bottom roughness," IEEE J. Ocean. **35**, 199–208 (2010).
[33]D. R. Jackson and M. D. Richardson, *High-Frequency Seafloor Acoustics* (Springer, New York, 2007).
[34]H. P. Bucker, "Sound propagation in a channel with lossy boundaries," J. Acoust. Soc. Am. **48**, 1187–1194 (1970).
[35]C. T. Tindle and D. E. Weston, "Connection of acoustic beam displacement, cycle distances, and attenuations for rays and normal modes," J. Acoust. Soc. Am. **67**, 1614–1622 (1980).
[36]L. M. Brekhovskikh, "The average field in an underwater sound channel," Sov. Phys. Acoust. **11**(2), 126–134 (1965).
[37]L. M. Brekhovskikh, "Elements of sound field theory in the ocean," in *Ocean Acoustics*, edited by L. M. Brekhovskikh (Nauka, Moscow, 1974), pp. 79–162 (in Russian).
[38]P. M. Smith, "Average sound transmission in range-dependent channels," J. Acoust. Soc. Am. **55**, 1197–1204 (1974).
[39]L. M. Brekhovskikh and Y. P. Lysanov, *Fundaments of Ocean Acoustics*, 3rd ed. (Springer-Verlag, New York, 2003), Sec. 5.6.
[40]B. G. Katsnelson and V. G. Petnikov, *Shallow-Water Acoustics* (Springer-Praxis, New York, 2002), Sec. 3.5.
[41]D. R. Jackson, R. I. Odom, M. I. Boyd, and A. N. Ivakin, "A geoacoustic bottom interaction model (GABIM)," IEEE J. Ocean. Eng. **35**(3), 603–617 (2010).
[42]J. X. Zhou, X. Z. Zhang, and D. P. Knobles, "Low-frequency geoacoustic model for the effective properties of sandy seabottoms," J. Acoust. Soc. Am. **125**, 2847–2866 (2009).
[43]B. G. Katsnelson and V. G. Petnikov, *Shallow-Water Acoustics* (Springer-Praxis, New York, 2002), Sec. 2.1.
[44]J. X. Zhou, X. Z. Zhang Z. H. Peng, and J. S. Martin, "Sea surface effects on shallow-water reverberation," J. Acoust. Soc. Am. **121**, 98–107 (2007).
[45]J. X. Zhou and X. Z. Zhang, "Physical parameters for four seabed geoacoustic models from low-frequency measurements," AIP Conf. Proc. **2712**, 163–172 (2010).
[46]F. Ingenito, S. Wolf, and J. Miller, "Modal acoustic transmission loss (MOATL)," Report 8429, NRL, Washington, DC, 1980.